This is to certify that the

dissertation entitled

THE ELECTRONIC AND GEOMETRIC STRUCTURES OF VARIOUS SMALL MOLECULES CONTAINING EARLY TRANSITION METALS

presented by

Jesse Edwards III

has been accepted towards fulfillment
of the requirements for

Ph.D. degree in Chemistry

James F. Harrison
Major professor

Date August 30, 1999

THE ELECTRONIC AND GEOMETRIC STRUCTURES OF VARIOUS SMALL MOLECULES CONTAINING EARLY TRANSITION METALS

By

Jesse Edwards III

A DISSERTATION

Submitted to
Michigan State University
in partial fulfillment of the requirements
for the degree of

DOCTOR OF PHILOSOPHY

Department of Chemistry

1999

ABSTRACT

THE ELECTRONIC AND GEOMETRIC STRUCTURES OF VARIOUS SMALL TRANSITION METAL CONTAINING MOLECULES

By

Jesse Edwards III

Earlier work on Scandium Nitride and Scandium Imide has prompted the study of this unique class of compounds through ab-initio methods. Computationally, the transition-metal nitrides have been studied in some detail. In these studies the ScN molecule was found to possess a $^1\Sigma^+$ ground state with a $^3\Sigma^+$ state lying only about 7 kcal higher in energy. The triplet state comes about by decoupling the weak sigma bond in the singlet state, leaving a diradical with the two remaining π bonds ($^{\cdot}Sc{=}N^{\cdot}$). The relative ordering of the low lying states predicted by Harrison and Kunze agrees extremely will with experiment. Coupling two of the diradicals leads to an alternating doubly-bonded dimer, $^{\cdot}Sc{=}N{-}Sc{=}N^{\cdot}$ with a lone electron found in the σ symmetry orbitals to the rear of the terminal Sc and N atoms. These lone electrons are left available to form additional bonds. This work will cover the studies conducted investigating the electronic structure of the scandium nitride dimer.

Ab-Initio studies of diatomic metal nitrides and phosphides provide a fundamental tool in understanding the bonding between nitrogen and phosphorus atoms and metals. The bond lengths, bond energies, dipole moments, and vibrational frequencies of the ground and several low-lying states of the YN and YP molecules, calculated using GVB

(Generalized Valence Bond), GVB+1+2, MCSCF (Multiconfigurational Self-Consistent Field), and MCSCF+1+2 techniques will be reported.

The basis sets used for the Y atom in the YN and YP calculations contained a relativistic effective core potential (RECP) to account for the relativistic effects on Y. There will be a comparison of the results of YP using two different all electron basis sets on the phosphorus atom. The calculated ground states of YN, YP, and ScN[1, 2] and ScP[5] are strongly bound $^1\Sigma^+$ states at each level of theory. The calculated bond length of YN is 1.8147 angstroms. The experimental value was reported as 1.8148 angstroms[4]. The ordering of states for the YN molecule was in agreement with experiment at each level of theory.

The early transition metal methylidynes provide another unique class of compounds to study. The electronic structure of ScCH, TiCH, VCH, and CrCH, as well as, their positive cations will be presented for the ground and selected excited states. The geometries, energies, and dipole moments, and electron distributions (populations) were calculated using RHF, MCSCF, and MRCI techniques. Density Functional Theory was used to calculate the vibrational frequencies, along with the other properties mentioned on the ground and selected excited states.

Our results are also in good agreement with the few experimental results available. The vibrational frequencies and bond lengths of TiCH in the $^2\Sigma^+$ ground state are compared to experiment, along with the separation (energetically) between the $^2\Sigma^+$ and $^2\Pi$ states of the TiCH molecule. The vibrational frequencies and bond lengths of the VCH molecule in the $^3\Delta$ state are also compared to our calculated results.

To Tyler and Anika

ACKNOWLEDGEMENTS

First of all, I would like to thank Dr. James Harrison for his support. He has not only provided me with guidance in my research, but with the many 'life' issues that have arisen during my stay. I feel very fortunate to have had him as an advisor. I would also like to thank the many members of my committee, new and old, Dr. Richard Schwendeman, Dr. Mecouri Kanatzitdas, Dr.Michael Rathke, Dr. Gary Blanchard, Dr. James Jackson, and Dr. Daniel Nocera. Although a few of these professors only served on my committee for a short period their support, good nature and advice will always be appreciated. I would like to offer a special thanks to Dr. Schwendeman who served as my second reader. His dedication definitely helped to make this dissertation possible.

My gratitude also extends to the Harrison group members who have helped me in so many ways. I would also like to thank the staff of the Chemistry Department, Dr. Thomas Atkinson and Mr. Paul Reed in particular, and the staff of the College of Natural Science for the many pep talks and assistance.

My parents, Jesse Edwards Jr. and Brenda E. Smith, deserve much more than a thank you for their encouragement, help, and endurance through this entire process. Finally, I would like to thank my friends and family, especially, my Aunt Reese and her family, Aricka, LaVetta, Ken, and Phil. I can not thank you all enough.

TABLE OF CONTENTS

LIST OF TABLES

Table **Page**

LIST OF FIGURES

Figure **Page**

Chapter II

Chapter III

Chapter IV

KEY TO SYMBOLS AND ABBREVIATIONS

Symbol or Abbreviation	
ψ	Wavefunction
H	Hamiltonian
SCF	Self-Consistent Field
RHF	Restricted Hatree-Fock
MCSCF	Multiconfigurational SCF
CI	Configuration Interaction
CASSCF	Complete Active Space SCF
GVB	Generalized Valence Bond
MCSCF+1+2	Single and double excitations from From a MCSCF reference space
GVB+1+2	Single and double excitations from From a MCSCF reference space
MRCI	Multireference CI (Single and double excitations out of a multireference space)
DFT	Density Functional Theory
ϕ / Φ	Spin orbital/ space orbital
ψ_i	Kohn-Sham ith orbital
∇	Laplace operator
B3LYP	Becke-Lee-Yang-Parr hybrid-exchange correlation functional

ECP/RECP	**Effective Core Potential/Relativistic Effective Core Potential**
$\hat{F}_{KS}$ / $\Im$	**Kohn-Sham Operator/Fock Operator**
F	**Fock Matrix**
χ_l / χ_μ	**Pseudo-orbital/μth basis function**
V_l^{eff}	**Effective Potential**
$\hat{K}_i$ / K_{ij}	**Exchange operator/Exchange integral**
$\hat{J}_i$ / J_{ij}	**Coulombic operator/Coulombic integral**
$\mathbf{R_{eq}}$	**Equilibrium distance**
CSF	**Configuration State Function**
NO	**Natural Orbital**

Chapter 1

METHODS SUMMARY

Introduction

The methods used in this dissertation are derived from the time independent Schroedinger equation, $H\Psi=E\Psi$.[3] These methods use the variation principle [1] to approach the exact wavefunction. This principle states that :

"Given a normalized wavefunction $|\Psi\rangle$ that satisfies the appropriate boundary conditions, then the expectation value of the Hamiltonian is an upper bound to the exact ground state energy; i.e., $\langle\Psi|H|\Psi \geq E_0$."[1] Therefore the energy calculated depends on the wavefunction that is constructed. The wavefunction is a mathematical function that depends on both spatial, and spin variables. The Hamiltonian is the operator for the motion of the electrons and nuclei in the Coulomb field of the electrons and nuclei of the system.

Hamiltonian

The Hamiltonian has the form,

$$H = -\sum \frac{1}{2}\nabla_i^2 - \sum_{k=1}^{m} \frac{1}{2M_k}\nabla_k^2 + \sum_{i=1}^{n}\sum_{j>i}^{n} \frac{1}{r_{ij}} + \sum_{k=1}^{m}\sum_{p>k}^{m} \frac{Z_p Z_k}{R_{kp}} - \sum_{i=1}^{n}\sum_{k=1}^{m} \frac{Z_k}{r_{ik}}$$

Here r_i denotes the coordinates of the i^{th} electron, R_k the coordinates of the k^{th} nucleus, and Z_k the charge of the k^{th} nucleus. The terms $-1/2(\nabla_i^2)$ and $(-1/2M_k)\nabla_k^2$ represent the kinetic energy of the i^{th} electron and k^{th} nucleus, respectively. The charges and masses are in atomic units (au) with $m_e = 1$ au. The terms $1/r_{ij}$, $(Z_pZ_k)/R_{kp}$, and Z_k/r_{ik} represent the electron-electron, nuclear-nuclear, and electron-nuclear Coulomb interactions. The Hamiltonian as written excludes relativistic effects that can be accounted for by using relativistic effective core potentials, which will be discussed later.

A simplification of the Hamiltonian is obtained by using the Born-Oppenheimer (B.O.) approximation. In the B.O. approximation the nuclei are assumed to move much slower than the lighter electrons and one considers the electrons to be moving in the field of the fixed nuclei. [1,3] The Hamiltonian then takes on the form,

$$H = -\sum \frac{1}{2}\nabla_i^2 + \sum_{i=1}^{n}\sum_{j>i}^{n} \frac{1}{r_{ij}} + \sum_{k=1}^{m}\sum_{p>k}^{m} \frac{Z_p Z_k}{R_{kp}} - \sum_{i=1}^{n}\sum_{k=1}^{m} \frac{Z_k}{r_{ik}}$$

The Hamiltonian can be divided into two parts, one being a one electron operator that includes the kinetic energy of the electrons and the nuclear-electron attraction.

$$h(i) = \frac{-1}{2}\nabla_i^2 - \sum_{i=1}^{n}\sum_{k=1}^{m}\frac{Z_k}{r_{ik}}$$

Then,

$$H_1 = \sum_{i=1}^{n} h(i)$$

The remaining part is

$$\sum_{i=1}^{n}\sum_{j>1}^{n}\frac{1}{r_{ij}} + \sum_{k=1}^{m}\sum_{p>k}^{m}\frac{Z_p Z_k}{R_{kp}}$$

In this part, the first term describes the electron-electron repulsion of the system and the second term describes the nuclear-nuclear repulsion, which is a constant for a particular nuclear configuration. Commonly the two body electron-electron interaction term is written as $g(1,2)=1/r_{12}$.

Wavefunction

Having specified the Hamiltonian, we can turn our attention to the wavefunction. There are various methods used to construct wavefunctions of atomic and molecular systems. All of the wavefunctions must follow the Pauli exclusion principle, which requires that a wavefunction must be antisymmetric with respect to the interchange of the coordinates of both space and spin of any two electrons,

$$\Psi(x_1,x_2,\ldots x_i,\ldots.x_j,\ldots x_n) = -\Psi(x_1,x_2,\ldots x_j,\ldots.x_i,\ldots x_n)$$

where x_I represents the space and spin coordinates of the i^{th} electron. While the nonrelativistic Hamiltonian does not include a contribution from the electron spin, the wavefunction often does, and this is usually accomplished by using spin orbitals.[1,2,9] The spin orbital is a product of a spatial function, Φ_i, describing the space in which the electron moves, and a spin function, with either spin up (α) or spin down (β); e.g., $\phi_a(i) = \Phi_a(i)\alpha(i)$.

One of the first wavefunctions to describe a system with this antisymmetric nature was the Hartree-Fock wavefunction.[1] A Hartree-Fock wavefunction is described by a Slater determinant [1, 9, 10] of spin orbitals selected so as to minimize the energy of the system.

$$\Psi_{HF} = \frac{1}{\sqrt{n!}} \begin{vmatrix} \phi_1(1) & \phi_2(1) & \cdots & \phi_n(1) \\ \phi_1(2) & \phi_2(2) & \cdots & \phi_n(2) \\ \vdots & \vdots & \ddots & \phi_n(3) \\ \phi_1(n) & \phi_2(n) & \cdots & \phi_n(n) \end{vmatrix}$$

The form of the orbitals is determined by varying the orbitals to minimize the energy under the following constraints:

a. the set ϕ_n is orthonormal

b. and the variation in each orbital is orthogonal to variations in the other orbitals.

This procedure leads to the Fock equation, $\Im\phi_i = \varepsilon_i\phi_i$, where $\Im$ is the Fock operator.

The Fock operator has the form,

$$\Im = \hat{h} + \sum_{j=1}^{n} (\hat{J}_j - \hat{K}_j)$$

where

$$\hat{h} = -\frac{1}{2}\nabla^2 - \sum_k \frac{Z_k}{r_k}$$

and

$$\hat{J}_i = \int \phi^*{}_i(2) g(1,2) \phi_i(2) d\tau(2)$$

is the Coulomb operator and

$$\hat{K}_i = \int \phi_i^*(2) g(1,2) \hat{P}_{12} \phi_i(2) d\tau(2)$$

is the exchange operator.

For a closed shell system the energy has the form,

$$E = \sum_{i=1}^{n} < h_i > + \sum_{i=1}^{n} \sum_{j>1}^{n} (2J_{ij} - K_{ij})$$

.

where $\langle h_i \rangle$ is the one electron energy of the i^{th} electron, J_{ij} is the coulombic repulsion between electron i and j and K_{ij} is the exchange energy between the two electrons.

Self-Consistent Field Procedure[1]

The unknown orbitals (spatial part) are expanded in a basis $\{\chi_\mu\}$ as

$$\phi_i = \sum_{\mu=1}^{m} C_{\mu i} \chi_\mu$$

where the $C_{\mu i}$ is the expansion coefficient of the μ^{th} basis function χ_μ. The basis functions used in this work are of the Gaussian type. These functions are of a form that is easy to use in calculating the integrals needed in the following procedures.[11, 12, 13] Upon substitution into the Schroedinger equation and variation of the $C_{\mu i}$ to minimize the energy, the Roothaan equations[3] are obtained as

$$\mathbf{FC_i = \varepsilon_i SC_i}.$$

$$\mathbf{F = H^{core} + G}$$

where **F** is the canonical Fock matrix whose elements are

$$F_{\mu\nu} = \int \chi_\mu^* \Im \chi_\nu d\tau;$$

S is the overlap matrix, whose elements are

$S_{\mu\nu} = \int \chi_\mu^* \chi_\nu \, d\tau$ and $\mathbf{C}_i$, is a column vector of coefficients $c_{\mu i}$, and ε_i is the energy of an electron in orbital *i*. The **G** term is the two electron part of the Fock matrix.

$$G_{\mu\nu} = \sum_a^{N/2} \int dr_1 \phi_\mu^*(1)[2J_a(1) - K_a(1)]\phi_\nu(1)$$

Here the *a* corresponds to the a^{th} orbital.

The Roothaan equations are solved by an iterative procedure. First, the geometry of the molecule is specified, a basis set is specified and the required integrals are calculated. The overlap matrix is diagonalized and a transformation matrix is obtained to transform the Fock matrix. One obtains a guess at the density matrix **P**

$$P_{\mu\nu} = 2\sum_a^{N/2} C_{\mu a} C_{\nu a}^*$$

often from the eigenvectors of the one electron Hamiltonian in the selected basis. The **G** matrix (obtained from the two electron intergrals) of the **F** matrix is calculated from the density matrix and the two-electron integrals. The $\mathbf{H}^{\mathbf{core}}$ **or** H_1 matrix is called the core-Hamiltonian. The transformed Fock matrix is calculated and diagonalized to obtain a new coefficient vector, **C′**, and orbital energy, ε. The new coefficients are used to form a new density matrix. This procedure is repeated until one obtains a solution that is consistent within a specified criterion on the energy or density, thus the idea of self-consistency. The field comes from the idea that there is an averaged field due to the electrons in the system.

Using this procedure it is possible to solve for a near Hartree-Fock wavefunction self-consistently. With a complete basis set this solution is considered the Hartree-Fock limit.

Correlation

The Hartree-Fock description does not provide adequately for the correlated motion of electrons in the system.[1,8] Therefore, this wavefunction description will not be adequate for quantitative studies. Correlation energy is by definition the energy difference between the exact energy and the Hartree-Fock energy.

$$E_{exact} - E_{Hartree\text{-}Fock} = E_{correlation}$$

This correlation energy may be (approximately) recovered by several methods including Generalized Valence Bond (GVB) Theory, [6,8,9] Multiconfigurational Self-Consistent Field (MCSCF)[5,7] and Configuration Interaction (CI)[3,7] techniques. In general, the exact wavefunction can be written as:

$$\Psi = c_0\Psi_0 + c_1\Psi_1 + c_2\Psi_2 + \cdots$$

where Ψ_0 is a single determinant wavefunction (possibly the Hartree-Fock solution), Ψ_1 consists of all determinants obtained as single excitations from Ψ_0, Ψ_2 consists of all determinants obtained as double excitations from Ψ_0, etc. Note that this is exact only when the expansion basis $\{\chi_\mu\}$ is complete. In CI calculations only the coefficients are permitted to vary; i.e., the orbitals $\{\phi\}$ are fixed at the SCF level. Practical considerations limit most calculations to single, Ψ_1, and double, Ψ_2, excitations and also to a finite or

incomplete basis $\{\chi_\mu\}$. Under these circumstances, a better approximation is to vary the coefficients of the basis functions themselves, as well as the coefficients of the selected determinants. This is the MCSCF technique. In the MRCI or multi-reference configuration interaction technique a MCSCF wavefunction is used as the reference space from which excitations are made to describe the MRCI wavefunction. The GVB method is just a special version of the MCSCF wavefunction. The MCSCF wavefunction is constructed under the constraints of orthonormality between the orbitals being constructed.

The final method to be discussed briefly is that of Density Functional Theory.[7,14] DFT is a development from the theory of Hohenberg and Kohn in 1963 which states that all the ground-state properties of a system are functions of the charge density. The Hohenberg-Kohn theorem thus enables us to write the total electronic energy as a function of density:

$$E(\rho) = \sum \int \psi_i (-\frac{\nabla^2}{2}) \psi_i dv + \int V_{nuclear} \rho(r) dv + \frac{1}{2} \iint dv dv' \frac{\rho(r)\rho(r')}{|r - r'|} + E_{xc}[\rho(r)]$$

where $E(\rho)$ is the energy as a function of the density, the first term is the kinetic component of the energy, the second term is the nuclear attractive component of the energy, the third term is the coulombic repulsive term, and the last term is the exchange-correlation functional.

The Ψ_i are the Kohn-Sham orbitals,[14c] defined so that the $\rho(\vec{r}) = \sum_{i=1} \Psi_i^2$ and obtained from a Hartee-Fock like eigenvalue problem.

$$\hat{F}_{KS}\Psi_i = \varepsilon_i \Psi_i$$

where $\hat{F}_{KS}$ is the Kohn-Sham operator

$$\hat{F}_{KS} = \hat{h} + \sum_{i=1}^{n} \hat{J}_i + \frac{\partial E_{xc}}{\partial \rho}$$

Unfortunately, E_{xc}, the exchange correlation energy is unknown and one is forced to use various approximate forms. We will use the Becke-Lee-Yang-Parr hybrid exchange-correlation functional called B3LYP.

Relativistic Effective Core Potentials

The Hamiltonian described earlier did not include relativistic effects; however, for atoms heavier than Al relativistic effects come into play. In the case of YN and YP discussed in a later chapter the relativistic effects are accounted for by using Relativistic Effective Core Potentials (RECP's).[15, 16]

The Effective Core Potential, ECP is also used in computational studies to provide computational savings. The number of integrals that need to be calculated in these systems scale on the order of M^4 where M is the number of basis functions. By using effective core potentials the core electrons on individual atoms are represented by a potential $V_{effective}$ or V_{eff} and are eliminated. The potential takes the form:

$$V_l^{eff} = \varepsilon_l + \frac{Z_{eff}}{r} - \frac{l(l+1)}{2r^2} + \frac{(\frac{1}{2}\nabla^2 - V'_{val})\chi_l}{\chi_l} .$$

Here, ε_l is the atomic orbital energy, Z_{eff} is the effective nuclear charge due to screening, and the third term represents the orbital kinetic energy. The last term consists of the kinetic energy of the electron in the orbital, V'_{val} represents the Coulomb and exchange potentials due to the other valence electrons, and χ_l represents the pseudo-orbital constructed from the Hartree-Fock orbitals that would see the potential due to the core electrons. Each valence orbital, χ_l, with a given angular momentum generates a unique potential. This decreases the number of integral calculations significantly because fewer basis functions are necessary to describe the system.

Relativistic Effective Core Potentials are generated in a similar manner, except the Dirac-Fock relativistic equations are solved and new relativistic pseudo-orbitals are generated with the relativistic effects already incorporated. These new pseudo-orbitals will then have an *l* and j dependence.

BIBLIOGRAPHY

BIBLIOGRAPHY

1. A. Szabo and N.S. Ostlund, "Modern Quantum Chemistry: Introduction to Advanced Electronic Structure Theory", Macmillan Pub. Co., Inc., New York, N.Y., 1982.

2. H. F. Schaefer III, "The Electronic Structure of Atoms and Molecules", Addison-Wesley Pub. Co., Reading, Mass., 1972.

3. I. Shavitt, "The Method of Configuration Interaction" in "Methods of Electronic Structure Theory", edited by H. F. Schaefer II, Plenum Press, New York, 1977.

4. A.C. Wahl and G. Das, "The Configuration Self Consistent Field Method" in "Methods of Electronic Structure Theory", edited by H.F. Schaefer III, Plenum Press, New York, 1977.

5. a) R. Shepard, "Ab-Initio Methods In Quantum Chemistry II," Advances in Chemical Physics, edited by K. P. Lawley, Wiley, New York, 1987.

   b) T. H. Dunning, Jr., "Multiconfigurational Wavefunctions for Molecules: Current Approaches" in "Methods of Electronic Structure Theory", edited by H.F. Schaefer III, Plenum Press, New York, 1977.

6. a) F.W. Bobrowicz and W.A. Goddard III, " The Self Consistent Field Equations for Generalized Valence Bond and Open-Shell Hartree –Fock Wavefunctions" in "Methods of Electronic Structure Theory", edited by H. F. Schaefer III, Plenum Press, New York, 1977.

   b) W. A. Goddard III, T. H. Dunning, Jr., W. J. Hunt, P. J. Hay, Acc. Chem. Res., 6, 368, (1973)

   c) W. A. Goddard III, L. B. Harding, Ann. Rev. Phys. Chem., 29, 363, (1978)

7. A. R. Leach, "Molecular Modeling: Principles and Applications", edited by Addison Wesley Longman Limited, Essex, England, 1996.

8. E. Merzbacher, "Quantum Mechanics", 2nd. Ed., John Wiley and Sons, New York, 1970.

9. I. N. Levine, "Quantum Chemistry", 2nd. Ed., Allyn and Bacon, Inc., Boston, 1974.

10. J. C. Slater, Phys. Rev. 34, 1293 (1929).

11. S. F. Boys, Proc. Roy. Soc. (London), A200, 542, (1950).

12. a) T.H. Dunning, Jr., J. Chem. Phys., 53, 2823, (1970).

    b) T.H. Dunning, Jr. and P.J. Hay, "Guassian Basis Sets for Molecular Calculations" in "Methods of Electronic Structure Theory", edited by H.F. Schaefer III, Plenum Press, New York, 1977.

13. a) B.H. Botch, T.H. Dunning, Jr. and J.F. Harrison, J. Chem. Phys., 75, 3466, (1981)
    b) P.J. Hay, J. Chem. Phys., 66, 4377, 1977.

14. a) J. A. Pople, P. M. W. Gill, and B.G. Johnson, Chemical Phys. Lett. 199, 557, 1992
    b) P. Hohenberg and W. Kohn, Phys. Rev. B 136, 864, 1964.
    c) W. Kohn and L. J. Sham, Phys. Rev. A 140, 1133, 1965.

15. Hay, P. J.; Wadt, W. R. J. Chem. Phys. 1986, 82, 5606.

16. Krauss, M.; Stevens, W. J., Ann. Rev. Phys. Chem., 1994, 34, 357.

CHAPTER 2

THE ELECTRONIC STRUCTURE OF YN AND YP

This chapter contains a detailed study of the electronic structure and various properties of YN and YP. Two of the central purposes of this work are to gain an understanding of the nature of the bonding between transition metals and main group elements and to characterize the effect of electronic structure on the properties of these compounds. This knowledge is important in the areas of astrophysics, organometallics, solid state chemistry, gas-phase spectroscopy, surface chemistry, and catalysis.

Yttrium nitride and phosphide have a variety of low-lying electronic states with an assortment of bonding possibilities. As has been seen in various studies of metal-main group diatomics, there are several bound single, double, and triply bonded states. It is our intention to investigate seven of the low-lying states of YN and YP. We will compare and contrast these two compounds and other first and second row transition metal diatomics

Background

There have been numerous experimental[3] and theoretical studies[1, 2] completed on the first row transition metals bonded to main group elements. Harrison and Kunze published ab-initio studies on several bound states of scandium nitride along with a significant compilation of work on transition metals bonded to other main group elements, including studies on TiN, VN, CrN and their mono and dipositive ions.[1] Other

researchers have produced work on the positive cations and also the dipositive ions of some of these unique metal-main group element diatomics.[2, 3] Very little has been done on the metal-phosphides. The ScN molecule was observed by Ram and Bernath by using Fourier transform emission spectroscopy,[4] and they found the ground state of ScN to be $^1\Sigma^+$ in keeping with the theoretical prediction. The experimental bond length of 1.654 Å [4] is in reasonable agreement with a predicted bondlength of 1.768 Å by Harrison and Kunze[1(h)]. Titanium nitride's electronic emissions were analyzed by Dunn, Hanson, and Rubinson and they observed a bondlength of 1.583 Å for the lowest energy state.[5] Harrison and Kunze reported the bond length to be 1.613 Å, in reasonable agreement.[1(j)]

Vanadium nitride was generated and observed by Dunn and Peter by way of electronic emission studies and they determined that it had the shortest bond length (1.566 Å) of any observed transition metal diatomic.[6] Theoretical calculations have predicted it be 1.588 Å.[1(j)] The term symbols of the ground states of TiN and VN, $^2\Sigma^+$, and $^3\Delta$, respectively, were the results found in both experiment and in theory. Theoretical calculations predict the ground state of CrN to be a $^4\Sigma^-$ with a bondlength of 1.597 Å.[1(j)]

The second row transition metal nitrides have been studied to a lesser extent theoretically, although significant work has been compiled in the experimental regime. Some of the earliest work was done on MoN and NbN in the 1960s.[7, 8] Since then there has been Fourier transform emission spectroscopy on YN,[3(r)] electronic emission spectroscopy on ZrN[9] and vibrational absorption spectrum observations on tantulum nitride[10] isolated in an argon matrix. Studies of MoN and Mo atoms in neon, argon, and krypton matrices using a hollow cathode ion sputter source for electron spin resonance

experiments followed some of this earlier work.[11] MoN has a ground state of $^4\Sigma^-$. Also, the compound yttrium imide has been studied by using jet-cooled spectroscopy. [12]

Theoretical studies have often provided valuable information relating experiment to theory. Balasubramanian[12] performed calculations on the yttrium imide molecule and found that the ground state was $^3\Sigma^-$, which Simard *et al.* were unable to confirm experimentally.[13] Gingerich calculated the dissociation energy of YN, LaN, HfN, NbN, TaN, MoN, WN, and several other first row transition metal nitrides using the experimental results of ZrN and UN.[2(k)] Gingerich and Shim[2(j)] performed calculations on YN to aid in the understanding of the bonding of this gaseous compound studied experimentally by Bernath and Ram.[3r] The molecule ZrN has also been examined experimentally and theoretically.[9, 2(k)] The experimental ground state detected was $^2\Sigma^-$.

In YN, the ground state has been found by Gingerich and ourselves to be the $^1\Sigma^+$ state.[2(j)] There are some differences in the bonding and other physical properties between Gingerich's results and ours. In the case of MoN the ground state was found theoretically by Goddard to be of sigma symmetry with a triple bond.[2i] This coincides with the chromium nitride $^4\Sigma^-$ ground state. [2(a, b, c, i)] The ScN ground state possesses a weak sigma bond. Daoudi et. al. calculated similar results for ScN using the CIPSI method,[2n] however, they suggested that the ground state, $^1\Sigma^+$, does not posses the weak sigma bond as suggested by Harrison.[2(n-p)] Harrison and Kunze calculate that the ground state lies only 7 kcal below that of the doubly bonded $^3\Sigma^+$ first excited state.[1j, 2o-p] This unique situation perseveres in the YN ground state, as will be discussed. This brings us to the significance of this work. As mentioned earlier, this work has import in areas of

catalysis, and organometallics and other areas where the question of bonding is important. Mulliken population[22] analysis and contour plots have been effective methods of examining the character and visualizing the structure of the bonding in this work, as has been noted by Goddard *et al.* in their examination of the electronic structure of MoN.[2(a, b, c, i)] The triple bonded species might form the bonds using pure atomic orbitals on Mo or hybrid orbitals, which would affect the bond length, bond energy, dipole moment, and an assortment of other physical properties.

The difference in the bond length affects the Coulombic interaction, electron distribution, and in turn the entire physical nature of these diatomic molecules. Referring back to MoN in the Goddard study and several triple-bonded metal nitride systems, the character of the sigma bond changes between the extensive valence s orbital character and the dσ character depending on the exchange energy and the ability of the orbital forming the bond to hybridize. In the case of catalysis and vapor deposition the ability of the metal nitride moieties to form stable bonds, affecting the surfaces in these systems, can be determined by the characteristics that have been cited. In the yttrium imide molecule Simard[13] and coworkers turned to theoretical calculations of Balasubramanian[12] to interpret their results.

Another factor that this type of study aids in disclosing is the nature and location of excited states and the relative ordering of these states. It is often difficult for a spectroscopist to examine some of the excited states in these systems because of the small separations in energy found between the states. Harrison and Kunze examined sixteen[1(h)] significant low-lying bound states relative to the separated ground state atoms. The

energy separations between states in these systems is sometimes as low as a few kcal/mol. This would be difficult for some spectroscopic techniques to uncover.

Methods

The computational work was completed using the COLUMBUS suite of programs.[14] There were two types of wavefunctions generated as references to the MRCI wavefunctions. Both sets of calculations were at the multiconfigurational self-consistent field (MCSCF) level; one set used the generalized valence bond (GVB) perfect pairing technique. The significance of near degeneracy in the Sc atom was noted by Harrison, Dunning and Botch.[15] It was not accounted for in either of the reference wavefunctions generated by these two techniques, but the single and double excitations out of the reference spaces in the (CI) calculations included the effect. The importance of the near degeneracy arises in that it affects the calculated dissociation energy. In the case of ScN including near degeneracy in the MCSCF wavefunction of Harrison and Kunze drops the ground state energy by 2-4 kcal/mol.[1(h)]

The MCSCF wavefunctions of YN and YP are described below:

N=nitrogen or phosphorus p_y or p_σ= 2p or 3p of N or P, respectively.

$^1\Sigma^+ \sim [\sigma(Y)\sigma(N) + \sigma(N)\sigma(Y)][\pi_y(Y)\pi_y(N)+\pi_y(N)\pi_y(Y)][\pi_x(Y)\pi_x(N)+\pi_x(N)\pi_x(Y)]$

$^3\Sigma^+ \sim [\pi_y(Y)\pi_y(N)+\pi_y(N)\pi_y(Y)][\pi_x(Y)\pi_x(N)+\pi_x(N)\pi_x(Y)]$ Y5s Npσ

$^3\Pi_{(\sigma,\pi)} \sim [\sigma(Y)\sigma(N) + \sigma(N)\sigma(Y)][\ \pi(Y)\pi(N)+\pi(N)\pi(Y)]$ Y5s Npy

$^3\Pi_{(\pi,\pi)} \sim [\pi_y(Y)\pi_y(N)+\pi_y(N)\pi_y(Y)][\pi_x(Y)\pi_x(N)+\pi_x(N)\pi_x(Y)]$ Y5py Npσ

$^1\Pi_{(\pi,\pi)} \sim [\sigma(Y)\sigma(N) + \sigma(N)\sigma(Y)][\pi_x(Y)\pi_x(N)+\pi_x(N)\pi_x(Y)]$ Y5py Npσ (singlet coupled)

$^3\Delta \sim [\pi_y(Y)\pi_y(N)+\pi_y(N)\pi_y(Y)][\pi_x(Y)\pi_x(N)+\pi_x(N)\pi_x(Y)]$ Yδ+ Npσ

$^1\Delta \sim [\pi_y(Y)\pi_y(N)+\pi_y(N)\pi_y(Y)][\pi_x(Y)\pi_x(N)+\pi_x(N)\pi_x(Y)]$ Yδ+ Npσ (singlet coupled)

In the MCSCF wavefunction the electrons are correlated without the pairwise constraint. Due to symmetry constraints the wavefunctions employed using the MCSCF and GVB techniques will not be significantly different, but the small difference in applying the perfect pairing has an effect on the manner in which the atoms separate. The GVB technique does not allow for the atoms to separate to the correct atom states and only the MCSCF and MCSCF+1+2 potential curves will be presented. However, the results of the GVB and GVB+1+2 calculations on the YN and YP molecules are presented in Tables 5a and 5b.

The calculations were performed using Hay and Wadt's relativistic effective core potentials (RECP's) with accompanying basis functions on the yttrium atom.[16] The Dunning double-zeta basis set was used on N.[17] The phosphorus basis set consisted of (16s10p3d2f)/[6s5p3d2f].[17] The yttrium basis was augmented according to Bauschlicher and Langhoff et. al. with polarization functions and a set of three uncontracted f-functions.[18, 19] In order to test the reliability of the Y basis, a comparison was made with the work of Bauschlicher and Langhoff *et. al.*[18] on the Y atom and the YH molecule. The Y atom was compared at the following levels of theory: RHF[a], SCF[b,c], single-reference SDCI[b,c], coupled-pair functional[c], and modified coupled-pair functional[c]. Table 1

displays the relative energy (eV) of three states of the Y atom relative to the ^{2}D ground state using the methods mentioned above, and compares them to the experimental results. In comparing the ^{2}P and the ^{4}F states at the SCF level our results are 0.02 and 0.04 eV lower in energy relative to the ground state of the atom. In the single-reference CI the difference increases to -0.05 and 0.08 eV for the two states. The differences can be attributed to symmetry and equivalence constraints placed on the orbitals in the Y atom by Langhoff et al.[18] Our calculations have no such constraints. Therefore, despite using the same basis sets with the same contraction schemes the resulting energies are different.

		SCF			CI		
State	Occupation	MH RHF[a]	LPB SCF[b]	EH SCF[c]	LPB SDCI[b]	EH SDCI[c]	Expt.[a]
^{2}D	$5s^24d^1$	0.00	0.00	0.00	0.00	0.00	0.00
^{2}P	$5s^25p^1$	1.19	1.41	1.39	1.08	1.13	1.33
^{4}F	$4d^25p^1$	0.75	0.69	0.65	1.36	1.44	1.36

[a]R. L. Martin and P.J. Hay, J. Chem. Phys. 75, 4539 (1981).
[b]S. R. Langhoff, L. G. M. Pettersson, and C. W. Bauschlicher, J. Chem. Phys. 86, 268 (1986).
[c]J. F. Harrison and J. Edwards, Department of Chemistry, Michigan State University.

Table 1. The relative energy (eV) of two states of the Y atom relative to the ^{2}D ground state.

Next, several states of the YH molecule were contrasted to continue our verification of the Y basis set. The same basis was used for the Y atom. The hydrogen basis set used was a duplicate of the hydrogen basis used by Langhoff and co-workers.[19] The H basis set consisted of 7s and 4p functions contracted to 4s and 3p functions as [4111/211], augmented with a diffuse function in an even-tempered manner.[20] A (211)

contraction of a Slater 2p function with an exponent of 1.0 was used for the p functions on the H atom.

Molecule	State	Level	ΔE(eV)	R_{eq}(a.u.)
YH	$^1\Sigma^+$	SDCI[a]	0.00	3.700
		SDCI[b]	0.00	3.700
		CPF[a]	0.00	3.706
		MCPF[a]	0.00	3.706
YH	$^3\Delta$	SDCI[a]	0.78	3.843
		SDCI[b]	0.86	3.842
		CPF[a]	0.86	3.842
		MCPF[a]	0.86	3.843
YH	$^3\Pi$	SDCI[a]	0.94	3.826
		SDCI[b]	1.01	3.824
		CPF[a]	1.01	3.825
		MCPF[a]	1.01	3.825

[a]S. R. Langhoff, L. G. M. Pettersson, and C. W. Bauschlicher, J. Chem. Phys. 86, 268 (1986).
[b]J. F. Harrison and J. Edwards, Department of Chemistry, Michigan State University.

Table 2. A comparison of various states of the YH molecule. The energy separation relative to the ground state YH molecule and the equilibrium geometry is reported.

As can be seen from the data above our results at the SDCI agree extremely well with those of Langhoff et. al. at the CPF and MCPF levels.[18] It appears that the small correlation energy difference evident in the atoms due to the symmetry and equivalence constraints may be accounted for in the CPF and MCPF calculations.

The Y atom and the Sc atom are obvious places to begin our comparison of the YN and ScN molecules. Figure 1 provides selected promotion energies of the Y

and Sc atoms averaged over the J values of each state.[21] The most striking difference in the ordering of these states is that the first excited states of each atom is different, yet similar in energy relative to the ^2D ground state. The ^2P, in a $5s^25p^1$ configuration, is the first excited state of the Y atom followed closely by the ^4F , $3d^24s^1$ configuration. On the other hand the Sc atom's first excited state is the ^4F , $4d^25s^1$ configuration. The promotion energies of these three states are all within about 32 kcal/mol. The $4s^24p^1$ configuration in the ^2P state for the Sc atom has not yet been observed experimentally. It was calculated using the basis set shown in Figure 1 at the SCF+1+2 level. The promotion energy puts it highest in energy amongst the states shown, about 8 kcal/mol higher than the ^4G, $3d^24p^1$ configuration. The isoelectronic configuration for Y is also a ^2P state and lies about 30 kcal/mole above the ground state of the Y atom. The only similarity displayed in Figure 1 between the atomic states of Y and Sc are the relative separation of the ^4F states corresponding to the configurations d^2s^1 and dsp configurations.

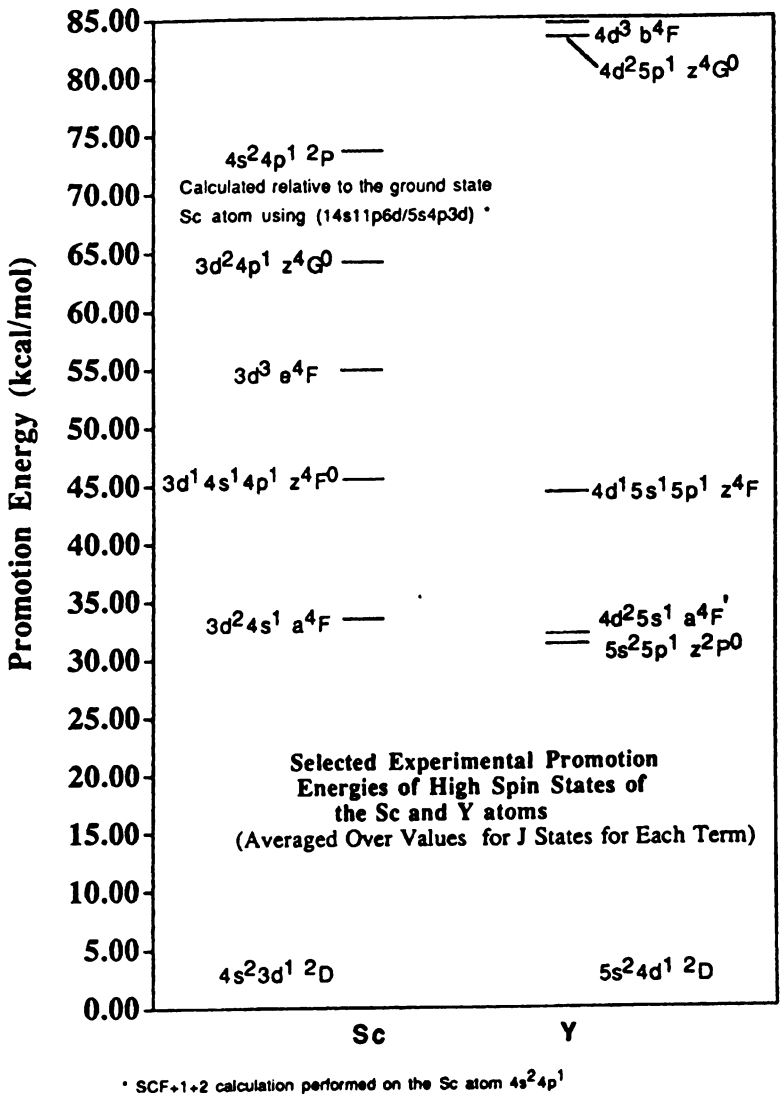

Figure 1. Selected experimental promotion energies of high spin states of the Sc and Y atoms averaged over values for J states for each term. Values taken from Moore (Reference 21) except for the calculated state shown above.

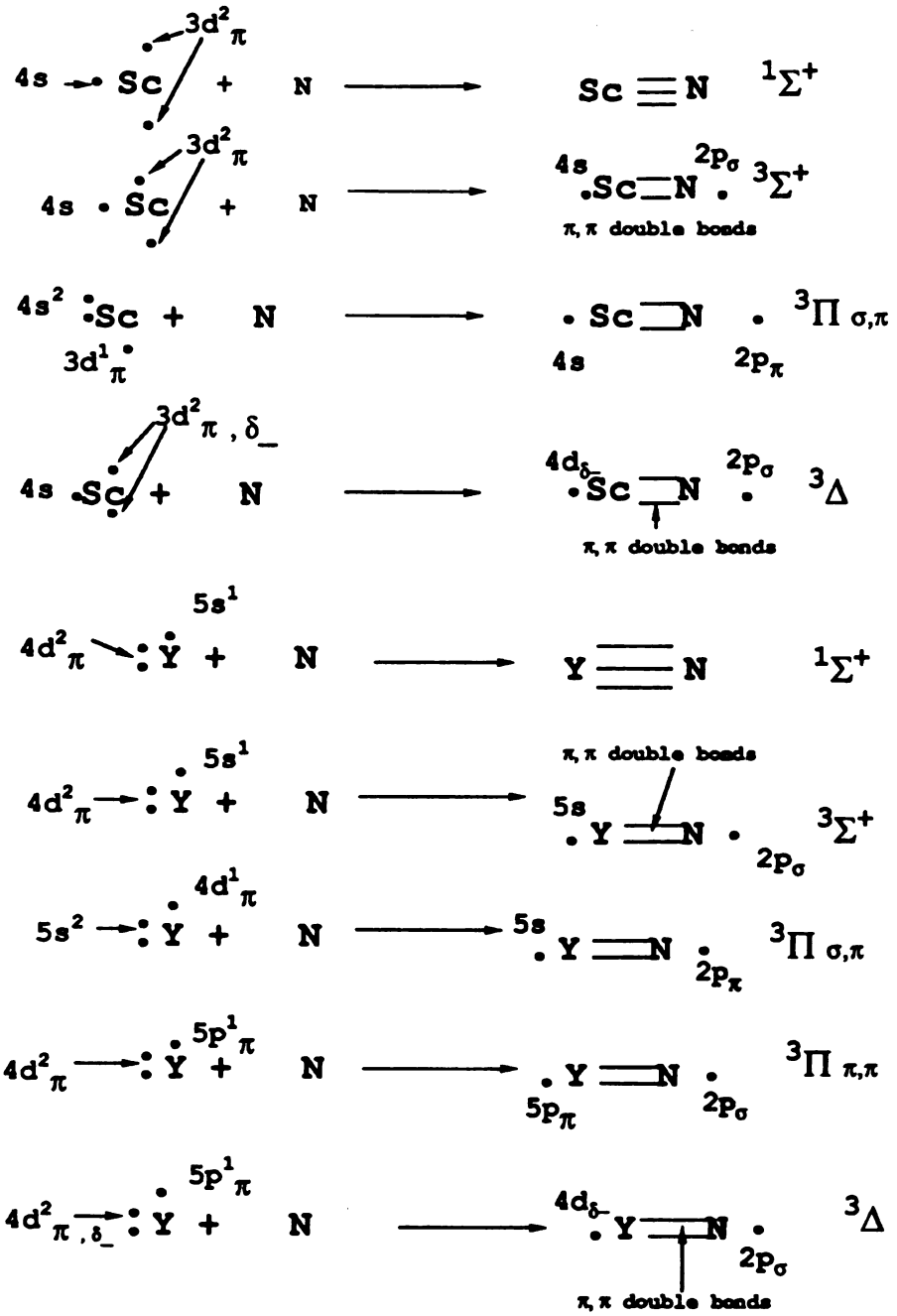

Figure 2. Bonding Scheme of analogous states of YN and ScN (Harrison and Kunze [1,2])

Results

Figure 2 presents the bonding scheme for the $^1\Sigma^+$, $^3\Sigma^+$, $^3\Delta$, $^1\Delta$, $^1\Pi_{\pi\sigma}$ and $^3\Pi_{\pi\sigma}$ states in the ScN and YN molecules and also the $^3\Pi_{\pi\pi}$ state of the YN molecule which would be analogous to those of YP with the difference being the atomic configuration of the phosphorus atom. The $^3\Pi_{\pi\pi}$, and $^3\Pi_{\pi\sigma}$ states are doubly bonded pi and double bonded sigma and pi bonded systems, respectively. Triplet coupled lone electrons are on the Y and N atoms. In the $^3\Pi_{\pi\pi}$ state the lone electron on the Y atom is localized in a $5p_\pi$ orbital, whereas in the $^3\Pi_{\pi\sigma}$ state the N atom possesses a $2p_\pi$ lone electron while the Y atom has a lone 5s electron making up the triplet coupling. The bonding in the $^3\Sigma^+$ state of both of these molecules consists of pi double bonds with lone electrons triplet coupled in an s orbital on the metal and in a $2p_\sigma$ orbital on N. In both molecules the triplet del state has a lone electron in a $d_{\delta+}$ orbital on the metal and in a $2p_\sigma$ orbital on the N.

Our MCSCF and MCSCF+1+2 wavefunctions provide the appropriate correlation to examine the molecules in a detailed fashion. The potential curves of the 7 states of interest are shown for YN and YP at both levels of theory in Figures 3, 4, 5, and 6. The ground state, $^1\Sigma^+$, of YN lies about 17 mH below the $^3\Sigma^+$ at the MCSCF level. In comparison, the ScN $^1\Sigma^+$ ground state is about 12 mH lower in energy than the $^3\Sigma^+$ first excited state at the MCSCF+1+2 level.[1h] The relative ordering of the $^1\Sigma^+$, $^3\Sigma^+$, $^3\Pi_{\pi\sigma}$, and

$^3\Delta$ states are the same in ScN at the MCSCF+1+2^{1h} and in YN (this work) at the MCSCF and MCSCF+1+2 levels.

The singlet coupled Δ and Π states are in close proximity in energy relative to the ground states for each of the systems examined. In contrast to the ScN systems studied, the YN molecule separates to a $5s^1 5p^1 4d^1$ valence configuration in the $^3\Delta$ state, while the ScN molecule separates to a $3d^3$ configuration of Sc with lone electrons in the $3d_{\pi x}$, $3d_{\pi y}$ and $3d_{\delta-}$ at the CI levels. In all of the states at each level of theory for both molecules, N separates to the ^4S ground state valence configuration of $2s^2 2p^3$. At the MCSCF level the $^3\Delta$ state valence configuration of YN matches that of the $^3\Pi\pi\pi$. At the asymptotic limit of the MCSCF+1+2 calculation the $^3\Pi\pi\pi$ state does not remain in the same configuration as the $^3\Delta$ state of YN; it falls to a lower energy configuration of $5s^1 4d^2$. The GVB calculations produce different results than those of the MCSCF. As mentioned earlier, constraints on the GVB wavefunctions do not allow for the atoms to separate smoothly to their proper limits. This can be corrected by modifying the GVB wavefunction as the molecule begins to separate. Despite this, the relative ordering of the energy levels was consistent with that of the MCSCF calculations. One significant difference arises in comparing the YN and YP molecular states. Figure 6 shows that the first excited state of the YP molecule is the $^3\Pi_{\pi\sigma}$ state at each level of theory. In the analogous diagram for YN this state lies slightly above the first excited state, $^3\Sigma^+$. The $^3\Sigma^+$ state lies several tenths of an of an electron volt above the ground state in the YP case at each level of theory. In the YN molecule at the CI level, the separation is slightly increased between the triplet

and singlet Δ and $\Pi_{\sigma,\pi}$ states, which was not evident in the MCSCF+1+2 calculations, as can be seen from Figure 4. The CI calculations for each of the MCSCF and GVB reference spaces lower the overall separations of the states relative to the ground state, but the overall ordering stays almost identical. The few exceptions arise in the ordering between the excited states $^3\Delta$, $^1\Delta$, and $^3\Pi_{\pi\pi}$. Despite this inconsistency, the lower lying states of $^3\Sigma^+$, $^3\Pi_{\pi\sigma}$ and $^1\Pi_{\pi\sigma}$ maintain a consistent order of separation of a little over 0.2 eV. Correlation introduced by the CI calculations accounts for these differences in ordering.

As mentioned earlier, one of the major differences predicted between the YN and YP molecules was the ordering between the $^3\Sigma^+$ and $^3\Pi_{\pi\sigma}$ states. In the $^3\Sigma^+$ state of YN the two pi bonds are made from the N $2p_x$ and $2p_y$ orbitals and Y d_{xz} and d_{yz} orbitals. In the case of the $^3\Pi_{\pi\sigma}$ state of YP the bonds are made from more spatially extensive orbitals of the P atom allowing for this state to be lower energetically than the $^3\Sigma^+$ state.

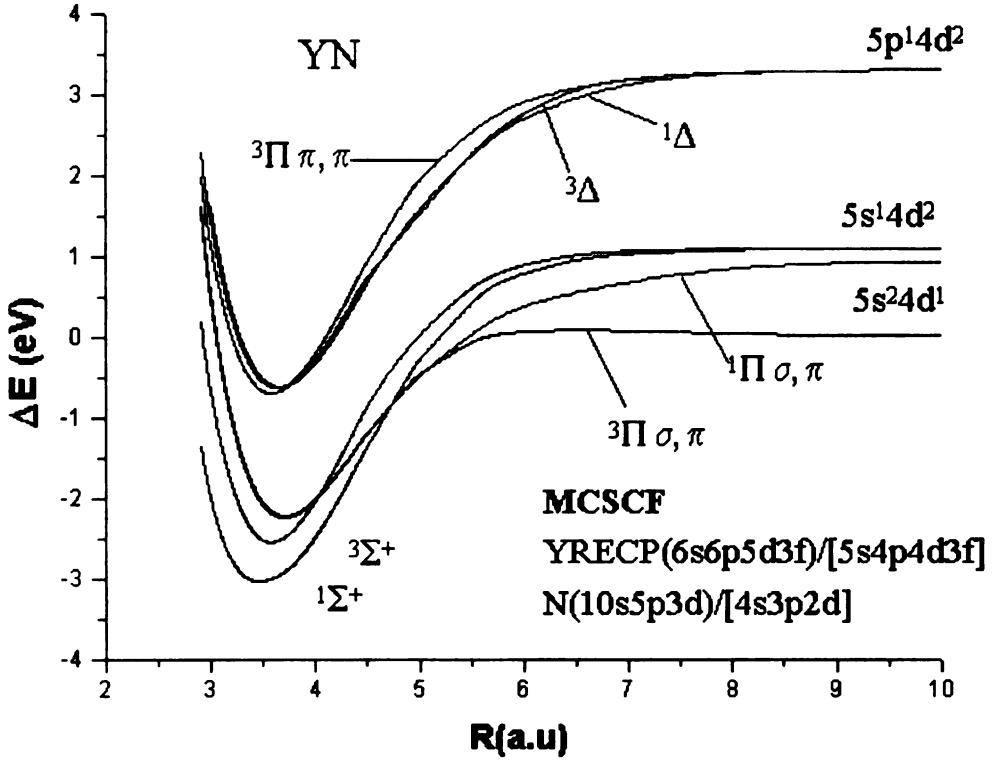

Figure 3. Potential energy curves of several electronic states of YN. MCSCF calculations performed in this work.

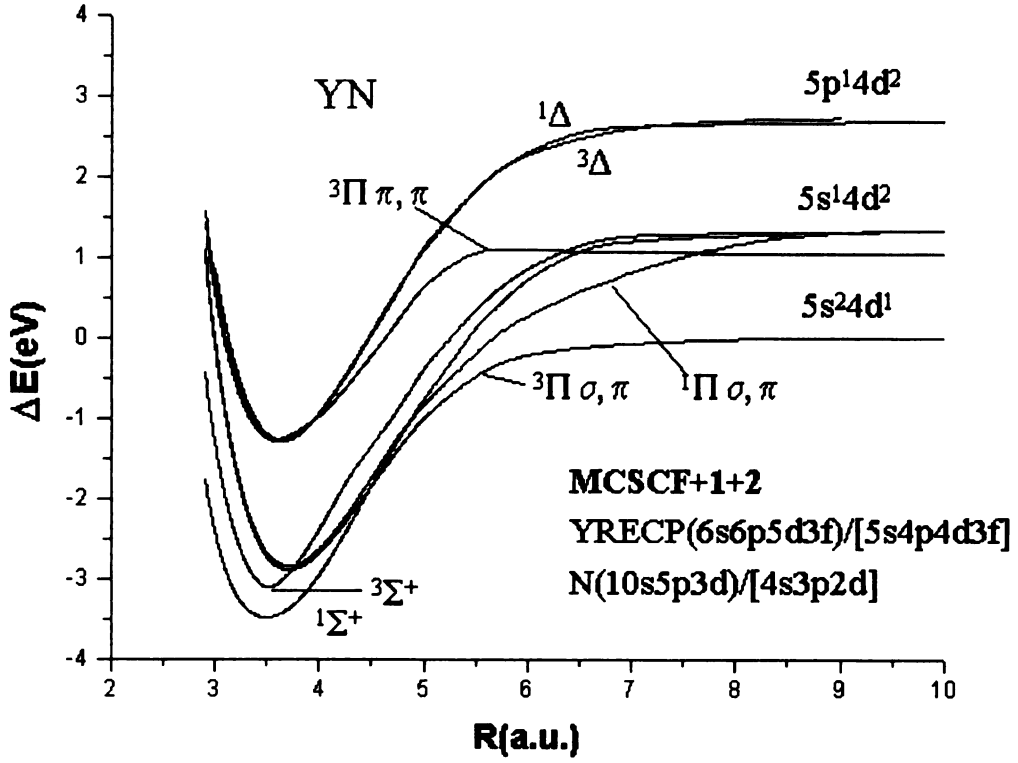

Figure 4. Potential energy curves of several electronic states of YN. MCSCF+1+2 calculations performed in this work.

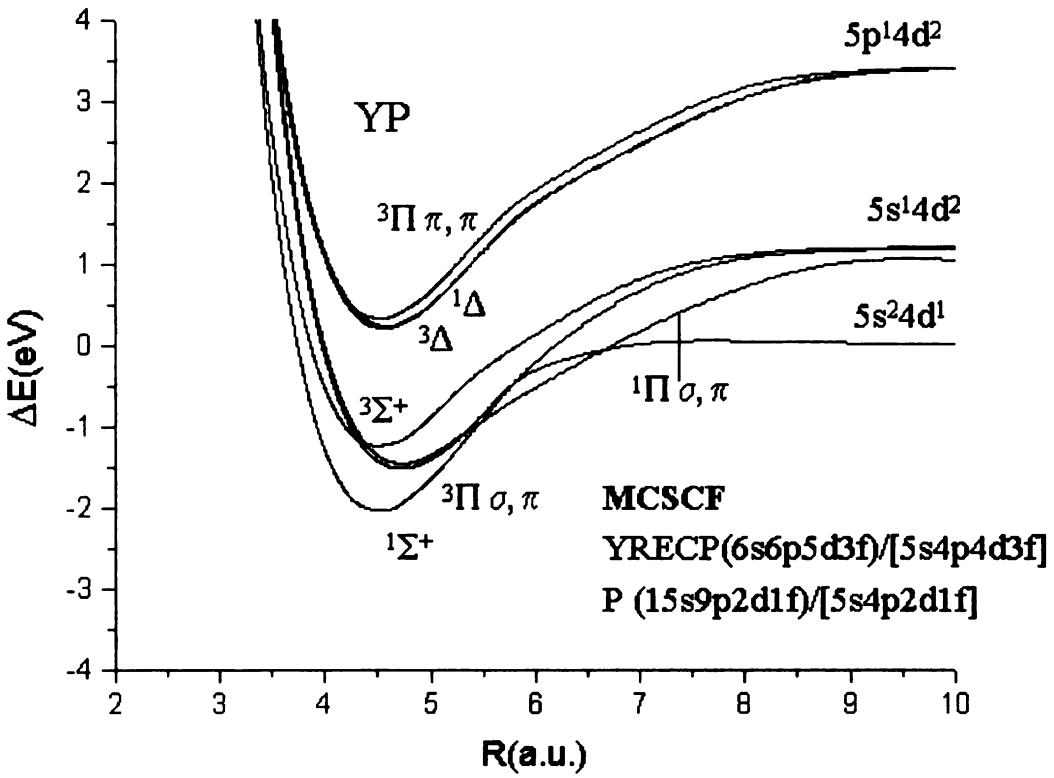

Figure 5. Potential energy curves of several electronic states of YP. MCSCF calculations performed in this work.

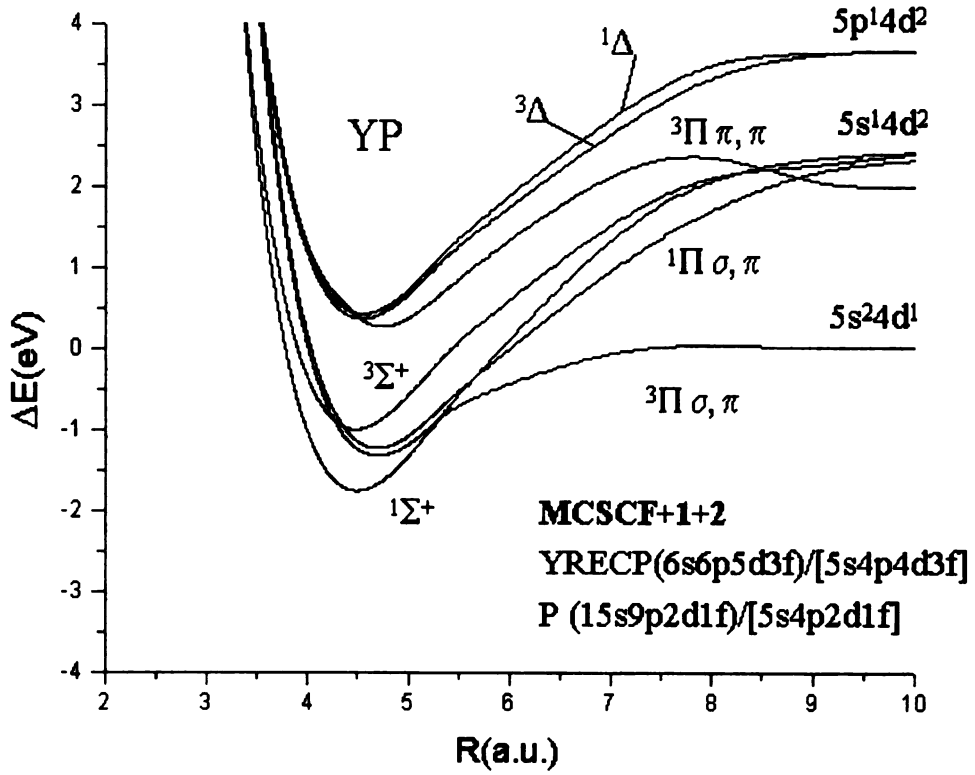

Figure 6. Potential energy curves of several electronic states of YP. MCSCF+1+2 calculations performed in this work.

Population Analysis

From Tables 3, 7 and 8 it can be seen that the populations of selected atomic orbitals for the YN and YP atoms are almost identical for each of the states shown. Figure 7a-7d show plots of the populations of selected atomic orbitals of YN versus the internuclear separation. Comparison of these plots with plots of the same type shown for ScN by Harrison and Kunze[1j] shows that the $^1\Sigma^+$ and $^3\Sigma^+$ states of YN and ScN follow similar bonding patterns. In each case there are large shifts of charge from π and d_σ orbitals of the metal atoms to the corresponding symmetry orbitals of the nitrogen atom. The shifts begin as the atoms approach the equilibrium bonding distances. Comparison of the population analyses of YP in this work and of ScP from the work of Tientega[5a] and Harrison shows that the populations at the equilibrium separation are very similar.

Bond lengths, bond energies, and vibrational frequencies are compared in Table 4 for YN and ScN and in Table 5 for YP and ScP. The data for the scandium diatomics, ScN and ScP, come from the work of Harrison and Kunze[1j] and Tientega and Harrison,[5a] respectively. The bond lengths of the phosphides are consistently larger than the nitrides, because of the larger phosphorus atom. The Sc atom being smaller than the Y atom leads to shorter bond lengths for the Sc species of the metal nitrides and phosphides. The vibrational frequencies are higher for the nitrides than the phosphides in keeping with the shorter bond lengths. This was also the case when comparing the scandium nitride and phosphide states with the corresponding states of

Table 3. YN Mulliken Population Analysis (a.u.)

MCSCF+1+2		Y atom								N atom			
State	Req(Å)	5s	5pσ	4dσ	4dδ+	5px	5py	4dπx	4dπy	2s	2pσ	$2p_x$	2py
$^1\Sigma^+$	1.847	0.22	0.32	0.55	0.00	0.07	0.07	0.65	0.65	1.8	1.1	1.3	1.3
$^3\Sigma^+$	1.863	0.86	0.20	0.32	0.00	0.58	0.58	0.51	0.51	1.8	0.80	1.4	1.4
$^3\Pi\pi\sigma$	1.857	0.91	0.21	0.67	0.00	0.01	0.06	0.16	0.53	1.9	1.4	0.79	1.4
$^3\Pi\pi\pi$	1.894	0.13	0.02	0.28	0.00	0.71	0.55	0.76	0.55	1.8	0.83	1.4	1.4
$^3\Delta$	1.830	0.08	0.05	0.25	0.00	0.08	0.08	0.49	0.49	1.8	0.81	1.4	1.4

Table 4. Comparison of equilibrium internuclear separations (Req) and vibrational frequencies (ω_e) for ScN and YN (This work)

State	Level[a]	ScN		YN	
		Req(Å)	$\omega_e(cm^{-1})$	Req(Å)	$\omega_e(cm^{-1})$
$^1\Sigma^+$	MCSCF	1.723	708	1.826	745
	MRCI	1.762	726	1.847	658
$^3\Sigma^+$	MCSCF	1.777	868	1.879	945
	MRCI	1.769	861	1.863	936
$^3\Pi\pi\sigma$	MCSCF	1.830	809	1.889	925
	MRCI	1.839	802	1.857	913
$^3\Pi\pi\pi$	MCSCF	-------	-------	1.889	911
	MRCI	-------	-------	1.894	874
$^3\Delta$	MCSCF	1.840	805	1.920	878
	MRCI	1.830	790	1.916	878

[a] MCSCF = MCSCF for YN molecule / GVB for the ScN molecule[1j]
MRCI= MCSCF+1+2 for YN molecule / GVB+1+2 for the ScN molecule[1j]

Table 5. Comparison of equilibrium internuclear separations (Req) and vibrational frequencies (ω_e) for ScP[1j] and YP[This work]

State	Level[a]	ScP			YP		
		Req(A)	ωe(cm^{-1})	D_e(kcal/mol)	Req(A)	ωe(cm^{-1})	D_e (kcal/mol)
$^1\Sigma^+$	MCSCF	2.272	459	17.8	2.382	562	49.5
	MRCI	2.277	446	35.6	2.375	568	65.4
$^3\Pi$ πσ	MCSCF	2.410	377	6.4	2.382	516	49.5
	MRCI	2.375	397	25.9	2.487	503	55.3
$^1\Pi$ πσ	MCSCF	2.419	384	6.2	2.503	489	36.8
	MRCI	2.392	319	21.6	2.485	516	53.2
$^3\Sigma^+$	MCSCF	.293	421	2.3	2.383	551	32.0
	MRCI	2.278	413	17.1	2.367	555	47.8
$^3\Pi$ ππ	MCSCF	-------	-------	-----	2.390	541	4.24
	MRCI	-------	-------	-----	2.509	540	17.7

[a]MCSCF = MCSCF for YP molecule / MCSCF(GVB) for the ScP molecule [5a]
MRCI= MCSCF+1+2 for YP molecule /MCSCF (GVB)(3s)+1+2 for the ScP molecule [5a]

Table 5a. YN equilibrium internuclear separations (Req), vibrational frequencies (ω_e), and energies.

State	Level[a]	Req(Å)	ωe(cm^{-1})	Energy (Hartree)
$^1\Sigma^+$	GVB	1.823	738	-91.97364
	MRCI	1.853	706	-92.04987
$^3\Sigma^+$	GVB	1.890	929	-91.95665
	MRCI	1.884	929	-92.03754
$^3\Pi\ \pi\sigma$	GVB	1.954	855	-91.94533
	MRCI	1.961	846	-92.02832
$^3\Pi\ \pi\pi$	GVB	1.888	919	-91.88766
	MRCI	1.893	887	-91.96859
$^3\Delta$	GVB	1.923	866	-91.88606
	MRCI	1.916	863	-91.96998

[a]MRCI= GVB+1+2 for YN molecule. This work.

Table 5b. YP equilibrium internuclear separations (Req), vibrational frequencies (ω_e), and energies.

State	Level[a]	Req(Å)	ωe(cm^{-1})	Energy (Hartree)
$^1\Sigma^+$	GVB	2.382	691	-378.26049
	MRCI	2.375	699	-378.34258
$^3\Sigma^+$	GVB	2.382	681	-378.23228
	MRCI	2.367	-----	-378.31439
$^3\Pi\ \pi\sigma$	GVB	2.486	-----	-378.24071
	MRCI	2.482	-----	-378.32556
$^3\Pi\ \pi\pi$	GVB	2.388	-----	-378.17289
	MRCI	2.512	-----	-378.26416
$^3\Delta$	GVB	2.416	-----	-378.17865
	MRCI	2.405	-----	-378.26422

[a]MRCI= GVB+1+2 for YP molecule

Table 6. ScN Mulliken Population Analysis (GVB) (a.u.). Taken from Harrison and Kunze reference 1(j).

		Y atom								N atom			
State	Req(Å)	5s	5pσ	4dσ	4dδ+	5px	5py	4dπx	4dπy	2s	2pσ	2px	2py
$^1\Sigma^+$	1.723	0.18	0.26	0.55	0.00	0.10	0.10	0.61	0.61	1.86	1.15	1.27	1.27
$^3\Sigma^+$	1.777	0.78	0.26	0.17	0.00	0.07	0.07	0.54	0.54	1.88	0.90	1.37	1.37
$^3\Pi\pi\sigma$	1.830	0.82	0.22	0.63	0.00	0.09	0.02	0.52	0.07	1.94	1.37	1.37	0.90
$^3\Delta(*)$	1.840	0.04	0.06	0.13	0.00	0.12	0.12	0.44	0.44	1.87	0.90	1.41	1.41

*$^3\Delta$ population for the dxy orbital on Sc is 1.0

Table 7. YP Mulliken Population Analysis (a.u.) at the MCSCF level.

		Y atom								P atom			
State	Req(Å)	5s	5pσ	4dσ	4dδ+	5px	5py	4dπx	4dπy	3s	3pσ	3px	3py
$^1\Sigma^+$	2.373	0.80	0.18	0.25	0.00	0.10	0.10	0.63	0.63	1.90	1.10	1.31	1.31
$^3\Sigma^+$	2.364	0.95	0.18	0.30	0.00	0.09	0.09	0.53	0.53	1.90	0.85	1.41	1.41
$^3\Pi\pi\sigma$	2.480	1.15	0.16	0.54	0.00	0.03	0.07	0.11	0.53	1.94	1.35	1.39	0.87
$^3\Pi\pi\pi$	2.509	0.23	0.07	0.18	0.00	0.10	0.54	0.54	0.97	1.91	0.82	1.50	1.40
$^3\Delta^a$	2.402	0.19	0.06	0.20	0.00	0.11	0.11	0.48	0.48	1.91	0.85	1.46	1.46
$^1\Pi\sigma\pi$	2.482	1.07	0.18	0.60	0.00	0.10	0.04	0.54	0.14	1.93	1.37	1.38	0.88
$^1\Delta^a$	2.406	0.19	0.06	0.22	0.00	0.13	0.13	0.41	0.41	1.88	0.85	1.54	1.54

[a] Y 4dxy population value is 1.04 for the $^3\Delta$ and $^1\Delta$ states.

Table 8. YP Mulliken Population Analysis (a.u.) at the MCSCF+1+2 level.

		Y atom								P atom			
State	Req(Å)	5s	5pσ	4dσ	4dδ+	5px	5py	4dπx	4dπy	3s	3pσ	3px	3py	
$^1\Sigma^+$	2.375	0.92	0.12	0.25	0.00	0.05	0.05	0.59	0.59		1.87	1.02	1.38	1.38
$^3\Sigma^+$	2.367	0.96	0.19	0.30	0.00	0.05	0.05	0.50	0.50		1.88	0.84	1.47	1.47
$^3\Pi\pi\sigma$	2.487	1.01	0.13	0.54	0.00	0.06	0.03	0.48	0.12		1.96	1.31	1.48	0.91
$^3\Pi\pi\pi$	2.510	0.13	0.02	0.28	0.00	0.55	0.55	0.76	0.76		1.8	0.83	1.40	1.40
$^3\Delta^a$	2.406	0.20	0.04	0.20	0.00	0.06	0.06	0.44	0.44		1.89	0.87	1.54	1.54
$^1\Pi\sigma$	2.485	1.10	0.15	0.59	0.00	0.06	0.01	0.50	0.12		1.97	1.33	1.46	0.93
$^1\Delta^a$	2.410	0.20	0.04	0.20	0.00	0.06	0.06	0.44	0.44		1.89	0.87	1.54	1.54

[a] Y 4dxy population value is 0.98 for the $^3\Delta$ and $^1\Delta$ states.

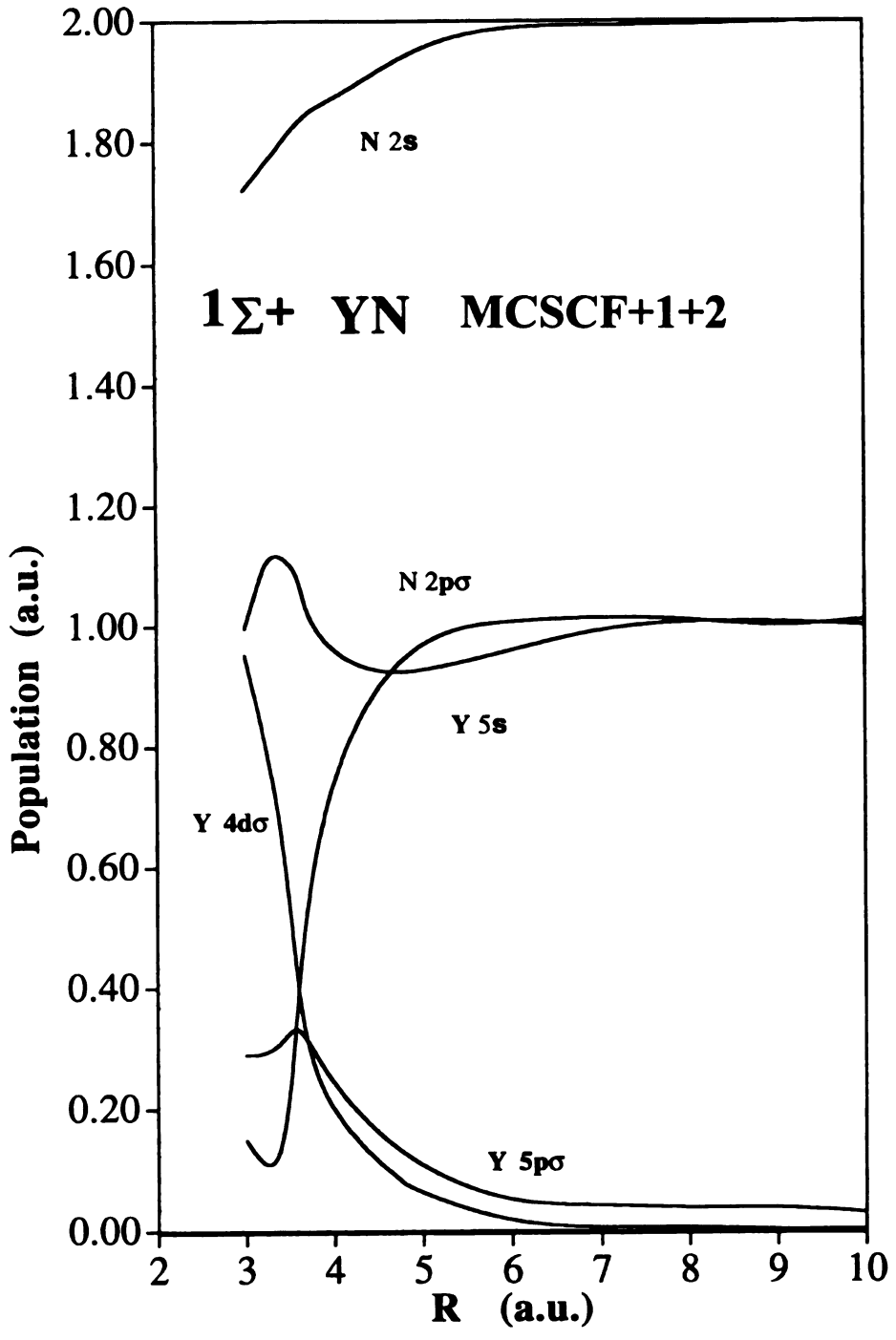

Figure 7a shows population curves of selected sigma symmetry orbitals taken from the natural orbitals of the YN molecule at the MCSCF+1+2 level.

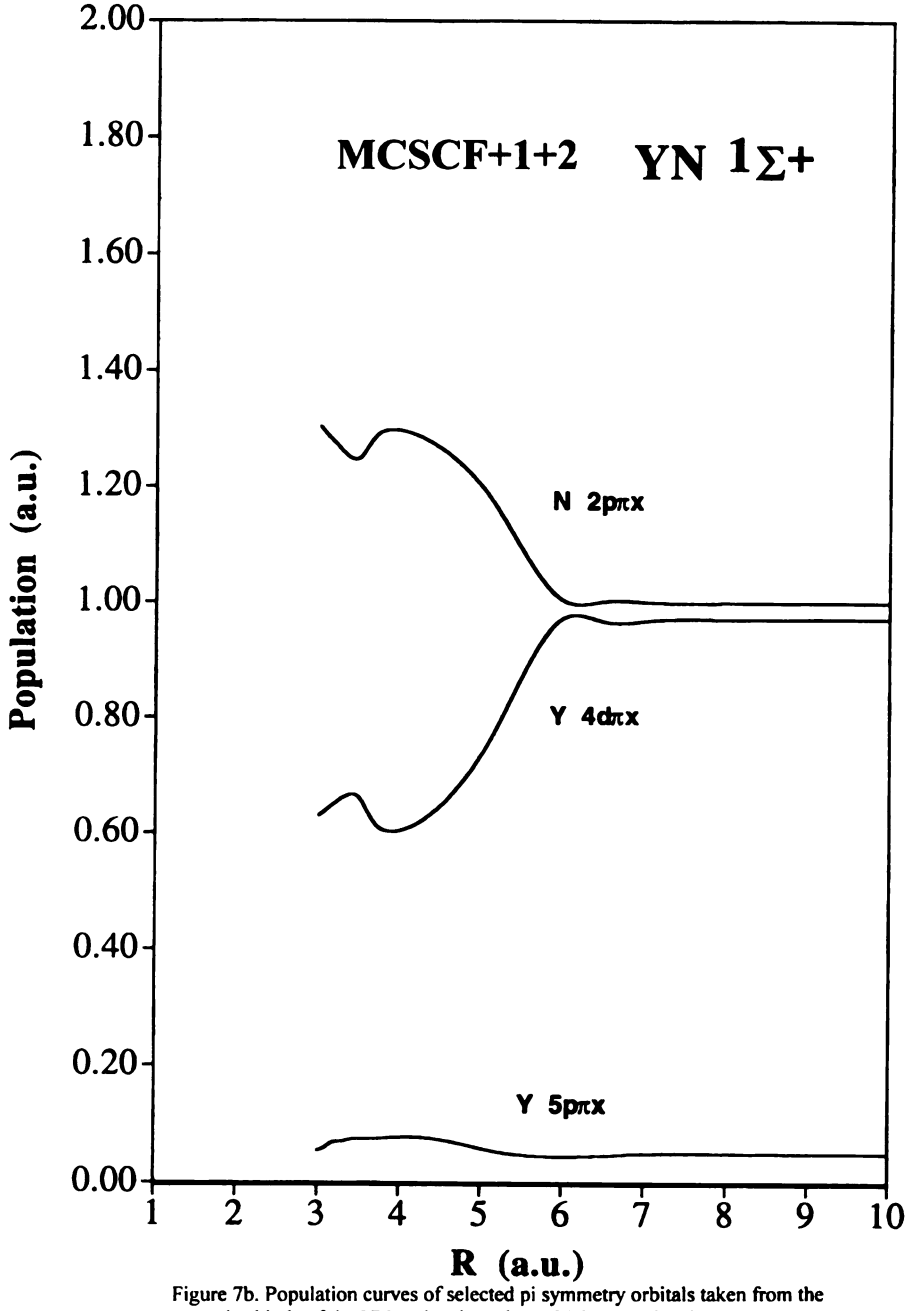

Figure 7b. Population curves of selected pi symmetry orbitals taken from the natural orbitals of the YN molecule at the MCSCF+1+2 level.

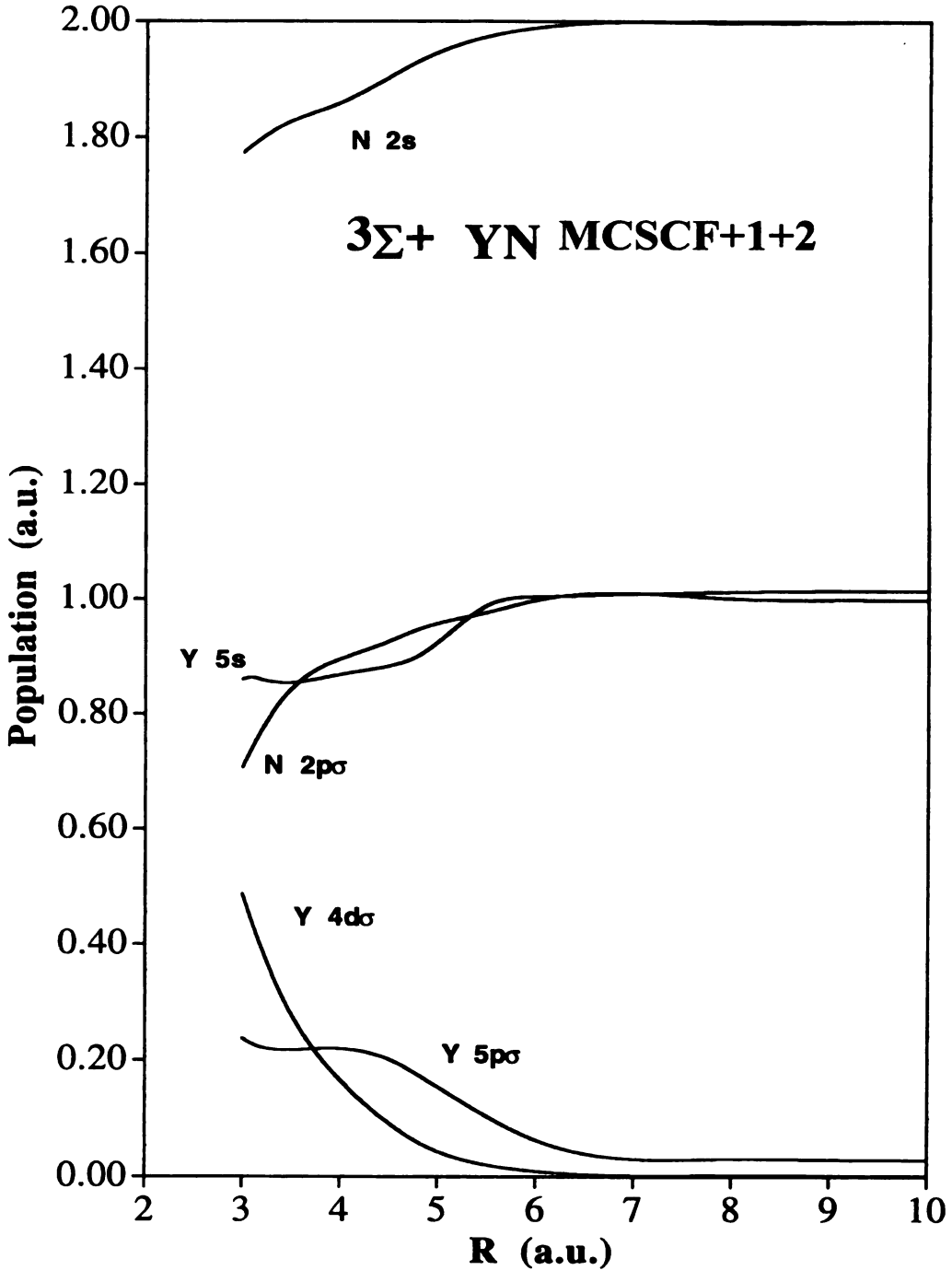

Figure 7c shows selected sigma symmetry orbitals taken from the natural orbitals of the first excited state of the YN molecule at the MCSCF+1+2 level.

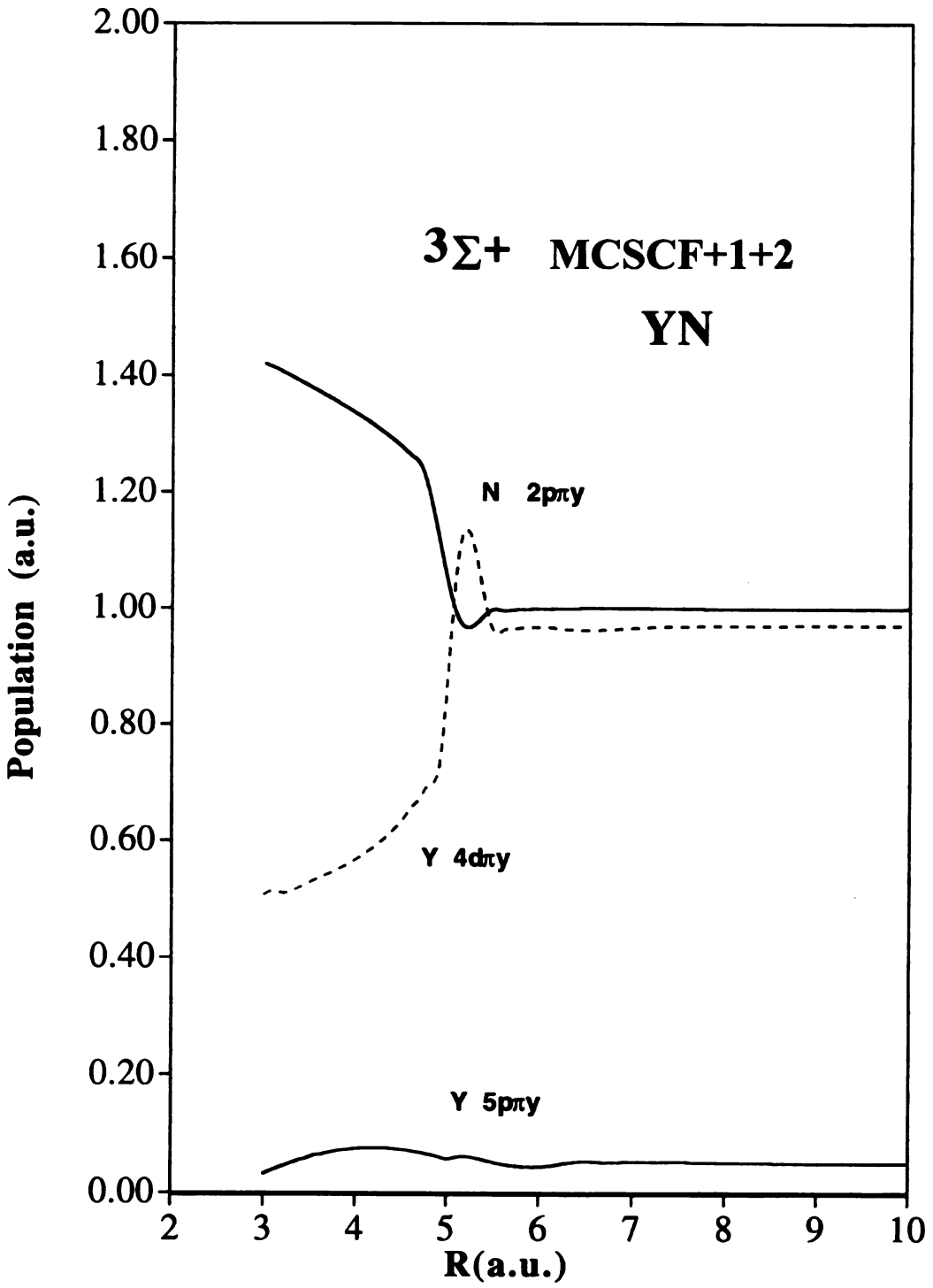

Figure 7d shows the population curves of selected pi symmetry orbitals from the natural orbitals of the first excited state of YN at the MCSCF+1+2 level.

YN and YP. The bond energies of YP were consistently greater than those of the same states of YN.

Another property that was examined was the dipole moment of the YP and YN diatomics. The scandium nitride and phosphide and the yttrium nitride and phosphide have similar valence structure, but the overall electronic structure does not translate to definite similarities in dipole moments.[1j,2i,2n-p,5a] Tables 9 and 10 report the dipole moments of YN and YP as calculated in this work, Table 9 also reports the dipole moments of ScN from the work of Harrison and Kunze.[1j] Comparison of the values of the dipole moments shows that the dipole moments of the various states of YP are 20-40% larger than the dipole moments of the corresponding states of YN, with the exception that the values of YN and YP are about the same for the ground state, $^1\Sigma^+$, and the dipole moment of the $^3\Pi_{\pi\pi}$ state of YP is about 50% larger than the corresponding state of YN.

Comparison to Experiment

The next logical comparison would be between experiment and theory, but unfortunately there are very few results to compare. Ram and Bernath have performed Fourier transform emission spectroscopy on YN in the gas phase. The bond length of the ground state, $^1\Sigma^+$, derived by Ram and Bernath [2r] (1.815 Å) was good agreement with our computed bond length (1.847Å). The bond length calculated by Shim and Gingerich [2j] (1.746Å) is in significant disagreement with these

Table 9. Dipole Moments (Debye) of YN.

State	GVB	GVB+1+2	MCSCF	MCSCF+1+2
$^1\Sigma^{+a}$	7.11	6.92	7.09	6.72
			(5.34)[b]	
$^3\Sigma^+$	3.60	3.79	3.53	3.68
			(2.46)	
$^3\Pi\ \sigma, \pi$	4.68	4.91	4.72	4.85
			(3.79)	
$^3\Pi\ \pi, \pi$	3.46	3.57	3.47	3.56
			(——)	
$^3\Delta$	8.31	7.97	8.31	7.97
			(9.38)	
$^1\Pi\ \sigma, \pi$	4.46	4.62	4.44	4.39
			(3.56)	
$^1\Delta$	8.26	7.97	8.26	7.97
			(9.22)	

[a]Shim and Gingerich report a dipole moment of 8.19 Debye[2j] for $^1\Sigma^+$ using a CASSCF with smaller basis set.
[b]Values in parenthesis are dipole moments of ScN from MCSCF wavefunctions of Harrison and Kunze[1j].

Table 10. Dipole Moments (Debye) of YP

State	GVB	GVB+1+2	MCSCF	MCSCF+1+2
$^1\Sigma^+$	6.22	7.04	6.28	7.09
$^3\Sigma^+$	4.31	4.80	4.30	4.81
$^3\Pi\ \sigma, \pi$	6.49	6.07	6.29	6.21
$^3\Pi\ \pi, \pi$	5.27	5.49	5.29	5.52
$^3\Delta$	9.83	9.56	9.83	9.57
$^1\Pi\ \sigma, \pi$	6.28	6.09	6.21	6.27
$^1\Delta$	10.9	10.6	9.81	9.57

results. In the work of Shim and Gingerich no effective core potentials were used and a smaller basis set was used on the nitrogen atom. Also our results are those of a multireference CI calculation, whereas their work is the result of calculations at the CASSCF level.

Conclusions

There are several conclusions that can be made from the work presented. First, the accuracy of the computational studies of the electronic structure of YN and YP depends greatly on the ability of the techniques to provide the proper correlation to describe the atomic states of the metal. The high level of correlation needed to discern the energetically close states of YN and YP is crucial. In comparison with calculations on ScN by Harrison *et al.*[1] the excited states of YN can be described with the same degree of precision at a lower level of theory than the MRCI.

Despite differences in the ordering of the low-lying states of Y and Sc, the nature of the bonding, character of the bonding, and the ordering of the lower energy states in the nitrides and phosphides of these two metals are the same. Also as seen in the metal hydrides, ScN, YN, and YP exhibit weak sigma bonding with the metal possessing largely $d\sigma$ character. Finally, the properties examined, bond length, bond energy, and dipole moment provide evidence of periodic trends, one of the goals of this work.

Future Work

The investigation of periodic trends in transition metal nitrides and phosphides is one of the goals of our future work. Extension of the results of this work to comparisons between VN and NbN, TiN and ZrN and the positive and dipositive ions of these compounds is planned. Also, comparisons can be made by replacing the nitrogen in the above diatomics with phosphorus. This would also result in an abundance of states and properties for comparison.

BIBLIOGRAPHY

BIBLIOGRAPHY

1. Publications in this series include: (a) Alvarado-Swaisgood, A. E.; Allison, J.; Harrison, J. F. J. Phys. Chem. 1985, 89, 2517. (b) Alvarado-Swaisgood, A. E.; Harrison, J. F. J. Phys. chem. 1985, 89, 5198. (c) Harrison, J. F. J. Phys. chem. 1986, 90, 3313. (d) Mavridis, A.; Alvarado-Swaisgood, A. E.; Harrison, J. F. J. Phys. Chem. 1986, 90, 2548. (e) Alvarado-swaisgood, A. E.; Harrison, J. F. J. Phys. Chem. 1988, 92, 2757. (f) Alvarado-Swaisgood, A. E.; Harrison, J. F. J. Phys. Chem. 1988, 92, 5896. (g) Alvarado-Swaisgood, A. E.; Harrison, J. F. 1988, 46, 155. (h) Harrison, J. F.; Kunze, K. L. Journal of Physical Chemistry 1989, 93, 2983.(I) Tientega, F.; Harrison, J. F. Chem. Phys. Letters, 1994, 223, 202. (j) (i) Harrison, J. F.; Kunze, K. L.. "Gas Phase Organomettaliic Chemistry", Freiser, B; Ed.; Kluwer Academic Publishers: Netherlands, 1995, Chapt. 2, 89-121.(j) Harrison, and Kunze, J. Am. Chem. Soc. Vol. 112, No. 10, 1990.

2. Publications of the theoretical groups: (a) Schilling, J. B.; Beauchamp, J. L.; Goddard, W. A., III; J. Am. Chem. Soc. 1987, 109, 4470. (b) Schilling, J. B.; Goddard, W. A., III; Beauchamp, J. L. J. Am. Chem. Soc. 1987, 109, 5573. (c) Schilling, J. B.; Beauchamp, J. L.; Goddard, W. A., III J. Am. Chem. Soc. 1987, 109, 5565. (d) Carter, E. A.; Goddard, W. A., III J. Am. Chem. Soc. 9186, 108, 2180, 4746. (e) Pettersson, L. G. M. ; Bauschlicher, Jr., C. W.; Langhoff, S. R.; Partridge, H. J. Chem. Phys. 1987, 87, 481. (f) Blomberg, M. R. A.; Siegbahn, P. E. M.; Backvall, J. E. J. Am. Chem. Soc. 1987, 109, 4450. (g) Siegbahn, P. E.; Blomberg, M. R. Chem. Phys. 1984, 87, 189. (h) Bauschlicher, C. W. Chem. Phys. Letters, 1983, 100, 515. (I) Allison, J. N.; Goddard, W. A. , III Chem. Phys. 1983, 81, 263. (j) Shim, I.; Gingerich, K. A. Int. J. Quant. Chem., 1993, 46, 145. (k) Gingerich, K. A. J. Chem. Phys. 1968, 49, 19. (l) Musaev, d. G.; Koga, N. ; Morokuma, K. J. Phys. Chem. 1993, 97, 4064. (m) Blomberg, R. A.; Siegbahn, P. E. M.; Svensson, Matts, Inorg. chem. 1993, 32, 4218. (n) Elkhattabi, S.; Daoudi, A.; Berthier, G.; Flament, J. P. 1997 to be published. (o) Harrison, J.F., J. Phys. Chem., 1996, 100, 3513.

3. Publications of experimental groups: (a) Elkind, J. L.; Armentrout, P. B. J. Chem. Phys. 1987, 86, 1868. (b) Sunderlin, L. ; Aristov, N.; Armentrout, P. B. J. Chem. Phys. 1987, 109, 78. (c) Aristov, N.; Armentrout,P. B. J. Phys. Chem. 1987, 91, 6178. (d) Reents, W. D.; Strobel, F.; Freas, R. B.; Wronka, J.; Ridge, D. P. J. Phys. Chem. 1985, 89, 5666. (e) Hettich, R. L.; Freiser, B. S. J. Am. Chem. Soc, 1987, 109, 3543. (f) Radecki, B. D.; Allison, J. Organometallics 1986, 5, 411. (g) McElvany, S. W.; Allison, J. Organometallics 1986, 5, 1219. (h) Hanratty, M. A.; Beauchamp, J. L.; Illies, A. J.; van Koppen, P.; Bowers, M. T. J. Am. Chem. Soc. 1988, 110, 1. (I) Schilling, J. L.; Beauchamp, J. L. J. Am. Chem. Soc. 1988, 110,

15. (j) Schilling, J. L.; Beauchamp, J. L. Organometallics 1988, 7, 194. (k) Tolbert, M. A.; Mandich, M. L.; Halle, L. F.; Beauchamp, J. L. J. Am. Chem. Soc. 1986, 108, 5675. (l) Kang, H.; Beauchamp, J. L. J. Am. Chem. Soc. 1986, 108, 5663. (m) Kang, H.; Beauchamp, J. L. J. Am. Chem. Soc. 1986, 108, 7502. (n) Lebrilla, C. B.; Schulze, C.; Schwarz, H. J. Am. Chem. Soc. 1987, 109, 98. (0) Lebrilla, C. B.; Drewello, T.; Schwarz, H. Int. J. Mass Spectrum. Ion Proc. 1987, 79, 287. (p) Schulze, C.; Schwarz, H. J. Am. Chem. Soc. 1988, 110, 67. (q) Stepnowski, R.; Allison, J. Organometallics, in press. (r) Bernath, P. F.; Ram, R. S. J. Mol. Spect. 1994, 165, 97.

3. Bernath, P. F.; Ram, R. S. J. Chem. Phys. 1992, 96, 6344.

5. Dunn, T. M.; Hanson, L. K.; Rubinson, K. A. Can. J. Phys. 1970, 48, 1657.

5a. Tientega, F.; Harrison, J. F. Chem. Phys. Letters, 1994, 223, 202.

6. Peter, S. L.; Dunn, T. M. J. Chem. Phys. 1989, 90, 5333.

7. Howard, J. C.; Conway, J. G. J. Chem. Phys. 1965, 43, 3055.

8. Dunn, T. M.; Roa, K. M. Nature 1969, 222, 266.

9. Bates, J. K.; Dunn, T. M. Can. J. Phys. 1976, 54, 1216.

10. Bates, J. K.; Gruen, D. M. J. Chem. Phys. 1979, 70, 4428.

11. Knight, L. B., Jr.: Steadman, J. J. Chem. Phys. 1982, 76, 3378.

12. Balasubramanian, K.; Das, K. K. J. Chem. Phys. 1990, 93, 6671.

13. Simard, B.; Balfour, J.; Vasseur, M.; Hackett, P. A. J. Chem. Phys. 1990, 93, 4481.

14. Lischka, H.; Shepard, R.; Brown, F. B.; Shavitt, I. Int. J. Quantum Chem., Quantum Chem. Symp. 1981, 15, 1991.

15. Botch, B. H.; Dunning, T. H.; Harrison, J. F.; J. Chem. Phys. 1981, 75, 3466.

16. a) Hay, P. J.; Wadt, W. R. J. Chem. Phys. 1986, 82, 5606.
b) Krauss, M.; Stevens, W. J., Ann. Rev. Phys. Chem., 1994, 34, 357.

17. Dunning, T. H. J. Chem. Phys. 1971, 55, 3958.

18. Langhoff, S. R.; Pettersson, L. G. M.; Bauschlicher, C. W. J. Chem. Phys. 1986, 86, 268.

19. Martin, R. L.; and Hay, P. J. J. Chem. Phys. 1981, 75, 4539.

20. Van Duijneveldt, F.B.; Research Report RJ 945, IBM, San Jose, California, December 10, 1971.

21. Moore, C. E. Atomic Energy Levels; National Standard Reference Data Series; National Bureau of Standards: Washington DC, 1971; Vol. I and II, Circular 35.

22. Mulliken, R. S. J. Chem. Phys. 1955, 23, 1833.

CHAPTER 3

AB-INITIO STUDIES OF THE SCANDIUM NITRIDE DIMER

INTRODUCTION

Work on the synthesis of metallic-nitride polymers has prompted the study of this unique class of compounds through ab-initio methods.[1,2] Computationally, the transition-metal nitrides have been studied in some detail.[3,4,11,12] In these studies the ScN molecule was found to possess a $^1\Sigma^+$ ground state with a $^3\Sigma^+$ state lying only about 7 kcal higher in energy. The triplet state comes about by decoupling the weak sigma bond in the singlet state, leaving a diradical with the two remaining π bonds. The relative ordering of the low lying states predicted by Harrison and Kunze agrees extremely well with experiment.[5,11] Coupling two of the diradicals leads to an alternating doubly-bonded dimer, with a lone electron found in the σ symmetry orbitals to the rear of the terminal Sc and N atoms. These lone electrons are left available to form additional bonds.

Ab-initio studies of transition-metal nitride dimers can serve as a tool to examine the electronic structure and nature of the bonding in systems that may be of importance in catalysis and surface chemistry. Also, these calculations can be used as a predictive tool in unraveling the reactivity of compounds. Along with these advantages, these

computational studies can provide an impetus for research in the area of mass spectroscopy, Fourier transform emission spectroscopy, and other areas of spectroscopy.[5]

Earlier work on the ScN molecule by Harrison and Kunze[3] predicted a $^1\Sigma^+$ ground state with a $^3\Sigma^+$ excited state, as mentioned above. The relative order of the low-lying states of ScN were later supported through emission spectroscopy experiments conducted by Bernath *et al.*[5] The closeness of the ground and first excited states of the ScN molecule suggests that the thermodynamically stable species, the $^3\Sigma^+$ state, is accessible for chemistry. Daoudi *et al* also examined the $^3\Sigma^+$ state for evidence of weak sigma bonding between monomers.[12] The ScN dimer was constructed by bringing two ScN molecules in the $^3\Sigma^+$ state together in a linear fashion, forming a sigma bond from two of the lone electrons, leaving two lone electrons on the terminal Sc and N atoms to propagate the linear chain, as shown in Figure 1.

Wavefunction Construction

The multiconfigurational self-consistent field (MCSCF) wavefunctions were constructed by correlating the sigma and pi bonds of the dimer with orbitals of proper symmetry. The sigma orbitals were correlated in (GVB) generalized valence bond fashion in order to allow the two monomers to separate to the proper SCF products. The wavefunction for the dimer was constructed with C_{2v} symmetry and there were a total of 37 configuration state functions. The ab-initio calculations on the ScN dimer were performed on Silicon Graphics IRIS^2 workstations in the Chemistry Department Visualization Center using the Columbus package.[6] The basis sets used were A. J. H.

Wachters' (14s11p6d)/[5s4p3d] on Sc and the (9s4p0/[3s2p] Dunning double zeta basis set (absent d-functions) on the N.[7,8] The d-functions were omitted for computational savings.

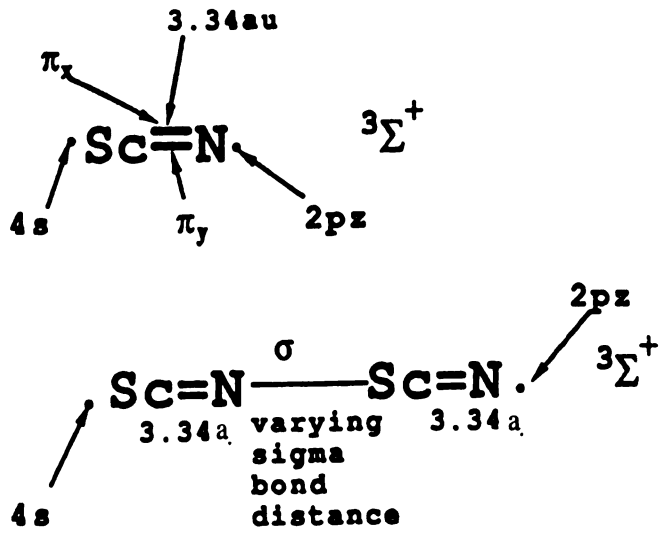

Figure 1. The geometries of the monomer and dimer of ScN in the triplet sigma plus state. The calculations were performed by varying the sigma bond distance of the dimer while maintaining a distance of 3.34 a. between the monomers, the equilibrium separation of the ScN molecule in the triple sigma plus state.

RESULTS

The potential energy curve for the scandium nitride dimer in the $^3\Sigma^+$ state generated from the wavefunctions is shown in Figure (2). Upon analysis of this potential curve there is evidence of two potential curves. At large separations, there is a sigma bond between the internal scandium and nitrogen, while nearer to the minima at shorter

bond lengths there exists an ionic interaction between the internal Sc and N. The calculations were performed by varying the intermonomer N-Sc distance shown in Figure 1, while maintaining the double π bond distances of the two monomers at the equilibrium internuclear separation of 3.34 a_o of the ScN molecule in the $^3\Sigma^+$ state. This bond length serves as a good starting point for the separation between the terminal and internal Sc and N atoms. The structure of the dimer with various double bond lengths can be examined in later work.

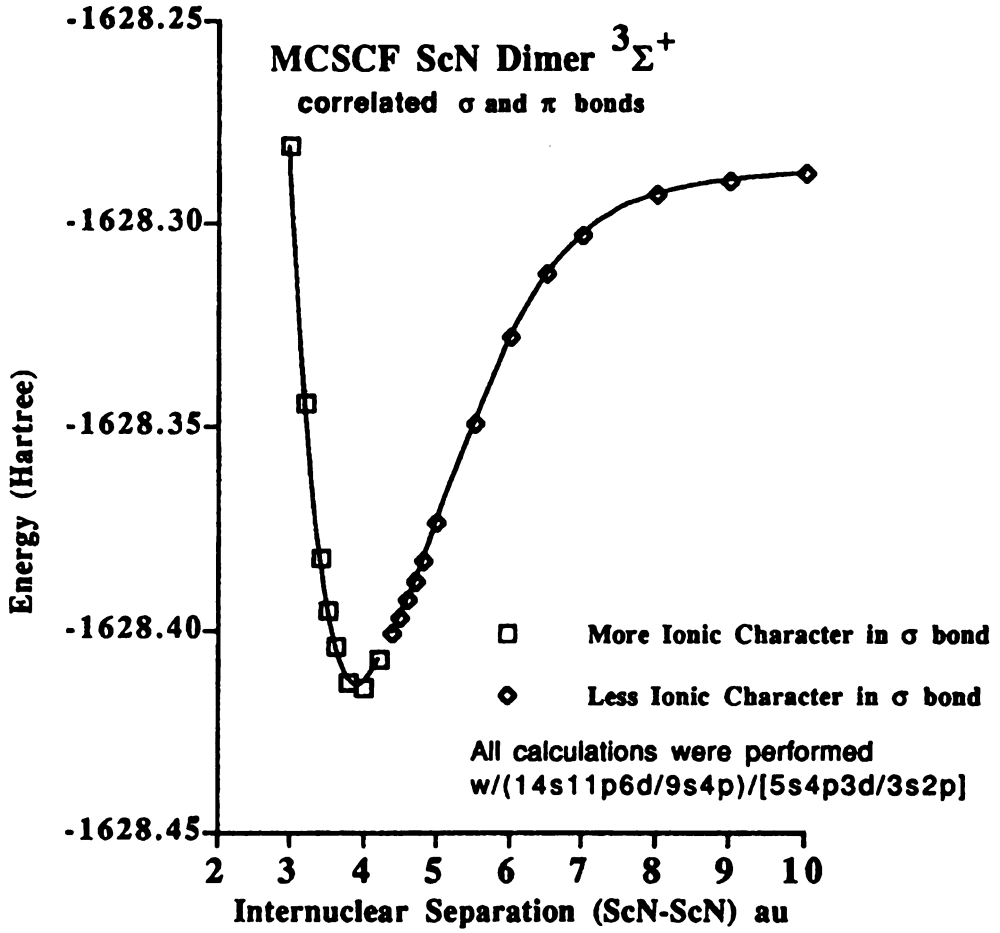

Figure 2. The potential curve of the ScN dimer in the $^3\Sigma^+$ state constructed from MCSCF wavefunctions at selected separations of N(2)-Sc(3). The single bond of σ symmetry was correlated in a GVB manner in order to insure that the two ScN monomers separate to the correct SCF products. The R_{eq} of the dimer is at about 4.0 au.

Charge Distribution and Population Analysis

In order to distinguish between the Sc and N atoms the individual atoms will be labeled one through four from left to right along the linear chain (i.e., Sc(1) N(2) Sc(3) N(4)) or referred to as an internal or terminal Sc or N, accordingly. Mulliken population analysis shows significant charge transfer, suggesting an electron transfer from the internal Sc to the internal N in the dimer. Figure 3 shows the charge on each of the Sc and N atoms at various sigma bond lengths on the potential curve shown in Figure 2. At 10 a_o of separation between the internal N and Sc the charge transfer is not apparent between the two internal atoms. At 5.0 a_o separation between the monomers there is a -0.74 charge on the internal N and +0.85 on the internal Sc atom. This signifies that a charge transfer of one electron has begun. With a further change in bondlength of 0.4 a_o the charge on the N(2) becomes -0.94 au. . The charge on the internal Sc(3) atom is at +0.88 atomic units at this point. This value decreases slightly as we go from 4.6 a_o separation between the monomers to 3.8 a_o separation in steps of 0.2 a_o. The change in the charge on the external Sc and N atoms is greatest going from 5.0 a_o separation to 4.6 a_o between the two monomers. The Sc(1) atom has a large charge change of -0.09 atomic units between 5.0 and 10.0 a_o separation between the two ScN monomers. The same atom experiences a charge change of positive 0.17 au. between 5.0 a_o and 4.6 a_o.

Figure (4) shows how the terminal Sc orbital populations decrease for the $3d_{xz}$ and $3d_{yz}$ orbitals, while the population remains relatively unchanged in the 4s orbital. As required by symmetry, the population of the $3d_{yz}$ orbital mirrors that of the $3d_{xz}$ orbital. The same thing occurs in the case of the p_y and p_x orbitals on N(2) and the d_π orbitals on

Sc(3). Therefore, only one of each pair will be displayed in the population plots that follow. Figure 5 shows that the internal nitrogen $2p_\sigma$ orbital population increases from about 0.89 to 1.4 au as the N(2)-Sc(3) internuclear separation decreases, while the $2p_x$ and the $2p_y$ orbitals exhibit small changes in population.

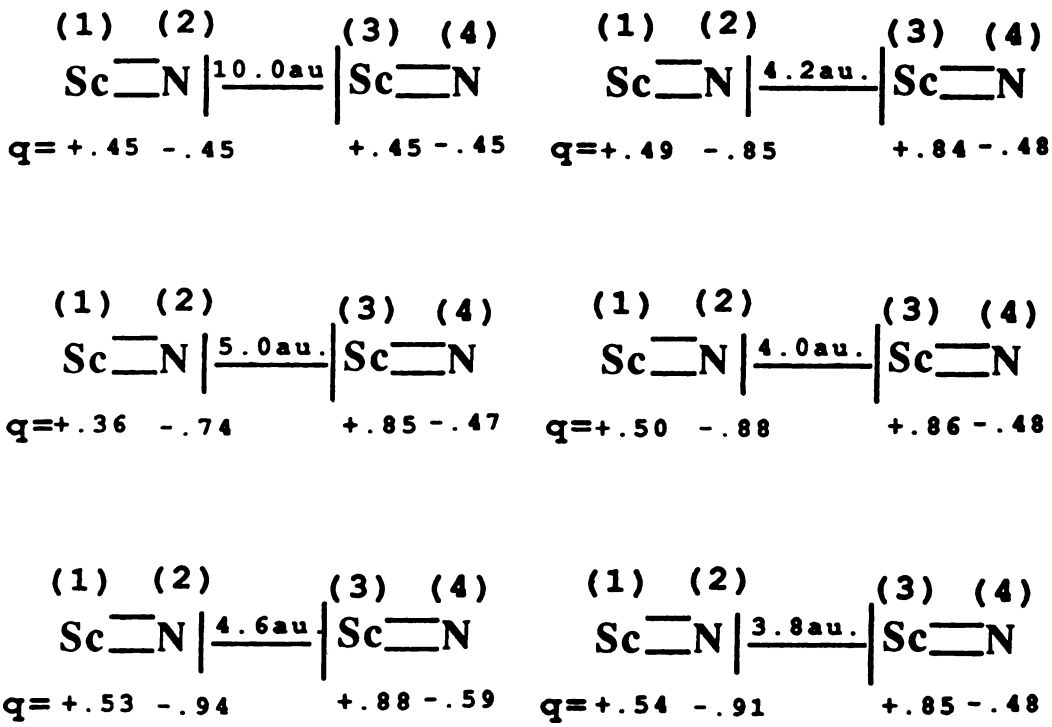

Figure 3. Total charge in atomic units is condensed to orbitals and summed on atoms from the valence electron population of the valence natural orbitals. Obtained from the MCSCF wavefunction of the ScN dimer at selected bond lengths.

The 2s orbital of N(2) decreases in population from about 1.9 to 1.75 (at 4.0 a_o) for the same change in monomer separation as shown in Figure (5). The internal Sc, Sc(3), gains population in the $3d_\sigma$, $3d_{xz}$ and $3d_{yz}$ orbitals.

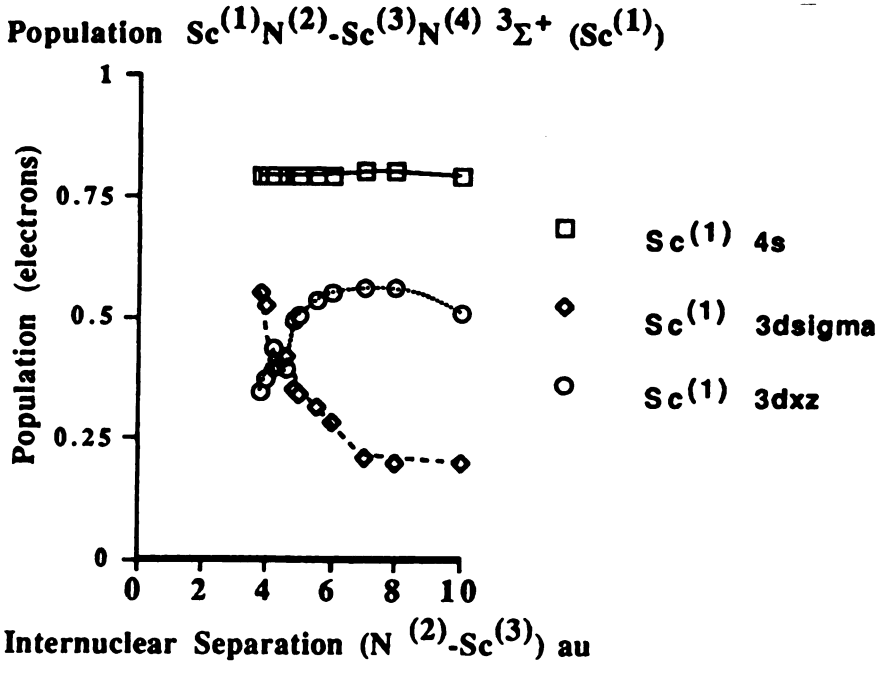

Figure 4. Total valence population of selected atomic orbitals of σ and π symmetry of Sc(1). Obtained from the valence natural orbitals of the MCSCF wavefunction. The R_{eq} is at about 4.0 au.

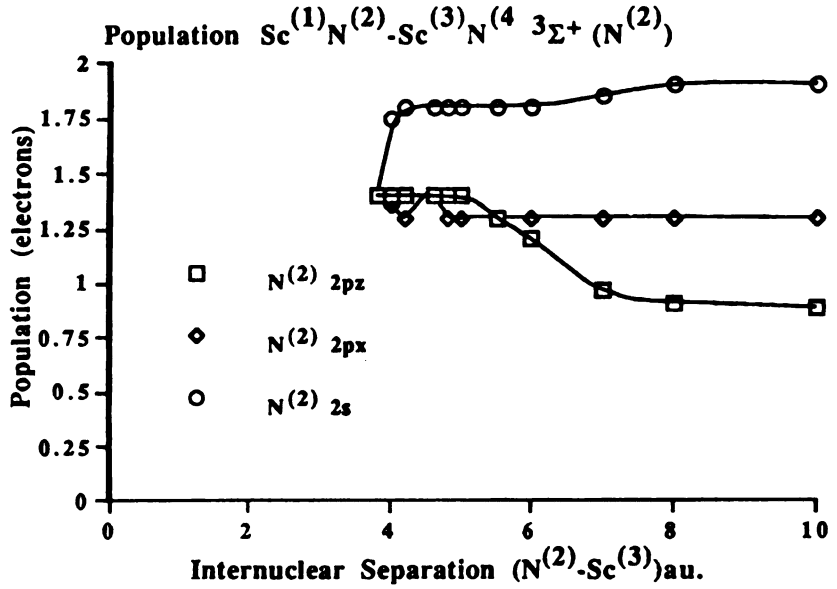

Figure 5. Total valence population of selected atomic orbitals of σ and π symmetry of N(2) Obtained from the valence natural orbitals of the MCSCF wavefunction. The R_{eq} of the dimer is at about 4.0 au.

However, there is a substantial decrease in the population of the 4s orbital of Sc(3) of about 0.65 electrons as shown in Figure (6). This large loss reflects the charge transfer coming from the 4s orbital. The terminal N atom, N(4), shows a variation in the charge on the atom as seen in Figure (3).

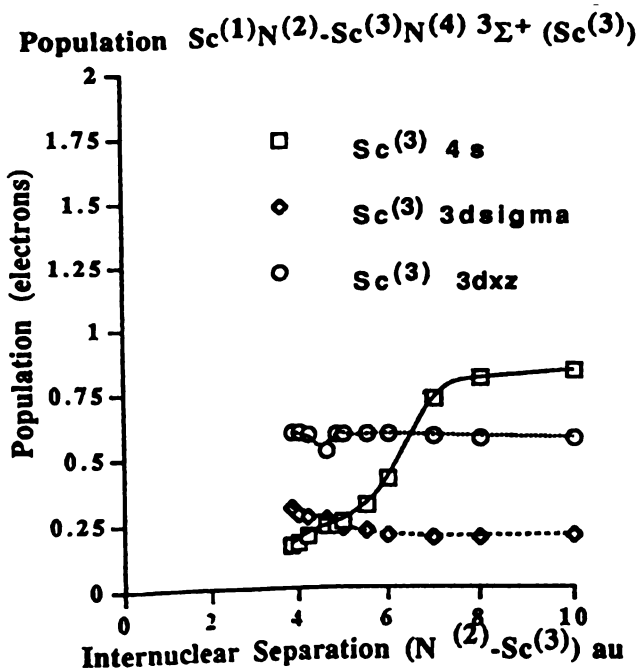

Figure 6. Total valence population of selected atomic orbitals of sigma and pi symmetry on Sc(3). Obtained from the valence natural orbitals of the MCSCF wavefunction. The equilbrium separation between the internal Sc and N atoms is about 4.0 au.

In all the population analysis shown, there exist sharp variations when the N(2) and Sc(3) atoms are separated about 4.4 a_o. This is the region of the potential curve, Figure 2, at which the charge transfer occurs or a curve crossing, as we go from the sigma bonded structure to the ionic species.

Discussion of Density Difference Contour and Mesh Plots

Density difference contours and mesh plots of the of the same density difference provide further evidence of charge transfer and possibly the formation of an internal dative sigma bond in the ScN monomer on the left. Figure 7 show this possible structure.

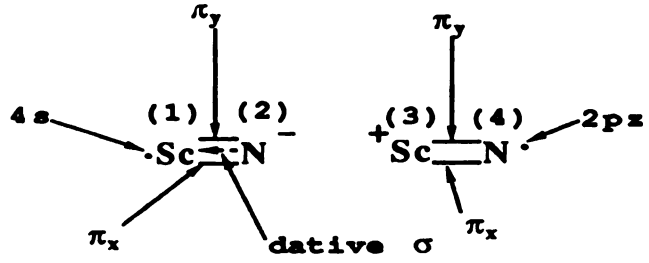

Figure 7. Possible structure of the ScN dimer in the triplet sigma plus state after electron transfer and formation of an internal dative bond between the internal N and external Sc atoms.

The density difference contours and mesh plots are constructed by subtracting the density of the two non-interacting ScN monomers in the $^3\Sigma^+$ state from the density of the dimer in the same state and appropriate geometry. Actually the plots and contours show where the electron density is coming from and going to during formation of the dimer in the $^3\Sigma^+$ state from the two non-interacting monomers in the same state.

The contour plots seen in Figures 8a-8d show gains in the electron density in the p_σ orbital of the internal, N(2) atom and to the rear of the Sc(1), external Sc atom. Also the p-π system of the Sc(1) experiences some increase in population as we bring the two ScN monomers together, whereas Sc(1) loses electron density in the dπ system. It appears that Sc(1) loses some electron density from the dπ bonds in order compensate for the gain in the sigma region. This suggests the formation of an internal dative sigma bond from N(2) to Sc(1). From Figures 5 and 6 it can be seen that the N(2) gains an electron from the 4s orbital of Sc(3). Although it may not be obvious from the contours presented, the most significant losses occur on the Sc(3) atom. The net differences that occur on the N(4) center appear not to be significant, possibly due to shifts and reorganization in the electron density due to polarization.

The density difference mesh plots seen in Figures 9a-9d show the same physical picture with a slightly different perspective. The grey regions lying in the plane bisecting the two spiked regions constitute zero change in the electron density. The spikes and raised regions above the plane depict positive differences (gains) in the electron density. The spikes below the plane and depressions display negative differences (losses) in

electron density. Inspection of the plots shows that there are more positive spikes than negative spikes. Since one would expect equivalent losses and gains, this is an artifact of large amounts of electron density lost from the diffuse 4s orbital of the internal Sc atom, which is too expansive relative to the other orbitals to appear in the plot.

Just as in the case of the contours, there exist major gains in the $p\sigma$ orbital of the internal N atom from the internal Sc atom. There also exist gains to the rear of the terminal Sc atom. This is also evidence of a dative sigma bond being formed between the terminal Sc and the internal N, as mentioned earlier. At 3.8 a_o the magnitude of the positive difference increases between these same centers. There seems to be a slight increase in the density to the rear of the terminal Sc atom as we squeeze the two monomers even closer. Also the plots depict larger losses on the terminal Sc atom. Indeed, at this geometry we have started back up the repulsive side of the potential well seen in Figure 2. The terminal N remains relatively unchanged.

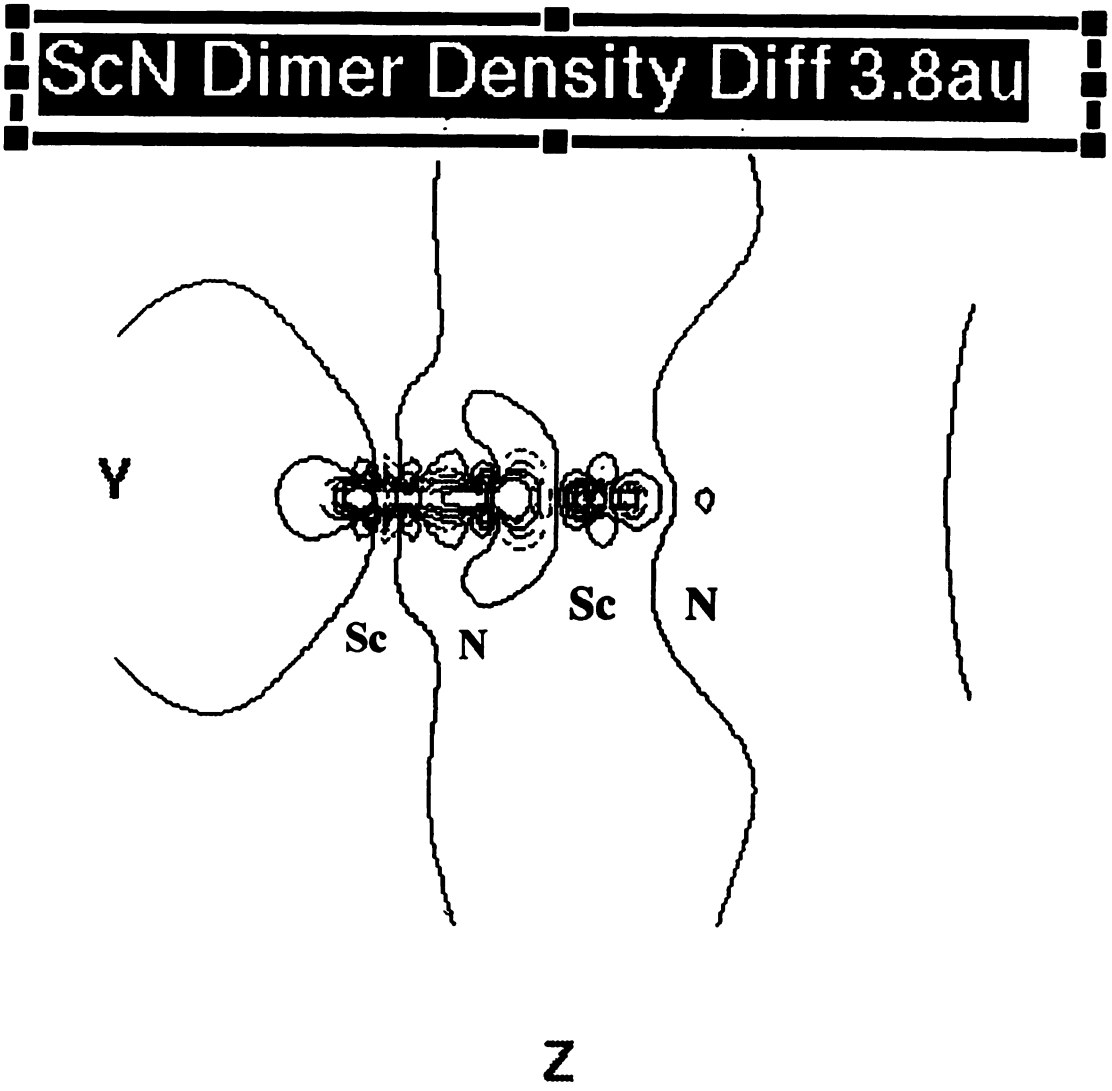

Figure 8a-8d show the electron density difference between two non-interacting ScN monomers in the $^3\Sigma^+$ state and the dimer in the same state at selected geometries. The broken lines depict significant increases in electron density. The solid lines depict significant losses in electron density. The contours range from 0.5 to –0.5 electrons/a_o^3 at separations of 3.8 a_o (stepsize of 0.1), 4.0 a_o (stepsize of 0.1), and 4.2 a_o (stepsize of 0.12). At 5.0 a_o the contour range is 0.05 to –0.05 with a step size of 0.01. All of the contour values and stepsizes were chosen in order to improve resolution. The large red balls denote the Sc atoms and the smaller balls denote the N atoms.

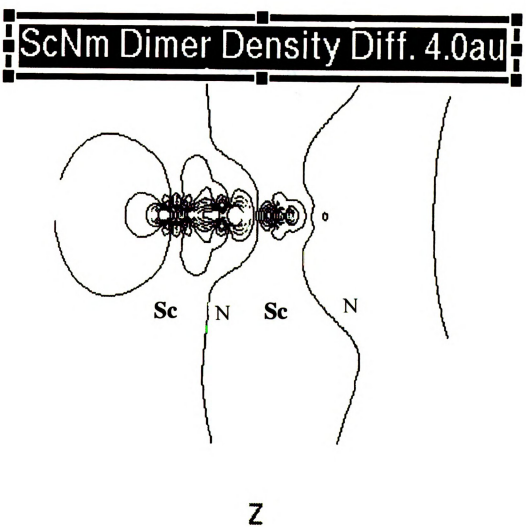

Figure 8b. Electron density difference contour plot at a selected geometry.

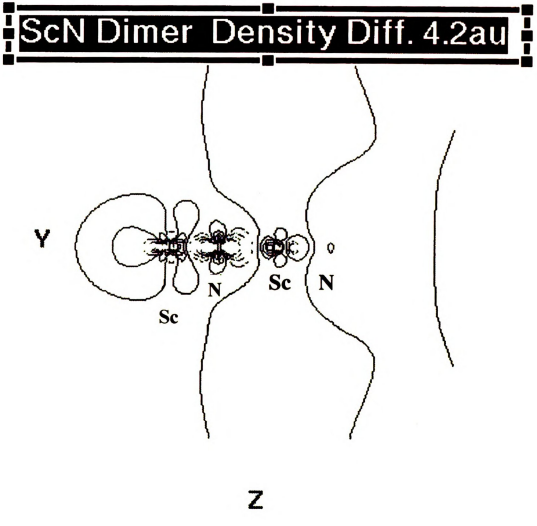

Figure 8c. Electron density difference contour plot at a selected geometry.

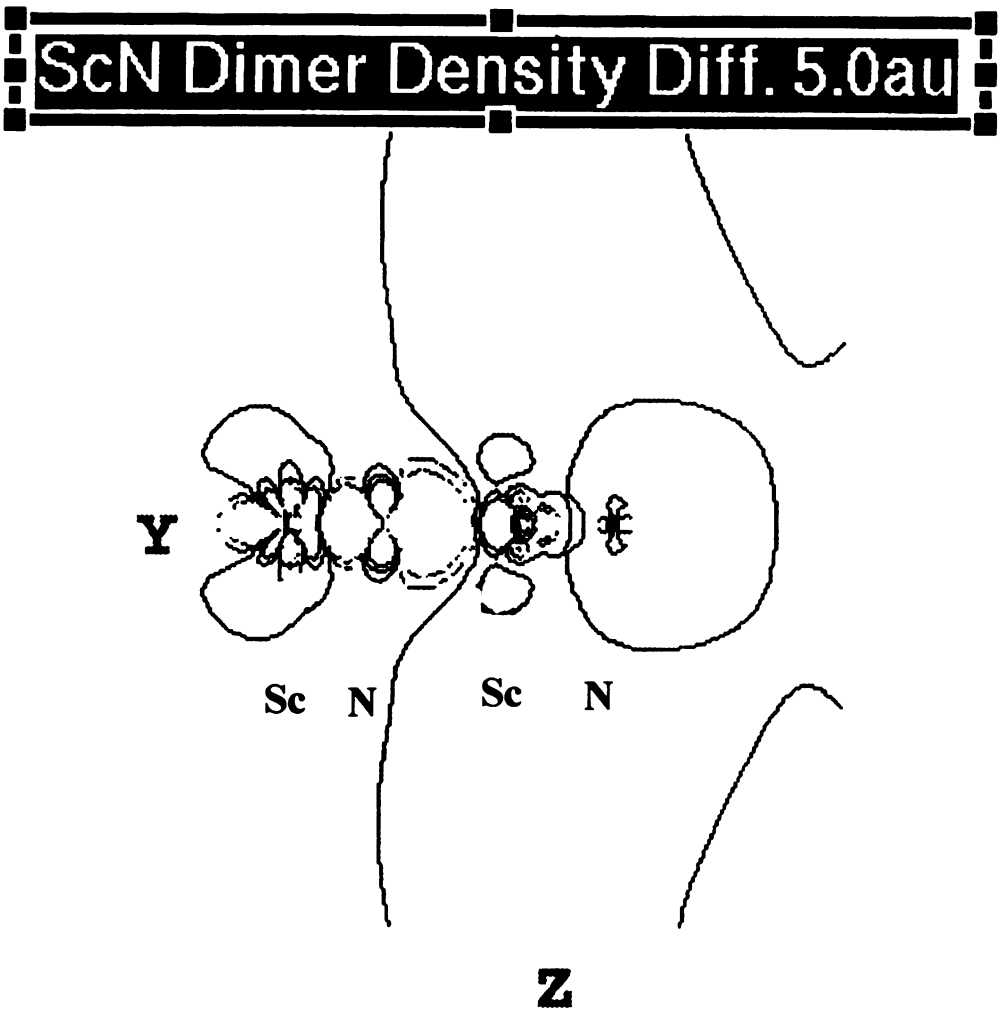

Figure 8d. Electron density difference contour plot at a selected geometry.

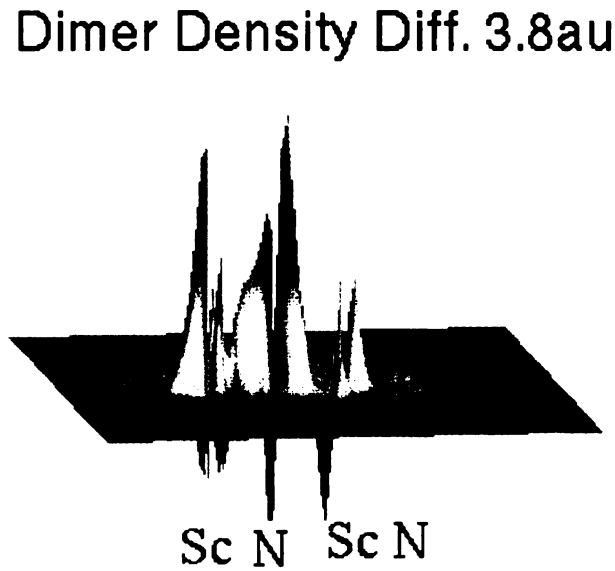

Figure 9a-9d show mesh plots of the electron density difference between two non-interacting ScN monomers in the $^3\Sigma^+$ state and dimer in the same state at selected geometries. The regions lying in the plane bisecting the two spiked regions constitute zero change in electron density. The spikes above the plane depict positive differences (gains) in electron density. The spikes below the plane depict negative differences (losses). The maximum and minimum values in electrons/a_o^3 for the density differences are as follows (separation between the internal Sc and N): -0.500, 0.886 (5.0a_o); -0.860, 1.116 (4.2a_o); -0.599, 1.123 (4.0a_o); -0.818, 1.241 (3.8a_o).

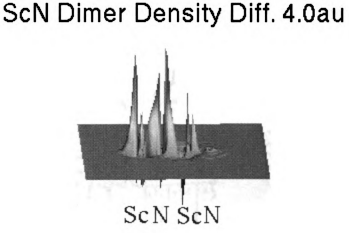

Figure 9b. Electron density difference mesh plot at a selected geometry.

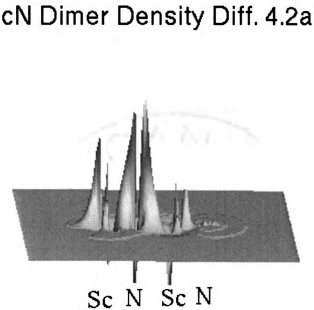

Figure 9c. Electron density difference mesh plot at a selected geometry.

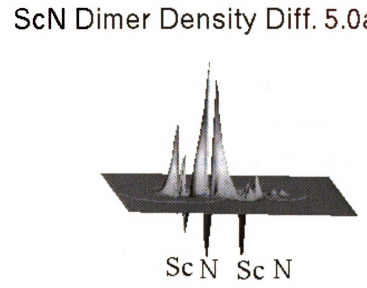

Figure 9d. Electron density difference mesh plot at a selected geometry.

At a separation of 4.0 a_o, there exists a state which effectively has the geometry of the $^2\Sigma^+$ ground state of the ScN^+ positive ion on the right experiencing an ionic interaction with a $^2\Sigma^+$ state of ScN anion on the left seen in Figure 7. This suggests that the ground state of the dimer may not be linear and might be indeed be cyclic.

Conclusions

Solid ScN has the same crystal structure as that of NaCl [5] and the cyclic structure shown in Figure 10 may be the dimer prelude to this crystal structure. In fact, Andrews has synthesized a dimer of ScN with a open rhombus structure.[11] The structure of this species is similar to that shown in Figure 10 with the open end of the rhombus possibly being the electrostatically interacting ends of the dimer shown in Figure 7.

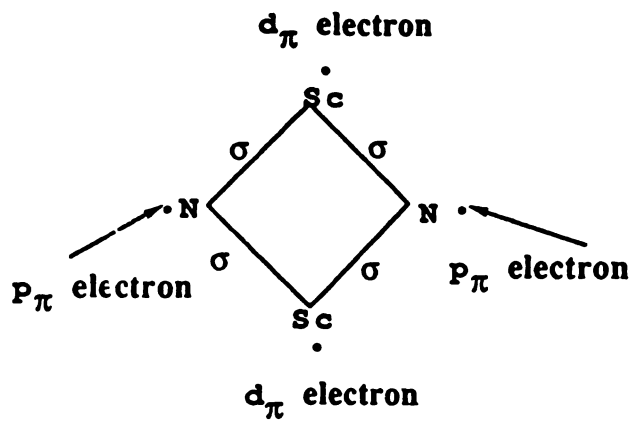

Figure 10. The proposed structure of the cyclic ScN dimer. The spin state for this structure is expected to be a triplet. The sigma bonds depicted in this structure are not necessarily equivalent.

BIBLIOGRAPHY

BIBLIOGRAPHY

1. C. M. Jones, M.E. Lerchen, C. J. Church, B. M. Schomber, and N. M. Doherty; Inorganic Chemistry 29, 1679 (1990).
2. S. C. Critchlow, M. E. Lerchen, R. C. Smith, N. M. Doherty, Journal of American Chemical Society 110, 8071 (1988).
3. J.F. Harrison, K.L. Kunze, Journal of Physical Chemistry 93, 2983 (1989).
4. J. F. Harrison, K.L. Kunze, Michigan State University, Department of Chemistry and Center of Fundamental Materials Research, to be published.
5. Bernath, P. F.; Ram, R. S.; J. Chemical Physics 1992, 9, 96.
6. R. Shepard, I. Shavitt, R. M. Pitzer, D. C. Comeau, M. Pepper, H. Lischka, P.G. Szalay, R. Ahlrichs, F. B. Brown, J. G. Zhao, International. J. Quantum Chemistry, 1988, S22, 149.
7. A. J. H. Wachters; J. Chemical Physics, 1970, 52, 1033.
8. T. H. Dunning; J. Chemical Physics, 1970, 53, 2823.
9. SciAn, Scientific Animation Package Version 0.853, Florida State University: E. Pepke, J. Murray, J. Lyons, and T Hwu., 1993.
10. AVS, Advanced Visualization Systems: Waltham, 1992.
11. Lester Andrews, Journal of Electronic Spectroscopy and Related Phenomena 97 (1998) 63-75.
12. A. Daoudi, and S. ElkHattabi Laboratoire de Chimie Theorique, Faculte des Sciences Dhar Mehraz, BP.; G. Berthier, Laboratoire de Radioastronomie Millimetrique, Ecole

Normale Superieure, France; J. P. Flament, Lavoratoire de Dynamique Moleculaire et Photonique, Universite USTL de Lille, France; submitted for publication.

CHAPTER 4

THE ELECTRONIC STRUCTURE AND VARIOUS PROPERTIES OF EARLY TRANSITION METAL METHYLIDYNES AND THEIR POSITIVE CATIONS

INTRODUCTION

The lack of experimental data on the gas-phase, biomolecular reactions of transition metals with main group elements has prompted a quantum chemical study of the transition metal methylidynes. There have been fairly extensive quantum chemical studies of the transition metal cations with various alkanes and other main group elements.[1, 2, 3] The prior work was prompted by an interest in understanding the chemistry of these transition metals bonding with main group elements as well as explaining the results of experimental studies of the gas-phase, bimolecular reactions of transition metal cations with alkanes and other main group elements. These studies have received impetus from developments in organometallic chemistry, surface chemistry, laser spectroscopy, and catalysis.[3, 4] In particular, reactions in which ions are involved can be studied by use of sophisticated mass spectroscopic techniques such as ion cyclotron resonance and guided ion beam mass spectrometry. The information obtained from these experiments has led to some understanding of the kinetic and thermochemical factors that allow these reactions to proceed. The neutral metal methylidynes have have been experimently observed, [32, 34] while the isoelectronic neutral metal nitrides, metal nitride cations, and transition metals bonded to other main group elements have been

studied previously.[3n-o, 4-13, 18] They have also been studied thoroughly by theoretical methods.[1, 2] The work reported here provides data to compare the properties and energies of these isoelectronic compounds.

Also, in the case of positive ions, the guided ion beam mass and the ion cyclotron resonance spectroscopic methods are used to study endothermic, as well as exothermic, reactions.[1a-c] The information gained can be applied to the analysis of the reactivity of C-H bonded systems with transition metals, reaction mechanisms, and surface reactions.

It is often difficult to experimentally determine the electronic and geometric structures of these species. This is the case for the positive ions, for while the data provide information on bond energies and reaction mechanisms, very little if anything can be said about the electronic and geometric structures. Mass spectrometers can only provide the mass ratios (m/z) of reactant and product ions.[3f,g,q] Most of the time, proposed structures are based on the structure of reactants, reactivity information, and chemical intuition about the reaction mechanism.[3q, 24] The possibilities are numerous for structural isomers, which increase with larger systems. By contrast, the necessary properties like bond lengths, bond angles, electron distributions, character of the bonding, etc., can be calculated through the use of ab-initio quantum mechanical techniques.[35]

Recent advances in the level of sophistication of electronic structure theory and its implementation in modern programs and the substantial increase in speed and accessibility of computers make it possible to study these important molecules computationally. The large number of closely spaced energy levels, the near degeneracy of ns-np shells, as well as other shells, and the importance of including or not including particular core orbitals in the correlation when working with the early transition metals,

and the as yet poorly understood relativistic effects of heavy atoms raise the required level of theory significantly. Work to date[8a, 9a, 15] suggests that an adequate description of the electronic structure of a first row transition element or a small molecule containing a transition element can be constructed using a multiconfigurational self-Consistent field (MCSCF) wavefunction. The MCSCF wavefunction often provides the proper correlation necessary to describe the molecule or atom effectively, and higher levels of theory that provide additional correlation, such as the configuration interaction technique, can be used when necessary.

In this work we will also explore the use of density functional theory to calculate the wavefunction for the ground and selected excited states. These wavefunctions are then used to calculate vibrational frequencies of these species at the equilibrium geometries. The density functional calculations used the Becke-3LYP functional, which has been used in related work on transition metals bonded to CH_2.[28] This functional should provide the proper correlation and exchange energies to give good geometry and vibrational frequencies.

The calculations presented in this work contain a large number of configuration state functions at the MCSCF level. Compared to the previous theoretical calculations performed on the positive ions of the transition metal methylidyne or corresponding methylidene, our MCSCF reference spaces are just as large as the Swaisgood and Harrison [1d] multireference configuration interaction spaces.

This work will permit a comparison between a neutral transition metal bonded to CH and the positive ion of the same molecule. Also, the positive ion and neutral molecule will be compared to the isoelectronic metal nitride cation and neutral metal

nitride, respectively. The effect of including the near degeneracy in these calculations will be discussed, including the possible necessity of higher levels of theory than the MCSCF level of theory. Along with these results, bond lengths, vibrational frequencies, energies, dipole moments, the nature of the bonding and the populations will be discussed. Descriptions of the wavefunctions, and possible transition metal-CH fragment bonding will be provided .

BASIS SETS AND MOLECULAR CODES

The primary basis sets used for transition metal atoms in the (TM)-CH (Sc,Ti,V, or Cr atom bonded to the CH) molecules are the Watchers' basis sets modified under scheme number 3, [15] using diffuse functions found in the work of Bauschlicher *et. al* in their calculations of (TM)CH_2^+ (Sc,Ti,V, or Cr atom bonded to CH_2^+) using Becke-3LYP density functional. However, we did not follow the same procedure for Sc and Ti in these calculations. It was felt that the inner shell correlation provided by using the scandium and titanium basis sets were not necessary because we were not going to be calculating bond energies. Instead, we followed the scheme (shown below) of the later early transition metals of vanadium and chromium in our Becke-3LYP calculations of these (TM)-CH systems.

To the Watchers' basis sets two diffuse p-functions were added; the exponents were those optimized by Watchers multiplied by 1.5. The d space was contracted in a (311) fashion. Then a diffuse d function[19] and three term fit to a Slater type f polarization function were

added to each metal atom. The f exponents vary from 1.6 for Sc to 4.8 for Cu in steps of 0.4 and are uncontracted. The f functions are constructed according to the paper by Stewart.[19a] The final basis sets of the metals had the contraction scheme:

(14s11p6d3f)/[8s6p4d2f]

because of the (3312) contraction of the p space maintained in all of the transition metal atoms. These basis sets will be referred to as the AWACH basis sets.[14] The C and H atoms used a 6-31G** basis set [23] in the DFT calculations.

The RHF, MCSCF, and MCSCF+1+2, and DFT calculations used the same AWACH basis set on the transition metal atoms. The C and H basis sets used in the RHF, MCSCF, and MRCI calculations were the Dunning augmented valence contracted quadruple-zeta basis sets with s, p, d-functions (on carbon atom). [33] However; the change in basis on these two atoms should be negligible, between the DFT and the other ab-initio methods used.

The DFT and frequency calculations were carried out using GAUSSIAN94[29] while the restricted Hartree-Fock, multiconfigurational self-consistent field, and multireference configuration interaction calculations used the MOLPRO96[20] set of codes. The calculations were performed on Silicon Graphics Indigo2 Workstations, supported by the Michigan State University Chemistry Department.

Another basis was also used in calculating wavefunctions and properties of the TiCH ground state, $^2\Sigma^+$, and the two excited states $^2\Delta$, $^2\Pi_{linear}$, and $^2\Pi_{bent\text{-}170^0}$ using MCSCF and MRCI techniques. This basis set is referred to as the AMES basis set.[31] It was developed by Partridge *et. al* and consists of (20s12p9d7f)/[7s6p5d2f]. This basis set is extremely large and proved to be computationally expensive.

MOLECULAR FRAGMENTS

Bond energies and separated fragments of the (TM)-CH and the positive ion were not calculated. However, the possible combination of fragments for the particular state of interest can be predicted by using spin and symmetry considerations and the bonding in the resulting molecule. We will focus this discussion on the ground states of ScCH, TiCH, VCH, and CrCH and their positive ions. Note that we label the $3d_{x^2-y^2}$ and $3d_{xy}$ orbitals on the TM as δ_+ and δ_- with the $3d_{z^2}$, $3d_{xz}$, $3d_{yz}$ represented as d_σ, $d_{\pi x}$, and $d_{\pi y}$, respectively.

First, the ScCH molecule has a unique bonding structure that arises from the $4s^13d^2$ configuration on the Sc atom. The CH fragment could be in a $^4\Sigma^-$ state or a $^2\Pi$ state if the Sc atom is in the ^2D or ^4F state, respectively. The $^3\Pi$ state of the ScCH molecule consists of a d_π-p_π bond between the Sc and C atoms with a lone electron in a hybrid orbital of the 4s of Sc and p and d sigma orbitals on Sc. The C atom forms a dative sigma bond with Sc and another sigma bond with the hydrogen atom. The remaining electron forms a one electron π bond significantly polarized toward carbon, suggesting that the *in situ* state of CH is $^2\Pi$.

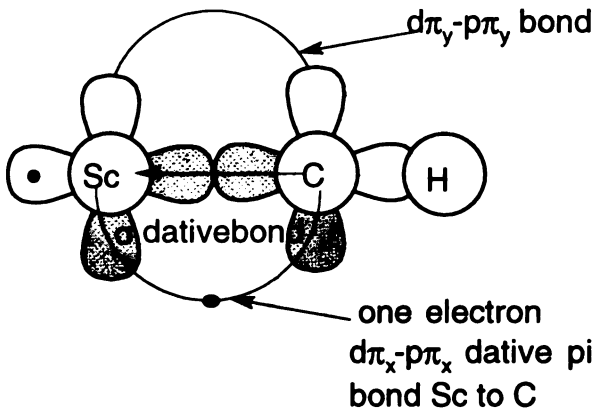

The positive ion, $ScCH^+$ has a ground state of $^2\Pi$. In this molecule the lone electron in the Sc 4s orbital of ScCH is removed to make the cation. Once again, dative sigma bonds and dative one electron pi bonds are made between the Sc and C, just as the case of the neutral compound.

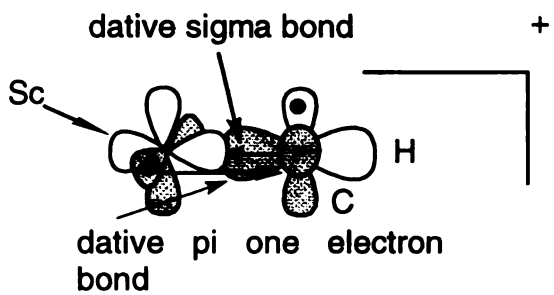

In the TiCH molecule the ground state is $^2\Sigma^+$ which results from the $4s^13d^3$ configuration on the Ti atom. The CH fragment would have to bond with titanium in a

$^4\Sigma^-$ state in order to form two pi bonds and one sigma bond; leaving a lone electron in the 4s orbital of titanium.

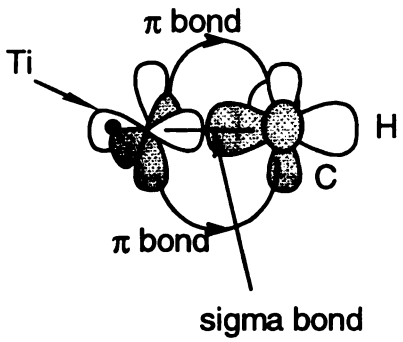

The $TiCH^+$ molecule is formed in the $^1\Sigma^+$ ground state by removing an electron from the 4s orbital of the titanium atom, leaving the two π bonds and one sigma bond between the Ti and C atoms intact.

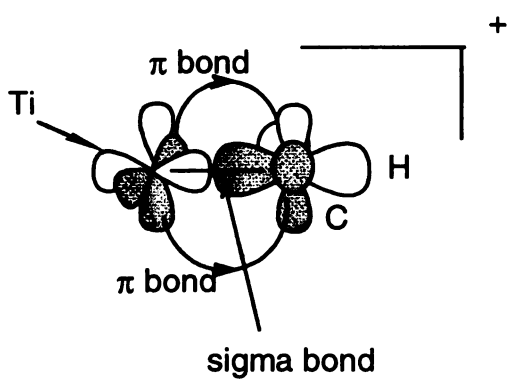

The VCH molecule has a just slightly shorter separation between the metal and C atoms than the TiCH molecule, and a structure that is similar to that of TiCH with vanadium's

extra electron in a δ_- orbital forming a $^3\Delta$ ground state. This results in a molecule with a triple bond between the vanadium and the C atoms.

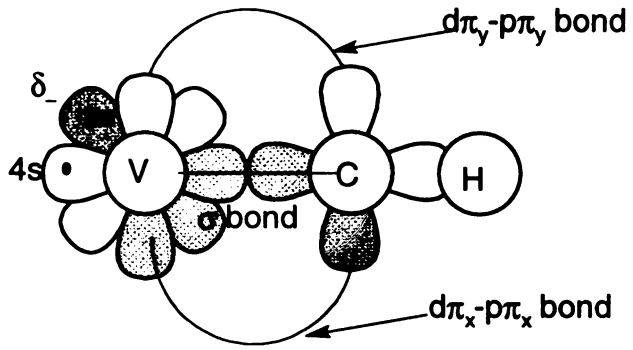

The VCH^+ molecule is the same structure as the VCH molecule absent the electron in the 4s orbital.

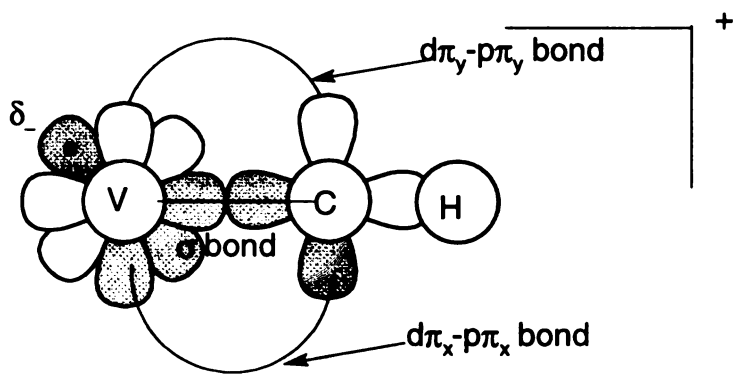

Note that both the electronic states of the VCH^+ and $TiCH^+$, $^2\Delta$ and $^1\Sigma^+$, correlate with the transition metal ion in its ground electronic state. In these molecular states the V^+ atom is in d^4 configuration and the Ti^+ atom is in a sd^2 configuration, respectively.[7a]

These configurations produce the atomic states ^5D and ^4F, respectively.[7a] The CH fragment exists *in situ* in the excited $^4\Sigma^-$ state.

The CrCH molecule consists of a Cr atom with a s^1d^5 configuration and the CH fragment once again in the $^4\Sigma^-$ state. Chromium in the $CrCH^+$ molecule exists in the d^5 configuration bonded to the CH fragment.

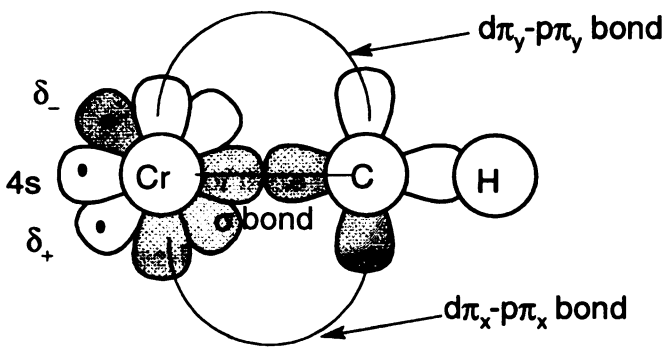

Shown above is the schematic representation of the CrCH molecule. The representation of the $CrCH^+$ molecule is shown below.

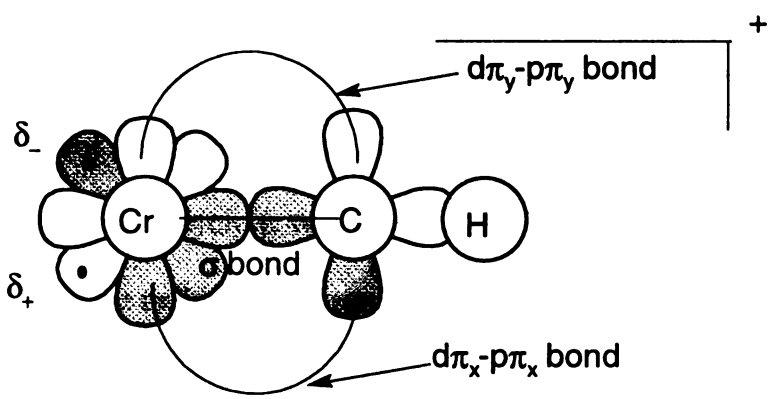

The ground state configurations for the Cr atom and the Cr^+ ion are the ^7S and ^6S, respectively.[8a, 15]

Wavefunctions and Computational Details

The wavefunctions for all of these molecules were constructed in a similar fashion. The restricted Hartree-Fock wavefunction was used as an initial guess for the positive ion of the carbyne at the MCSCF level; on most occasions only the sigma and pi bonds were correlated with orbitals of the corresponding symmetry. This was done in a generalized valence bond fashion; one sigma bonding orbital at a time or pair of pi bonding orbitals at a time. In this way the wavefunction was built up slowly until an electron was added back into the wavefunction and the corresponding carbyne was constructed. Later calculations added an additional orbital of a_1 symmetry to the correlation in each of the MCSCF calculations. In this way some of the near degeneracy was taken into account. Therefore, two sets of MCSCF calculations were used as reference spaces for the multireference configuration interaction calculations that followed. One set of calculations accounted for some of the near degeneracy in the correlation and the other set neglected the additional orbital in the sigma space. The

following are the wavefunctions for the carbynes and the positive cations in the generalized valence bond fashion:

$CrCH\ ^4\Sigma^- \sim [\sigma(Cr)\sigma(C)+\sigma(C)\sigma(Cr)]\ [\pi_x(Cr)\pi_x(C)+\pi_x(C)\pi_x(Cr)]$

$[\pi_y(Cr)\pi_y(C)+\pi_y(C)\pi_y(Cr)]3d_{\delta-}3d_{\delta+}4s$

$VCH\ ^3\Delta \sim\ [\sigma(V)\sigma(C)+\sigma(C)\sigma(V)]\ [\pi_x(V)\pi_x(C)+\pi_x(C)\pi_x(V)]$

$[\pi_y(V)\pi_y(C)+\pi_y(C)\pi_y(V)]3d_{\delta-}4s$

$TiCH\ ^2\Sigma^+ \sim [\sigma(Ti)\sigma(C)+\sigma(C)\sigma(Ti)]\ [\pi_x(Cr)\pi_x(C)+\pi_x(C)\pi_x(Cr)]$

$[\pi_y(Ti)\pi_y(C)+\pi_y(C)\pi_y(Ti)]4s$

$ScCH\ ^3\Pi \sim [\sigma(Sc)\sigma(C)+\sigma(C)\sigma(Sc)]\ [\pi_y(Sc)\pi_y(C)+\pi_y(C)\pi_y(Sc)]^1 4s2p_{\pi x}$

$CrCH^+\ ^3\Sigma^- \sim [\sigma(Cr)\sigma(C)+\sigma(C)\sigma(Cr)]\ [\pi_x(Cr)\pi_x(C)+\pi_x(C)\pi_x(Cr)]$

$[\pi_y(Cr)\pi_y(C)+\pi_y(C)\pi_y(Cr)]3d_{\delta-}3d_{\delta+}$

$VCH^+\ ^2\Delta \sim\ [\sigma(V)\sigma(C)+\sigma(C)\sigma(V)]\ [\pi_x(V)\pi_x(C)+\pi_x(C)\pi_x(V)]$

$[\pi_y(V)\pi_y(C)+\pi_y(C)\pi_y(V)]3d_{\delta-}$

$TiCH^+ {}^1\Sigma^+ \sim [\sigma(Ti)\sigma(C)+\sigma(C)\sigma(Ti)]\ [\pi_x(Ti)\pi_x(C)+\pi_x(C)\pi_x(Ti)]$

$[\pi_y(Ti)\pi_y(C)+\pi_y(C)\pi_y(Ti)]$

$ScCH^+ {}^2\Pi \sim [\sigma(Sc)\sigma(C)+\sigma(C)\sigma(Sc)]\ [\pi_y(Sc)\pi_y(C)+\pi_y(C)\pi_y(Sc)]^1 2p_{\pi x}$

Also presented are two excited states of TiCH, and two excited states of VCH. The excited state wavefunctions are represented in the GVB fashion as such:

$TiCH\ {}^2\Delta \sim [\sigma(Ti)\sigma(C)+\sigma(C)\sigma(Ti)]\ [\pi_x(Ti)\pi_x(C)+\pi_x(C)\pi_x(Ti)]$

$[\pi_y(Ti)\pi_y(C)+\pi_y(C)\pi_y(Ti)]3d_{\delta-}$

$TiCH\ {}^2\Pi_{linear} \sim [\sigma(Ti)\sigma(C)+\sigma(C)\sigma(Ti)]\ [\pi_x(Ti)\pi_x(C)+\pi_x(C)\pi_x(Ti)]$

$[\pi_y(Ti)\pi_y(C)+\pi_y(C)\pi_y(Ti)]4p_{\pi y}$

$VCH\ {}^3\phi_{\delta-,\pi} \sim\ [\sigma(V)\sigma(C)+\sigma(C)\sigma(V)]\ [\pi_x(V)\pi_x(C)+\pi_x(C)\pi_x(V)]$

$[\pi_y(V)\pi_y(C)+\pi_y(C)\pi_y(V)]3d_{\delta-}4p_{\pi}$

$VCH\ {}^3\Pi \sim\ [\sigma(V)\sigma(C)+\sigma(C)\sigma(V)]\ [\pi_x(V)\pi_x(C)+\pi_x(C)\pi_x(V)]$

$[\pi_y(V)\pi_y(C)+\pi_y(C)\pi_y(V)]4s4p_{\pi}$

Results and Discussion

The following will provide structural information on the carbynes and their cations and a comparison between the metal nitrides[1j] and corresponding metal nitride cations[1h]. Also, previous work by Alvarado-Swaisgood and Harrison[1d] will be compared. This previous work consists of MCSCF, and MCSCF+1+2 calculations with fewer configuration state functions and, therefore, smaller reference spaces than the present calculations.

Contour plots[27] of the electron density of selected natural orbitals will be presented. [25, 26] The contour plots were constructed by using positive and negative contour values of 0.02, 0.04, 0.08, 0.16, 0.32, and 0.64 au. The positive contours are solid lines, while the negative contours are dashed lines. The nodes are depicted by dotted lines. Occupations and populations condensed to basis function groups for the each of the natural orbital (NO) contour plots are also presented. The occupations and populations presented on the contour plots are calculated using the MSU properties program developed by Harrison.[26] The populations presented in the tables are from the Mulliken population[22] program of the MOLPRO96 [20] suite of codes.

The following methods are listed in the tables: RHF, MCSCF, and Configuration Interaction. The configuration interaction calculations refer to a MRCI calculation in each case. The MCSCF wavefunctions refer to wavefunctions constructed in a GVB fashion. Several of the tables will point out that an extra a_1 symmetry orbital was added to the correlation of the MCSCF wavefunction.

ScCH and $ScCH^+$

The first of the TM-CH series is ScCH, which has a $^3\Pi$ state. It offers a unique structure and corresponding geometry. The Sc-C bondlength is 1.954 Å at the multireference configuration interaction level (MRCI) (Table 1). The relatively long bond length is attributed to the double bond between the Sc and C atoms, rather than the triple bond found in the other TM-CH molecules. The Sc-C bondlength obtained from a DFT calculation is 1.892 Å. The dipole moment from the DFT calculation is 2.79 Debye (metal end positive), while that from the MRCI calculation is 2.18 Debye. The MCSCF calculation predicts a much longer bondlength of 1.996 Å with a dipole moment of 1.83 Debye (Table 1).

Removing a 4s electron from Sc in ScCH produces the $^2\Pi$ state of $ScCH^+$. The $^2\Pi$ state of $ScCH^+$ has a shorter Sc-C bond than that of the $^3\Pi$ state of ScCH as shown in Table 2. Also, the C-H bond length shortens to a length of 1.089 Å, comparable to the C-H bondlengths in the other early TM-CH molecules. Swaisgood and Harrison [1d] predicted a Sc-C bondlength of 1.940 Å and a C-H bondlength of 1.082 Å for the $^2\Pi$ state of $ScCH^+$ at the MRCI level.

The ScCH molecule is isoelectronic with ScN. The ScCH molecule in the ground state has a much longer bondlength than the other early TM-CH molecules. This is also the case for ScN when compared with the other transition metal nitrides. In fact, early work suggests a weak sigma bond in the triply bonded ScN [1j]; and the existence of a

doubly-bonded low-lying excited state. The calculated dipole moment of ScN is 6.04 Debye[1j] while that of ScCH is 2.18 (metal end positive).

$ScCH^+$ is isoelectronic with ScN^+. Comparing the $^2\Pi$ ground state of $ScCH^+$ to the ground state, $^2\Sigma^+$, of ScN^+, the transition metal nitride cation is reported to have a double bond and a lone electron in the sigma system of the Nitrogen atom.[1h] The $ScCH^+$ molecule also has a double bond, but places the lone electron in the π system of the carbon atom. The $^2\Sigma^+$ state of ScN^+ has a longer bond length of 1.804 Å relative to the Sc-C separation in the $ScCH^+$.

The energies of the ScCH $^3\Pi$ state at the MCSCF level are reported for two different wavefunctions in Table 1. The energy difference between the two wavefunctions is about 8mH and the optimized geometries are almost identical. At the MRCI level the differences are even smaller using these two wavefunctions as references.

The extra flexability provided by including another a_1 symmetry orbital in the correlation is important in describing the separation of the ground and excited states of TiCH described later in this chapter.

For ScCH, Tables 1 and 2 provide a comparison between the $^3\Pi$ state of the neutral molecule and the positive cation in the $^2\Pi$ state, with a energy difference of 213 mH. The MCSCF wavefunction (Table 1 and Table 2) have a difference in energy of 204 mH. The vibrational frequencies of the ScCH and $ScCH^+$ are given in Tables 7 and Table 8. The antisymmetric bending modes lend support to a lone electron in the π_x system of the C atom.

The contour plots of ScCH in the $^3\Pi$ state are in Figures 1-8. First the C-H sigma bonding natural orbital (NO) 7 shows a C s-p hybrid bonded to H s orbital (Figure 1). This orbital contour plot of C-H is typical of all of the C-H σ bonds in the early TM-CH molecules; therefore, this particular contour and that of $ScCH^+$ NO 7 , Figure 8, will serve as a reference to all of the other C-H bonding orbitals of this class of compounds. The contour plot of NO 8 (Figure 2) shows a dative sigma bond between the Sc and C atoms. The Sc spd hybrid follows in NO 9 (Figure 3) a sigma antibonding orbital. Natural orbital 11 (Figure 5) is the Sc-C σ antibonding orbital. Figure 6 shows a one electron dative π bond between Sc $\Rightarrow$ C. Swaisgood *et al*[1d] also found a dative sigma bond and one electron π bond in $ScCH^+$. This is also shown in the $ScCH^+$ contour plot of NO 23 in Figure 13 from this work. The bonding π_y orbitals of ScCH and $ScCH^+$ are shown in Figure 7 and Figure 14, respectively. The occupations are slightly different in these natural

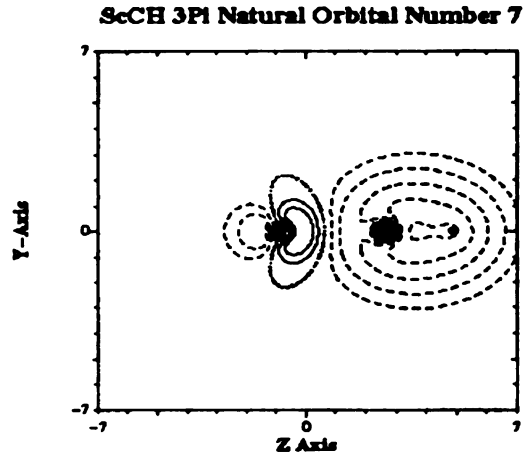

Occ=1.96
Cs=1.23
Cp=0.18
Hs=0.55

Figure 1

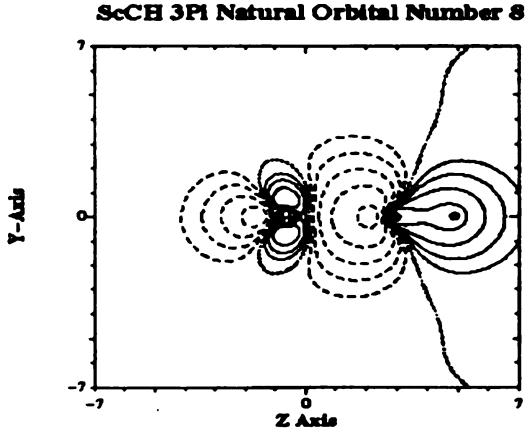

Occ=1.94 Cs=0.67 Cp=0.87
Hs=0.29 Scd=0.20

Figure 2

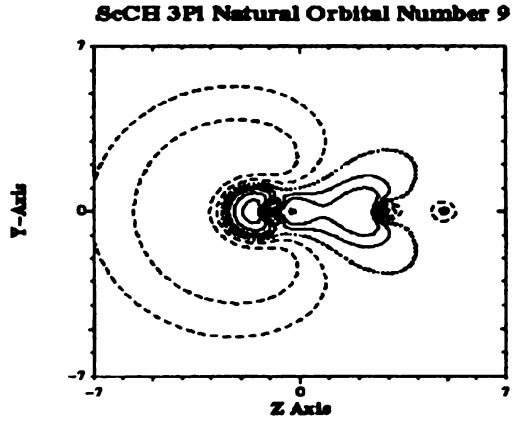

Occ=0.990 Scs=0.92
Scp=0.17 Scd=0.04

Figure 3

Figures 1, 2, and 3 are electron density contour plots of natural orbitals seven eight and nine of the ScCH molecule in the ground $^3\Pi$ state. The occupation and the mulliken population condensed to a basis function type are reported for each orbital.

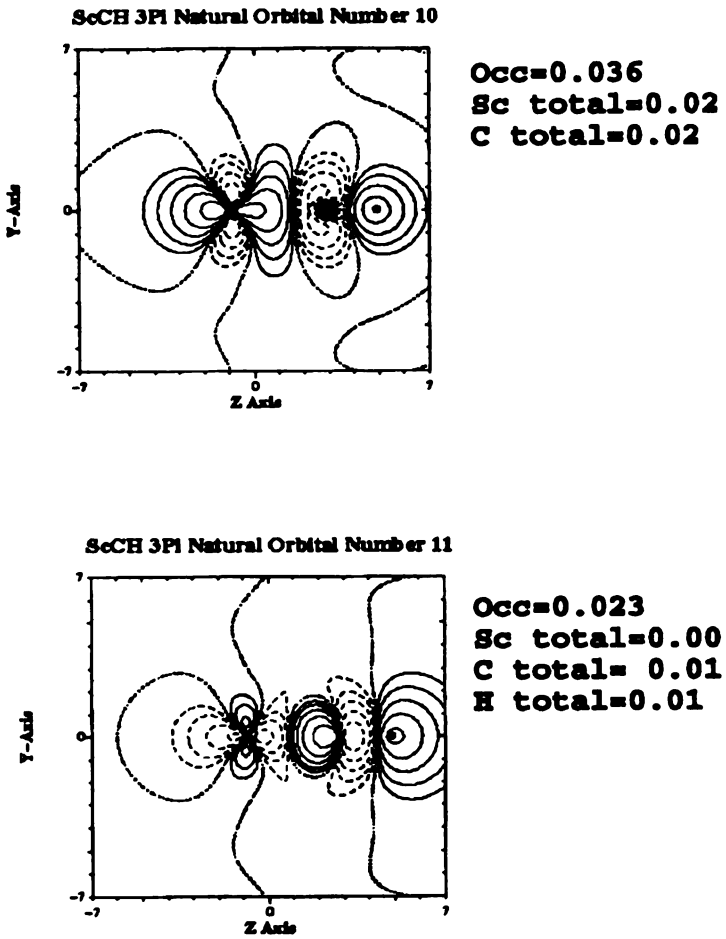

Figure 4 and Figure 5

Figures 4 and 5 are the electron density contour plots of natural orbitals 10 and 11 of the ScCH molecule in the $^3\Pi$ ground state. The occupations and the mulliken population condensed to a basis function type are reported for each orbital.

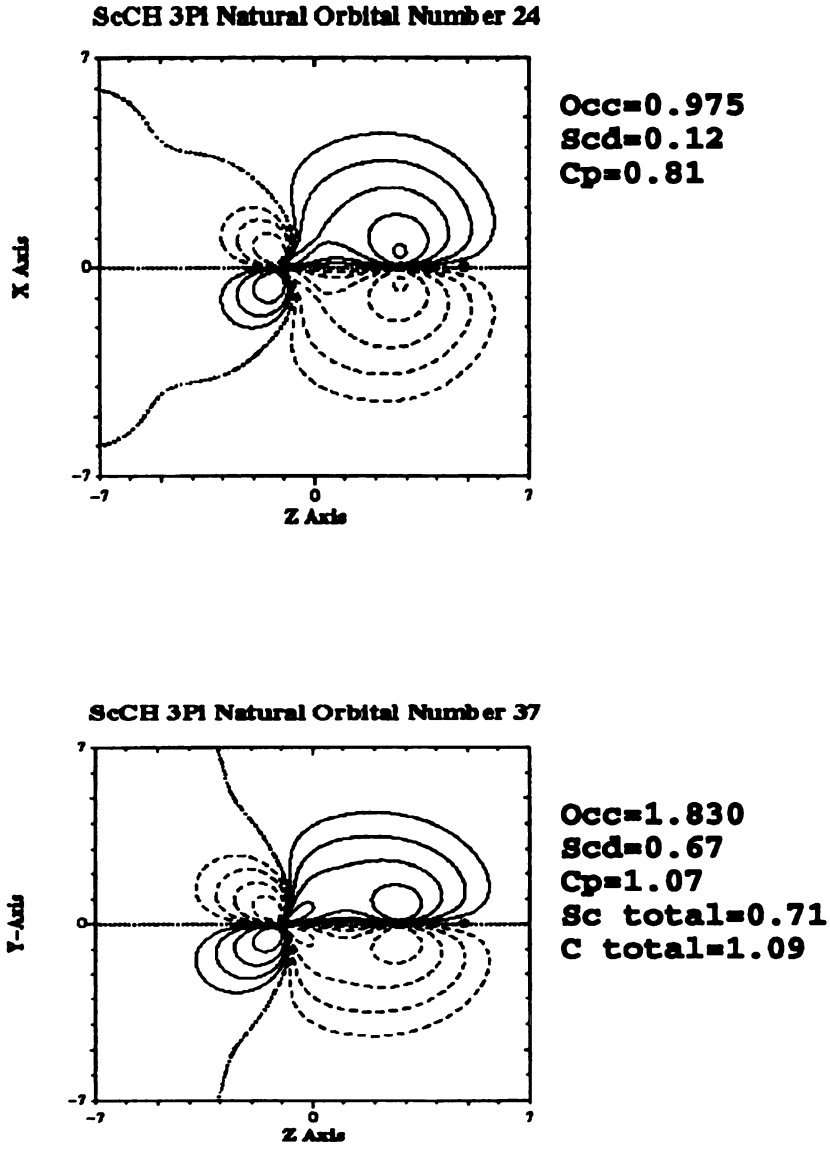

Figure 6 and Figure 7

Figures 6 and 7 are the electron density contour plots of natural orbitals 24 and 37 of the ScCH molecule in the $^3\Pi$ ground state. The occupations and the mulliken population condensed to a basis function type are reported for each orbital.

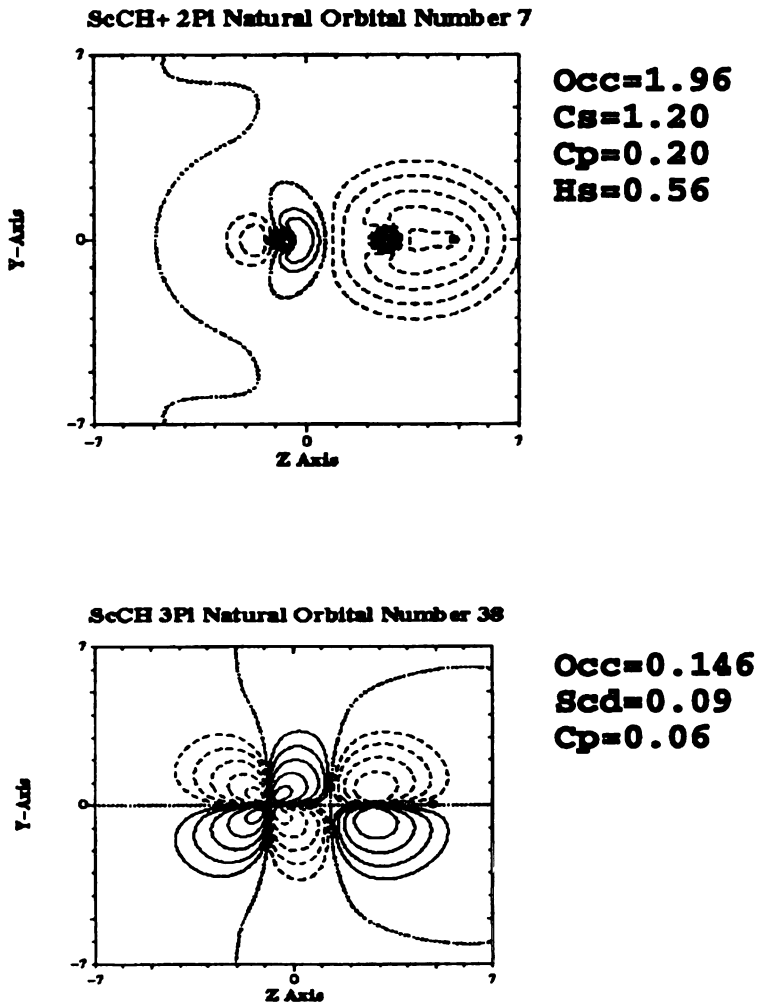

Figure 8 and Figure 9

Figures 8 and 9 are the electron density contour plots of natural orbitals 7 and 38 of the ScCH molecule in the $^3\Pi$ ground state. The occupations and the mulliken populationcondensed to a basis function type are reported for each orbital.

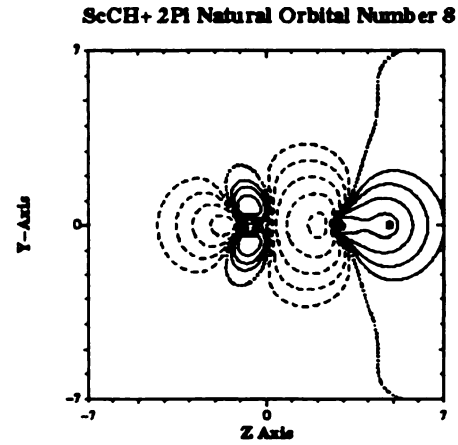

Occ=1.94
Scd=0.25
Cs=0.66
Cp=0.89
Hs=0.23

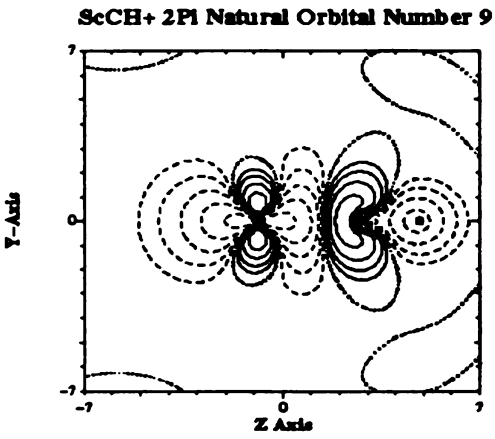

Occ=0.04
Sc total=0.02
C total=0.02

Figure 10 and Figure 11

Figure 10 and 11 are the electron density contour plots of natural orbitals 8 and 9 of the $ScCH^+$ molecule in the $^2\Pi$ ground state. The occupation and the mulliken population condensed to a basis function type are reported fro each orbital.

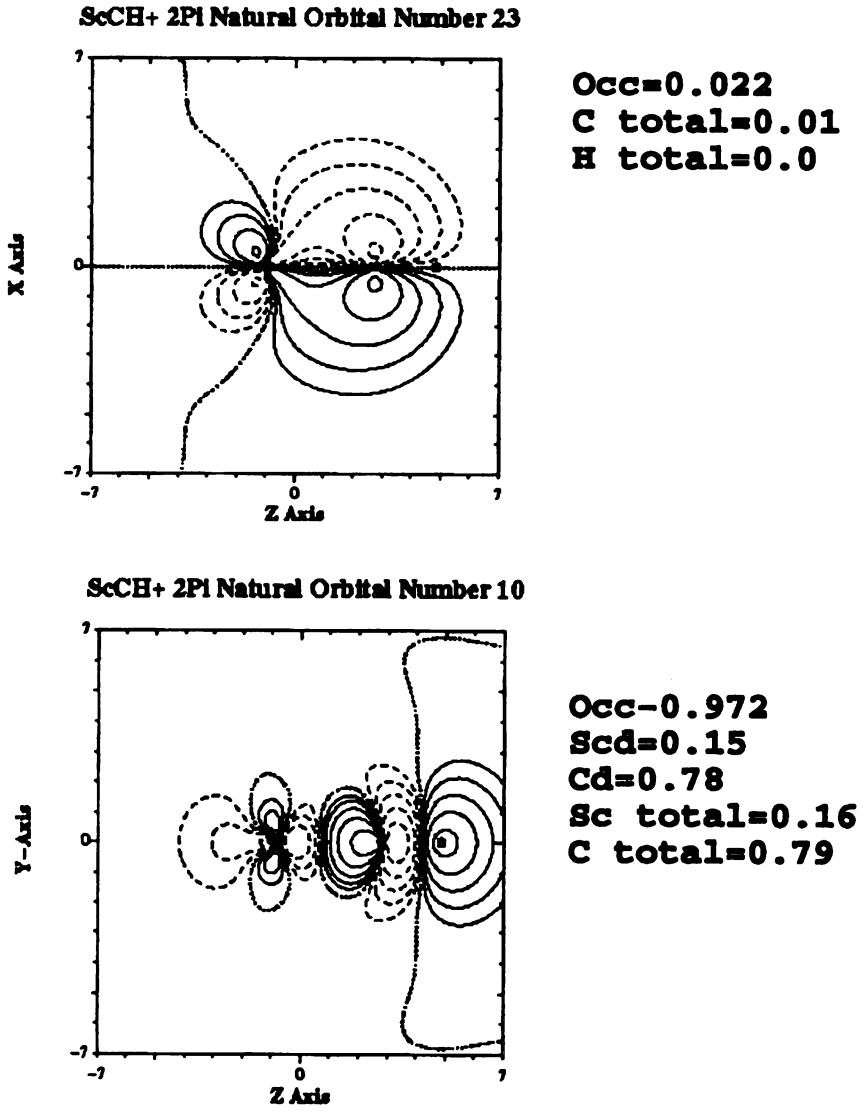

Figures 12 and 13 are electron density contour plots of natural orbitals 10 and 23 of the $ScCH^+$ molecule in the $^2\Pi$ ground state. The occupations and the mulliken population condensed to a basis function type are reported for each orbital.

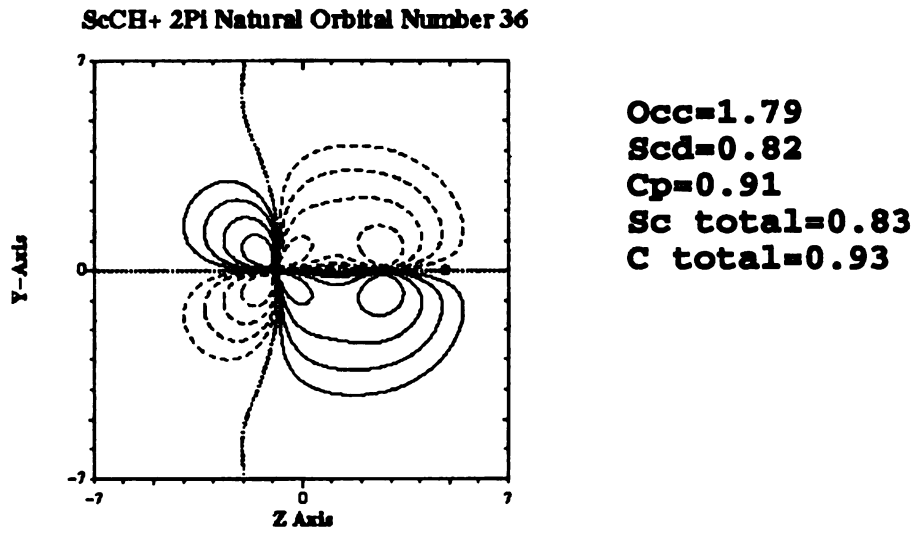

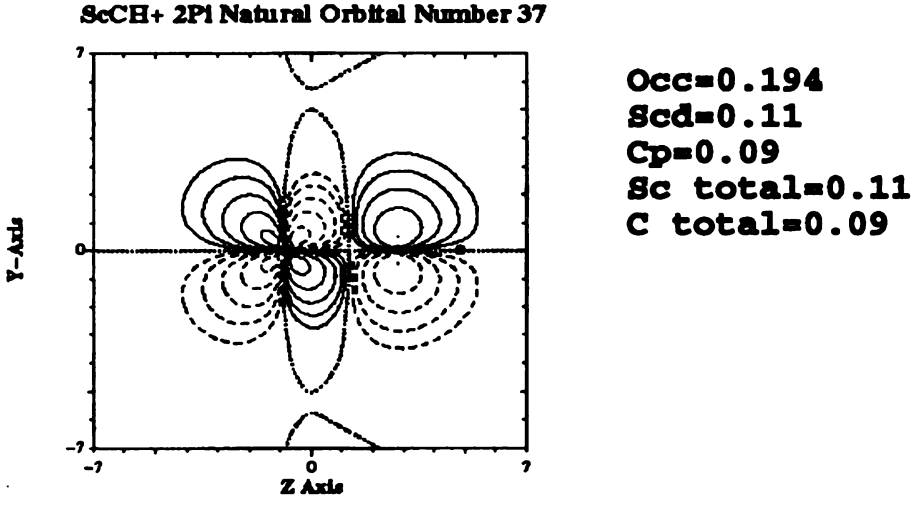

Figures 14 and 15 are electron density contour plots of natural orbitals 36 and 37 of the $ScCH^+$ molecule in the $^2\Pi$ ground state. The occupations and the mulliken population condensed to a basis function type are reported for each orbital.

orbitals with increases in the Sc $d\pi_y$ population and decrease in C $p_{\pi y}$ population going from the $^3\Pi$ state to the $^2\Pi$ state.

The ScN ground state has a d_σ orbital participating strongly in the sigma bond.[1j, 30] The ScCH molecule in the $^3\Pi$ state exists with a dative sigma bond. The charge on the Sc atom in ScN is +0.59 au.[1j, 30] The $ScCH^+$ molecule also has a dative bond with a charge transfer of +1.45, while the ScN^+ molecule in the $^2\Pi$ state has a +1.49 charge transfer[1j] from Sc to the N atom.

TiCH and TiCH+

The bond lengths, energies, and dipole moments (dipole moments of positive $TiCH^+$ are not reported) for TiCH and $TiCH^+$ are summarized in Tables 5 and 6, respectively. The $^2\Sigma^+$ ground state wavefunction has a Ti-C bondlength of 1.751 Å using the AWACH basis set. The wavefunction was constructed in a GVB fashion correlating the bonding pairs with the antibonding counterpart. Also an additional orbital was included in the active spave with a_1 symmetry. The TiC bond length using the same framework for the wavefunction and the AMES basis set is 1.750 Å. The C-H separations were almost identical at 1.0887 and 1.0892 Å, respectively. Dunning augmented quadrupole zeta basis[33] sets were used on both atoms.

The MCSCF calculations produced slightly longer Ti-C bond lengths than the MRCI calculations for all of the states of TiCH (Table 5). The same can be said for the

$TiCH^+$, $^1\Sigma^+$ state (Table 6). The C-H bondlength is predicted to be slightly shorter than the MRCI predictions.

The DFT calculations predict much shorter Ti-C bondlengths and slightly loner C-H bondlengths than the MRCI calculations. The DFT calculations predict a $^2\Sigma^+$-$^2\Pi_{linear}$ separation of 59.5 mH. The experimental separation is around 62.8mH.[32] These experimental results along with others can be found in Table 7.[32, 34]

The experimental TiC bondlength is 1.728 Å [32] compared to the CI values of 1.750 and 1.751 Å for the AWACH and AMES basis on the Ti atom. We calculate the separation between the $^2\Sigma^+$-$^2\Pi_{linear}$ states to be 64.3 mH with the AWACH basis on Ti and 65.1 mH with the AMES basis on Ti, using MRCI techniques with additional correlation provided to the sigma system by adding an a_1 symmetry orbital to the correlation in the reference space. The experimental separation between the two states is near 62.8 mH [32]. The $^2\Pi$ state in the experiment is thought to be bent.[32] Our imaginary (negative valued) vibrational frequency calculations on the $^2\Pi_{linear}$ state add support to the experimental results. A single point calculation on the $^2\Pi$ state bent at an angle of 170 degrees using the experimental geometry for the ground state yielded an energy 2mH higher than our linear prediction. The experimental frequencies are shown in Table 7 [32]. These values are in close agreement with our results also shown in Table 7.

To move the lone electron in the 4s orbital of the $^2\Sigma^+$ state of TiCH to the $d_{\delta-}$ orbital on Ti to make the $^2\Delta$ state takes 31mH, according to both MRCI calculations in Table 5. However, DFT predicts a value of 20.5 mH as shown in Table 6.

The TiCH molecule can be ionized to $TiCH^+$ by removing a lone electron of Ti. The $^2\Sigma^+$ and $^1\Sigma^+$ energies differ by 0.221 hartree or 5.99 eV. The ionization potential of Ti is 6.58 eV [21]. The energies are reported in Table 5 and Table 6, respectively.

Now, for a comparison of the electronic states of TiCH and $TiCH^+$ with the isoelectronic TiN, TiN^+, and other positive ion results. The bondlength in TN [1j] is much shorter than the Ti-C separation at 1.602 Å. The energy separation between the $^2\Sigma^+$ and the $^2\Delta$ states of TiN calculated by Harrison *et. al* is 0.95 eV or 34.9 mH [1j]. The $^2\Pi$ state of TiN is 73.9 mH above the ground state. Both of these values are very close to the same electronic state separations relative to ground state for TiCH at the MRCI level.

Contour Plot TiCH

The contour plot of TiCH $^2\Sigma^+$ NO 8 is shown in Figure 16. This contour shows a Ti-C sigma bond consisting mainly of a carbon s-p hybrid bonded to a smaller contribution of 0.35 au from the Ti d_σ. The Ti 4s orbital is the primary contributor in NO 9 (Figure 17). Figure 19 shows the contour plot of the anti-bonding sigma orbital of the C-H fragment.

The $TiCH^+$, $^1\Sigma^+$, NO contour plots, populations, and occupations are similar to those of $^2\Sigma^+$ in TiCH. The contour plots of $TiCH^+$ are shown in Figures 24-31 while the populations of TiCH and $TiCH^+$ are in Tables 7 and 8, respectively. The population of TiN $(^2\Sigma^+)^{1h,1j}$ is also comparable to that of the TiCH ground state. The sigma bond is consists mainly of N p_σ character bonded to Ti d_σ, with the lone electron in the 4s of the Ti atom. However, the N $2p_\sigma$ contributes 1.20 au. [1j] to the bond while the d_σ contributes 0.78 to the sigma bond. The lone electron in the TiN is calculated to be 0.79 [1j] 4s on Ti which is in agreement with experiment [1h]. In the TiCH NO 9 (Figure 17) the lone electron is almost completely the 4s orbital (1.11 au) on Ti with a small contribution from the $3d_\sigma$ orbital on Ti (0.091au). Figures 20 and Figure and 21 show

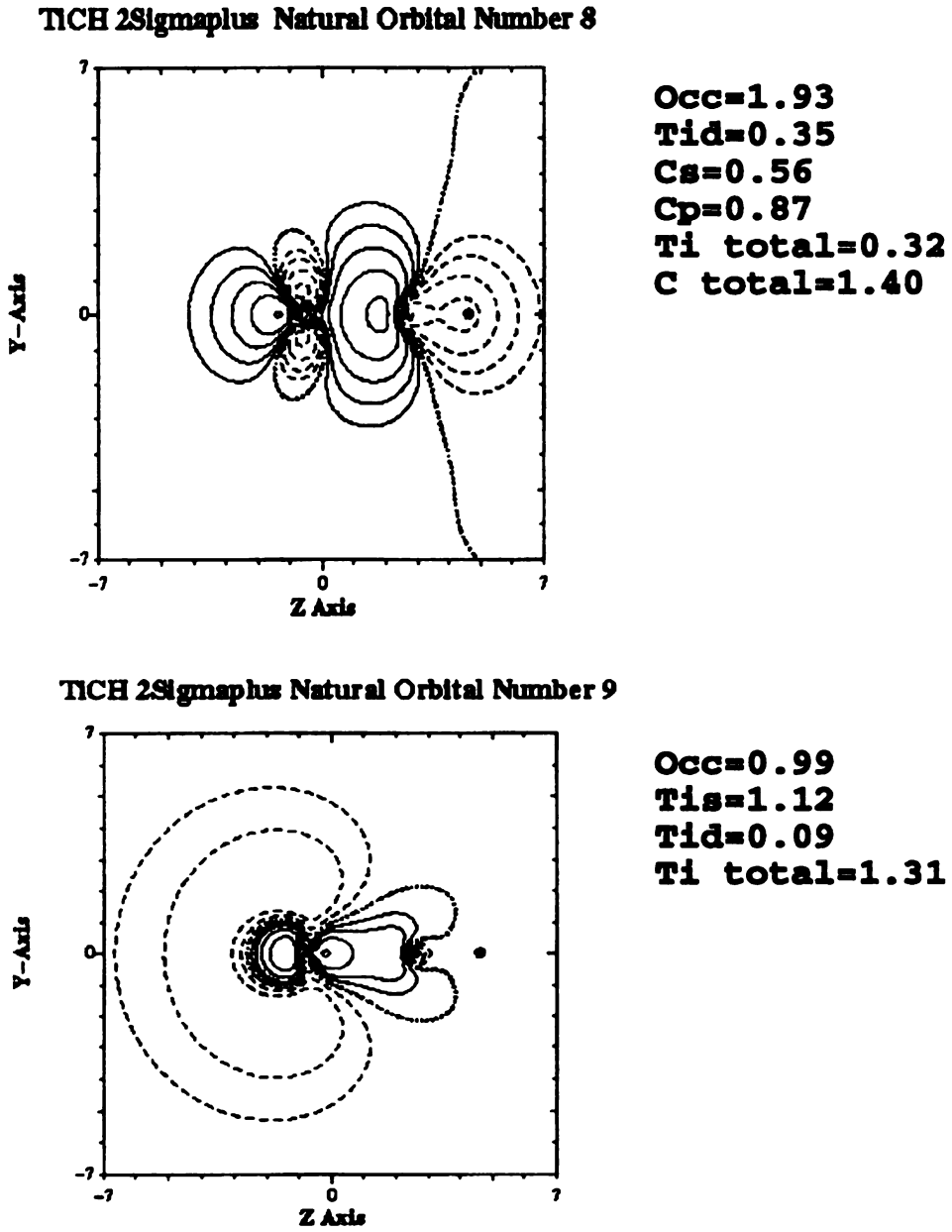

Figures 16 and 17 are electron density contour plots of natural orbitals seven 8 and 9 of the TiCH molecule in the $^2\Sigma^+$ ground state. The occupations and the mulliken population condensed to a basis function type are reported for each orbital.

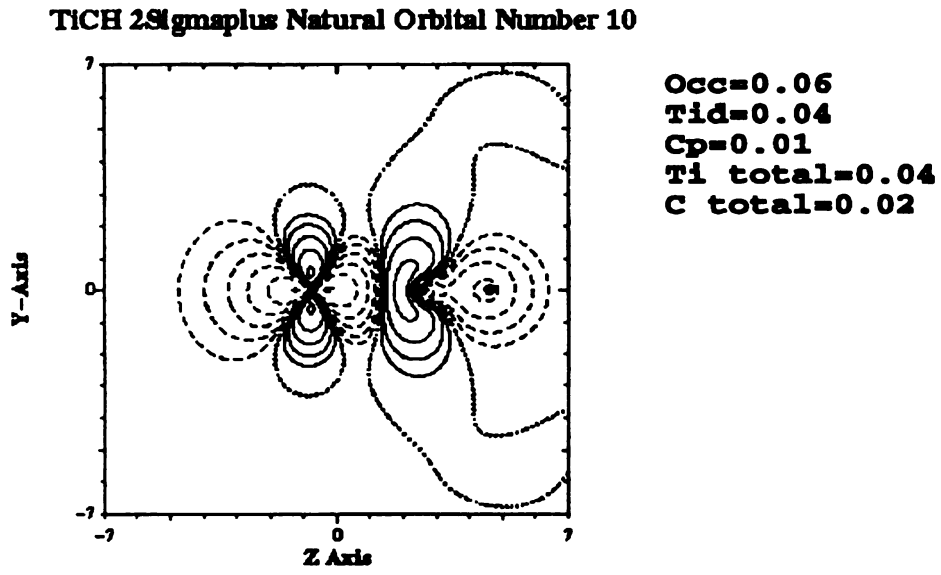

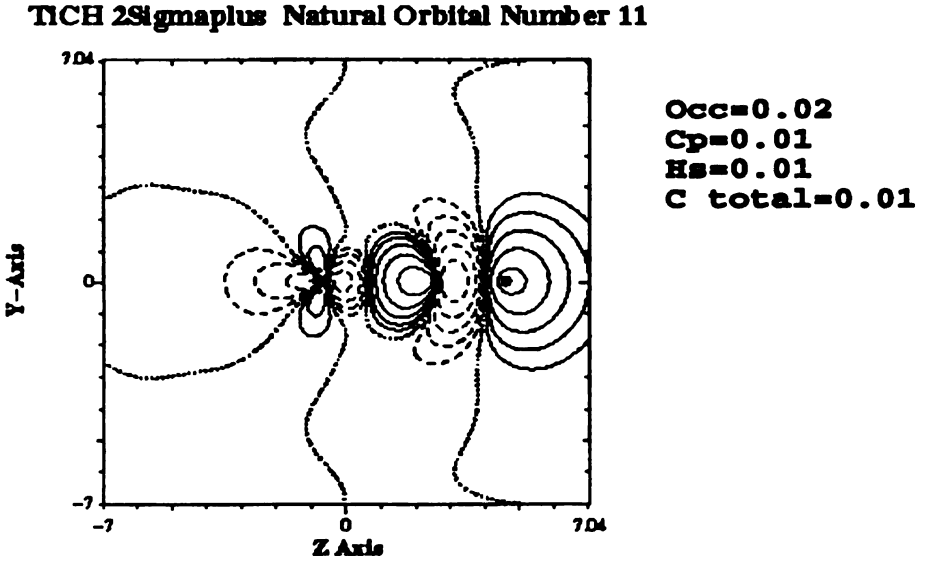

Figure 18 and Figure 19

Figures 18 and 19 are electron density contour plots of natural orbitals 10 and 11 of the TiCH molecule in the $^2\Sigma^+$ ground state. The occupations and the mulliken population condensed to a basis function type are reported for each orbital.

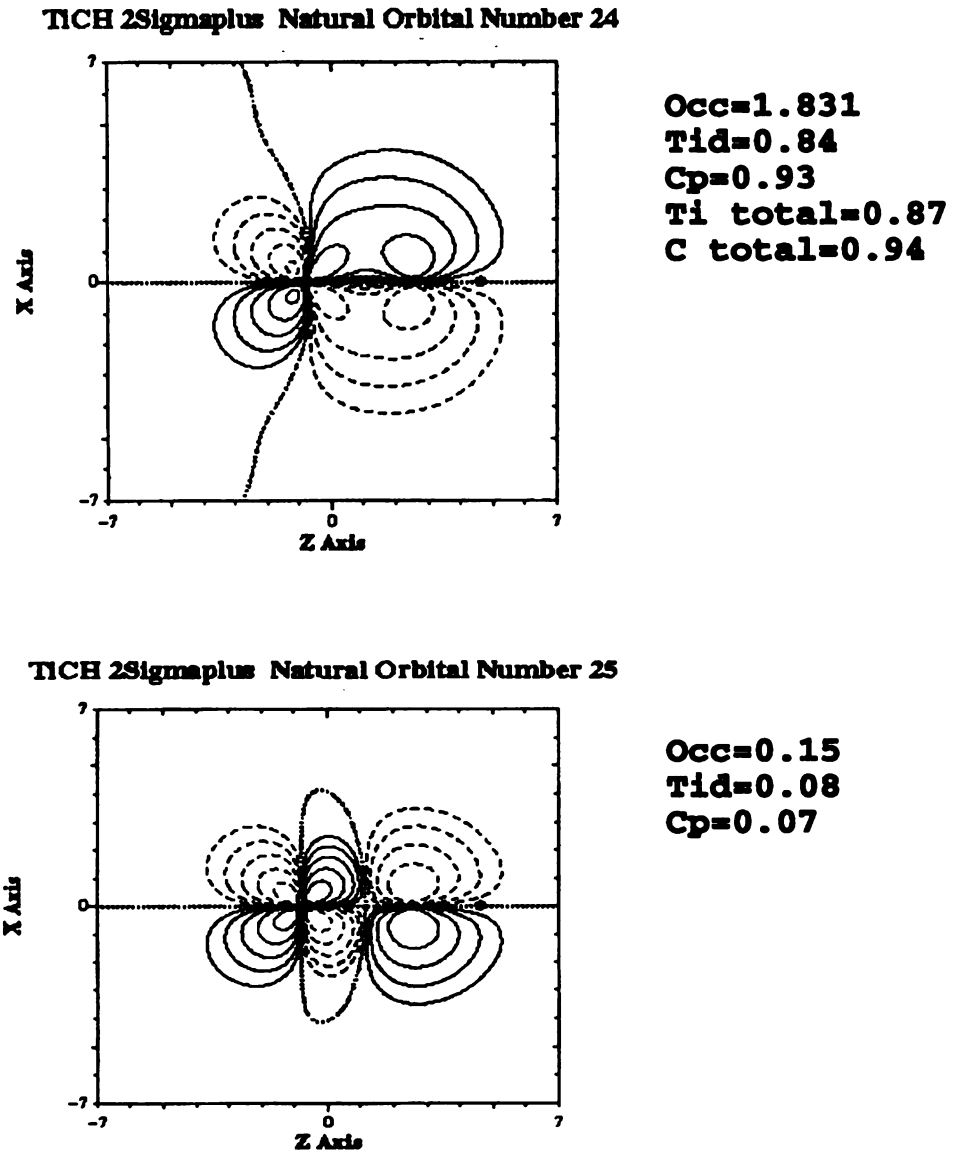

Figure 20 and Figure 21

Figures 20 and 21 are electron density contour plots of natural orbitals 24 and 25 of the TiCH molecule in the $^2\Sigma^+$ ground state. The occupations and the mulliken population condensed to a basis function type are reported or each orbital.

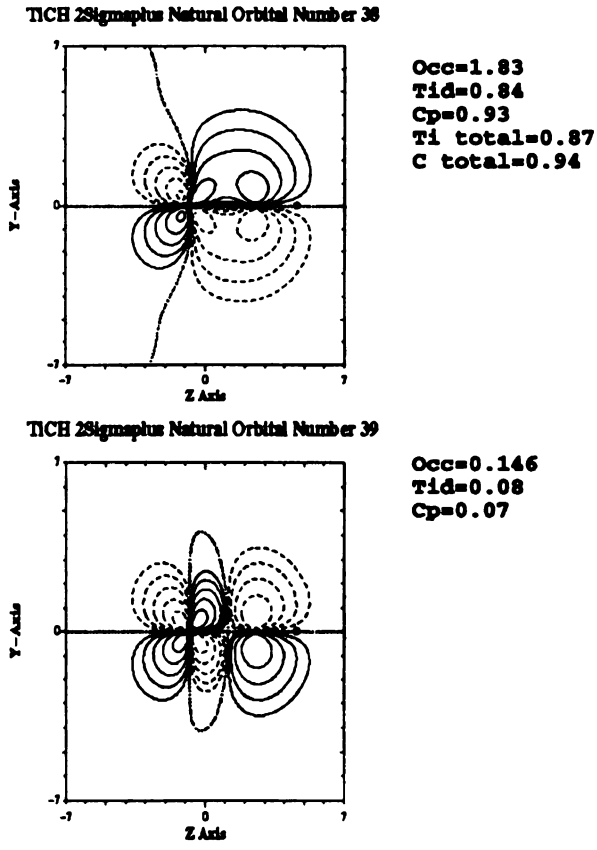

Figure 22 and Figure 23

Figures 22 and 23 are electron density contour plots of natural orbitals 38 and 39 of the TiCH molecule in the ground state. The occupations and the mulliken population condensed to a basis function type are reported for each orbital.

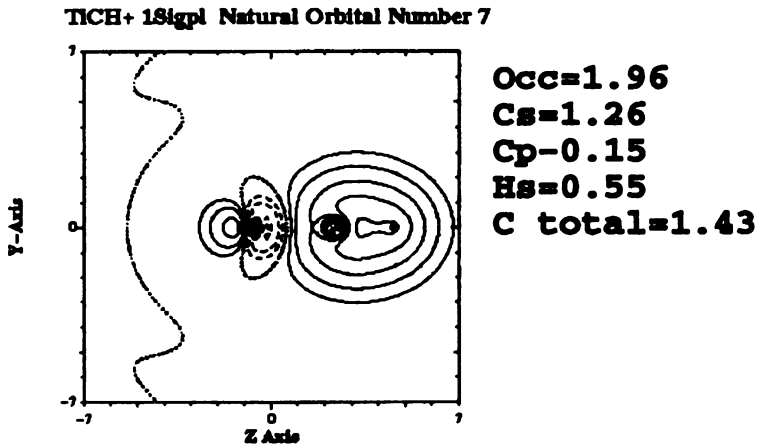

Figures 24 and 25 are the electron density contour plots of natural orbitals 8 and 9 of the $TiCH^+$ molecule in the $^1\Sigma^+$ ground state. The occupations and the mulliken population condensed to a basis function type are reported for each orbital.

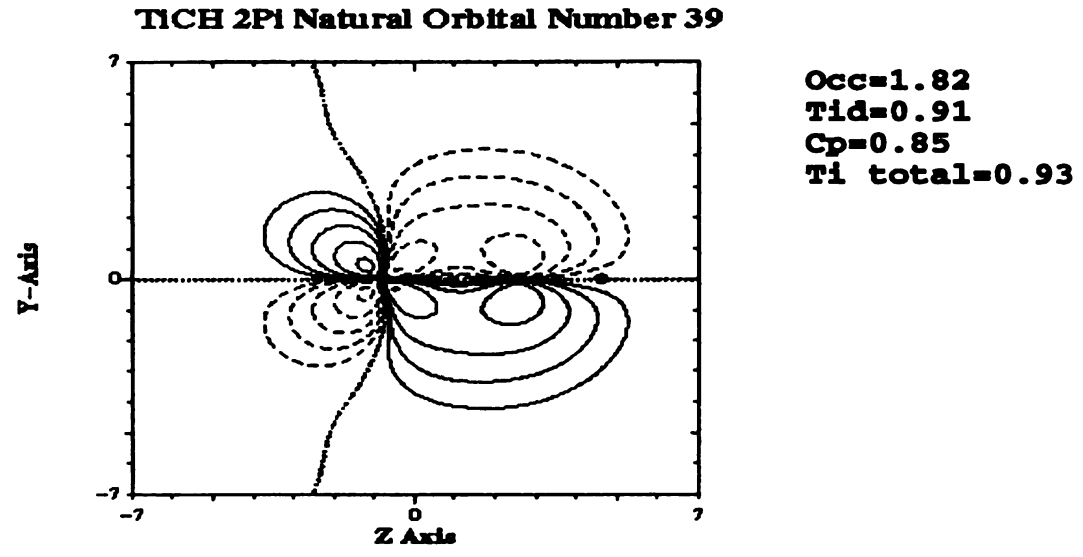

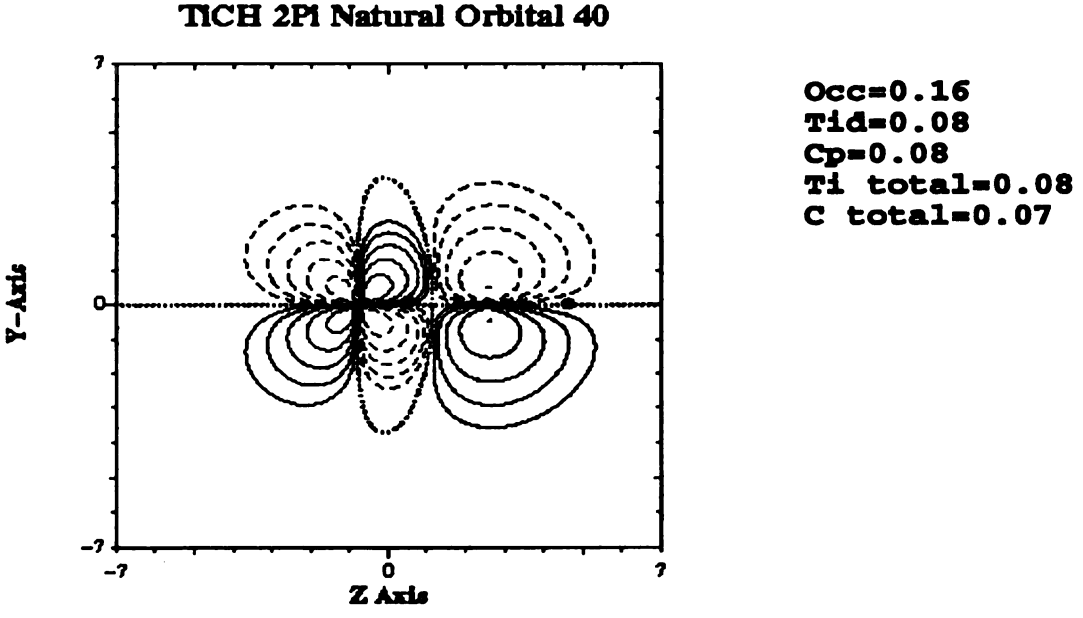

Figures 26 and 27 are the electron density contour plots of natural orbitals 39 and 40 of the TiCH molecule in the $^2\Pi$ excited state. The occupations and the mulliken population condensed to a basis function type are reported for each orbital.

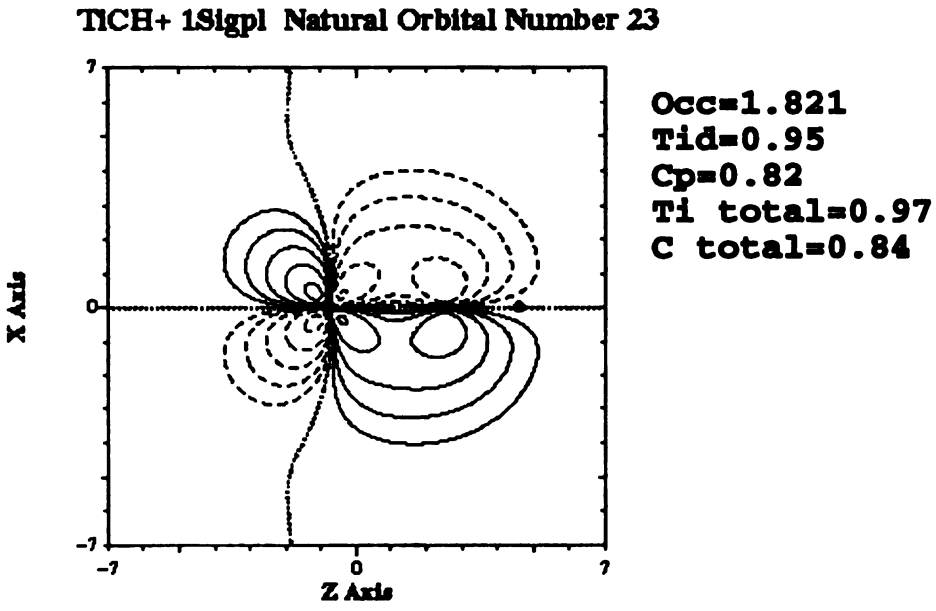

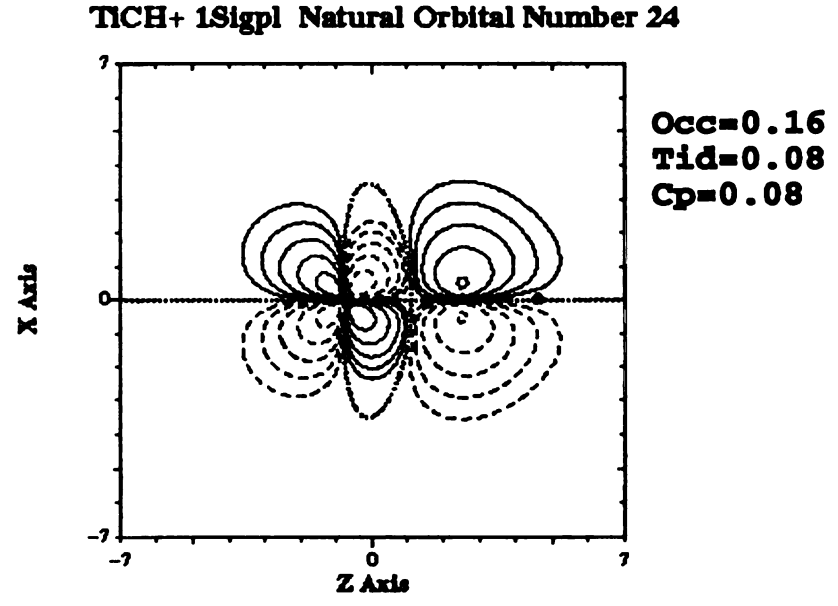

Figures 28 and 29 are the electron density contour plots of natural orbitals 23 and 24 of the $TiCH^+$ molecule in the $^1\Sigma^+$ ground state. The occupations and the mulliken population condensed to a basis function type are reported for each orbital.

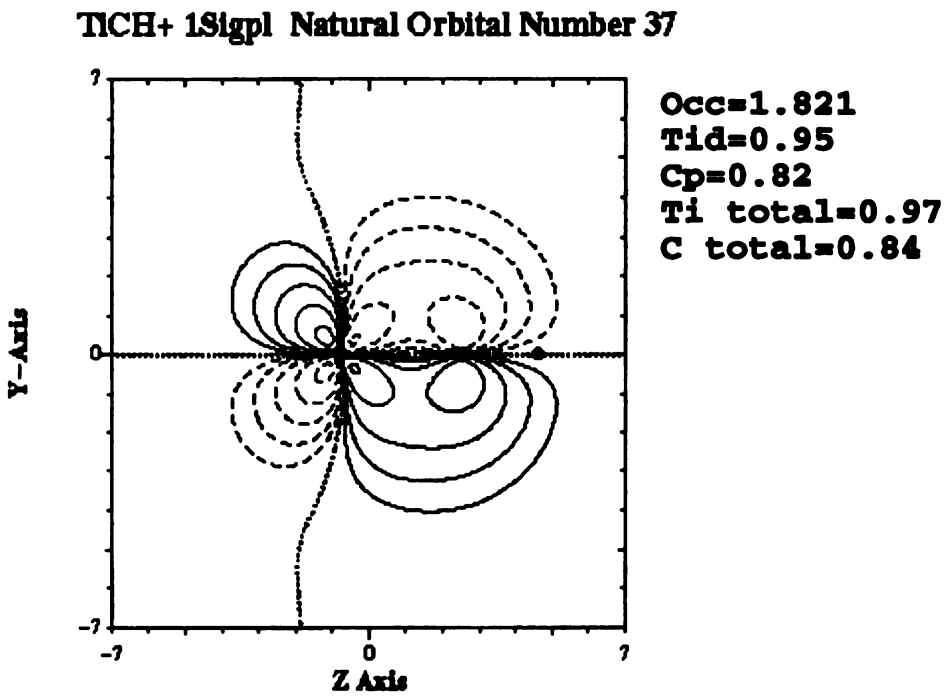

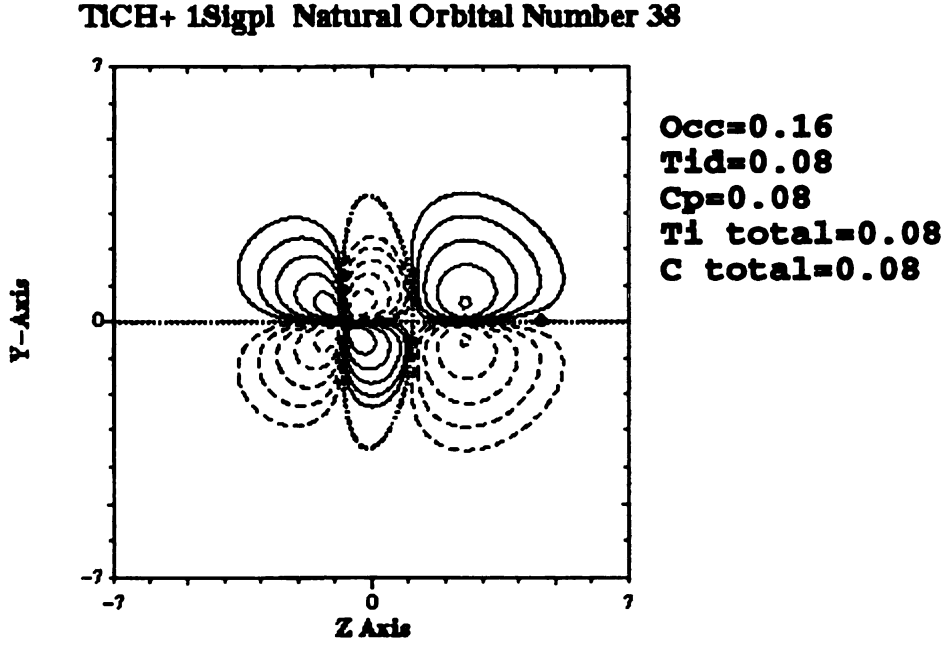

Figures 30 and 31 are electron density contour plots of natural orbitals 37 and 38 of the $TiCH^+$ molecule in the $^1\Sigma^+$ ground state. The occupations and the mulliken population condensed to a basis function type are reported for each orbital.

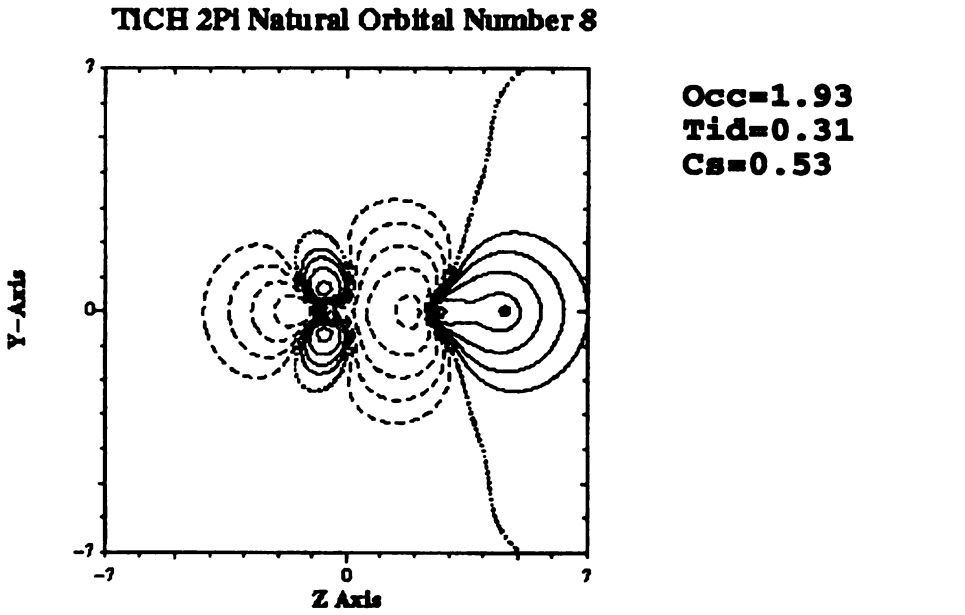

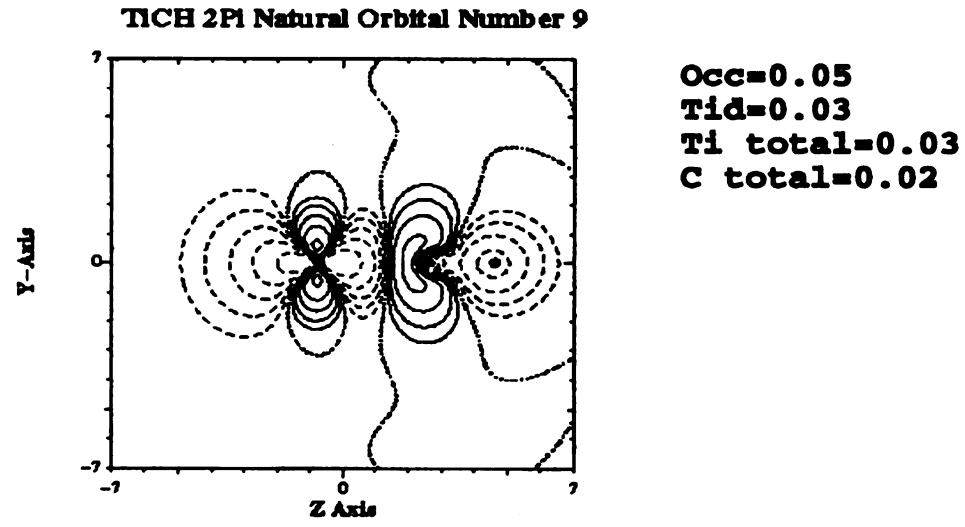

Figures 32 and 33 are the electron density contour plots of natural orbitals 8 and 9 of the TiCH molecule in the $^2\Pi$ state. The occupations and the mulliken population condensed to a basis function type are reported for each orbital.

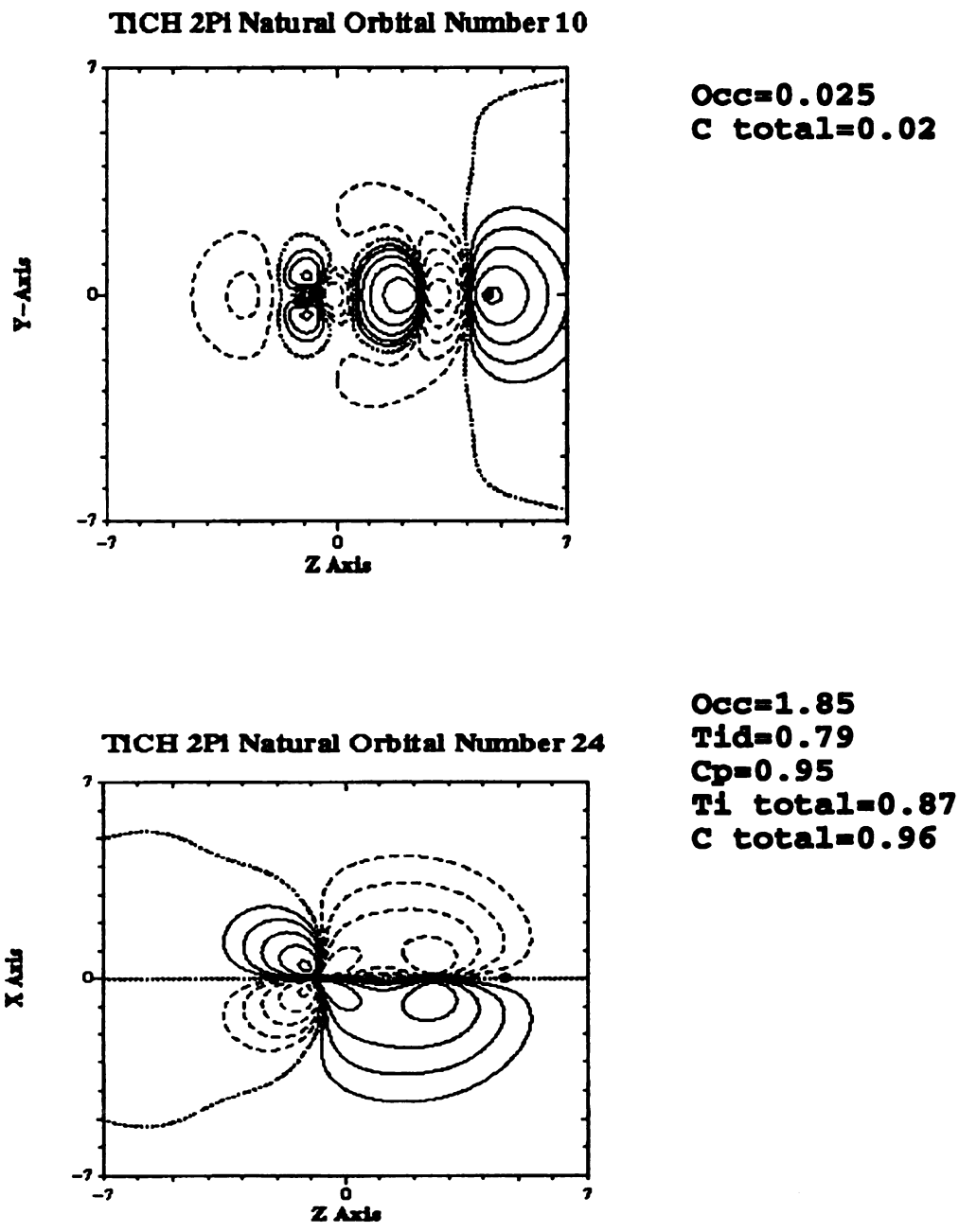

Figures 34 and 35 are electron density contour plots of natural orbitals 10 and 24 of the TiCH molecule in the $^2\Pi$ state. The occupations and the mulliken population condensed to a basis function type are reported for each orbital.

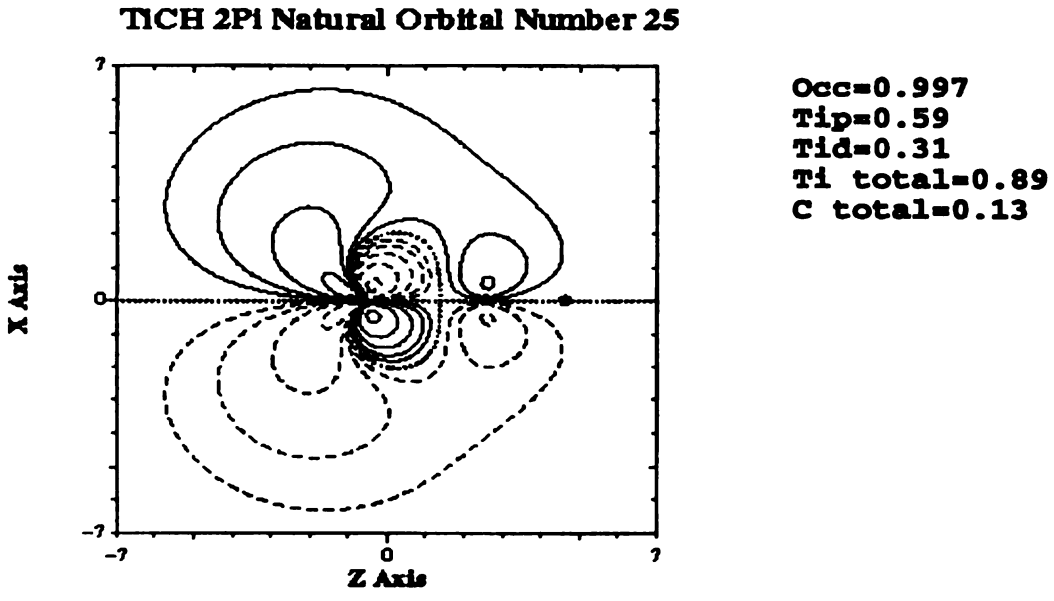

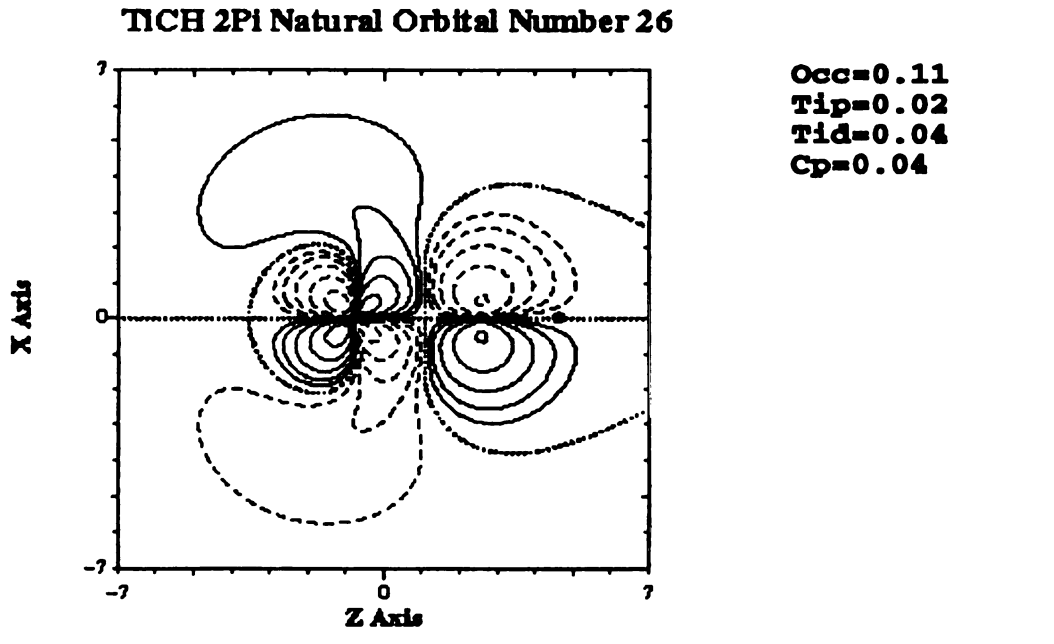

Figures 36 and 37 are the electron density contour plots of natural orbitals 25 and 26 of the TiCH molecule in the $^2\Pi$ state. The occupations and the mulliken population condensed to a basis function type are reported for each orbital.

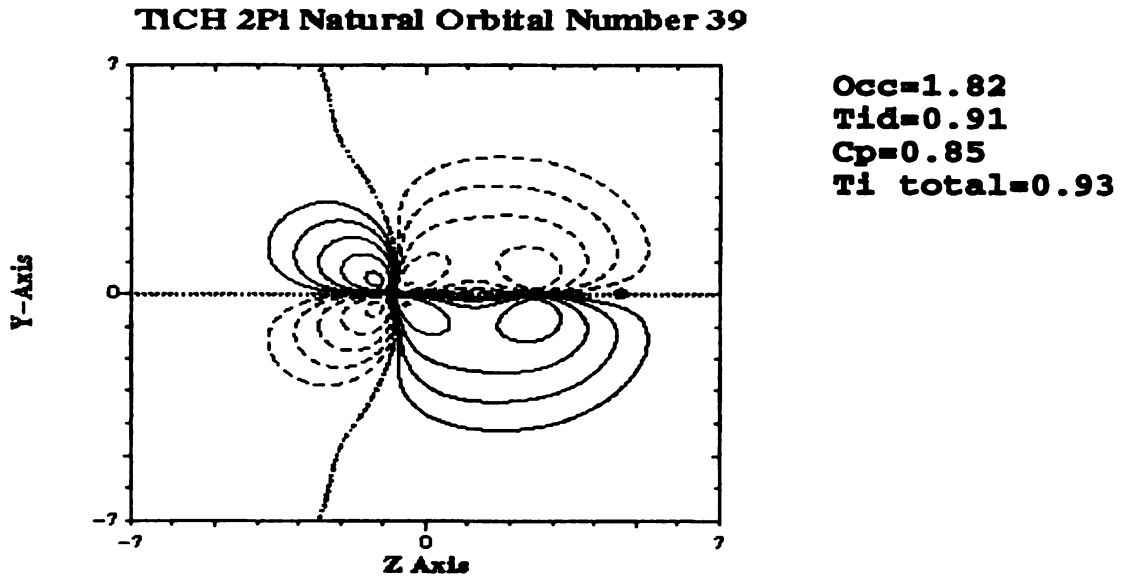

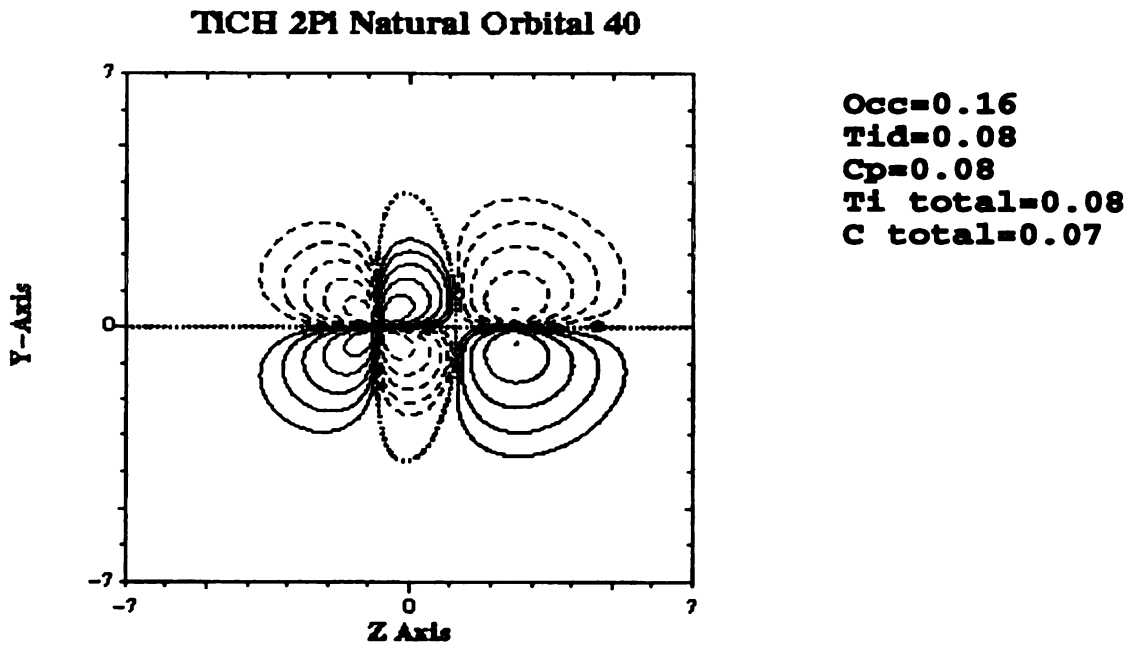

Figures 38 and 39 are the electron density contour plots of natural orbitals 39 and 40 of the TiCH molecule in the $^2\Pi$ state. The occupations and the mulliken population condensed to a basis function type are reported for each orbital.

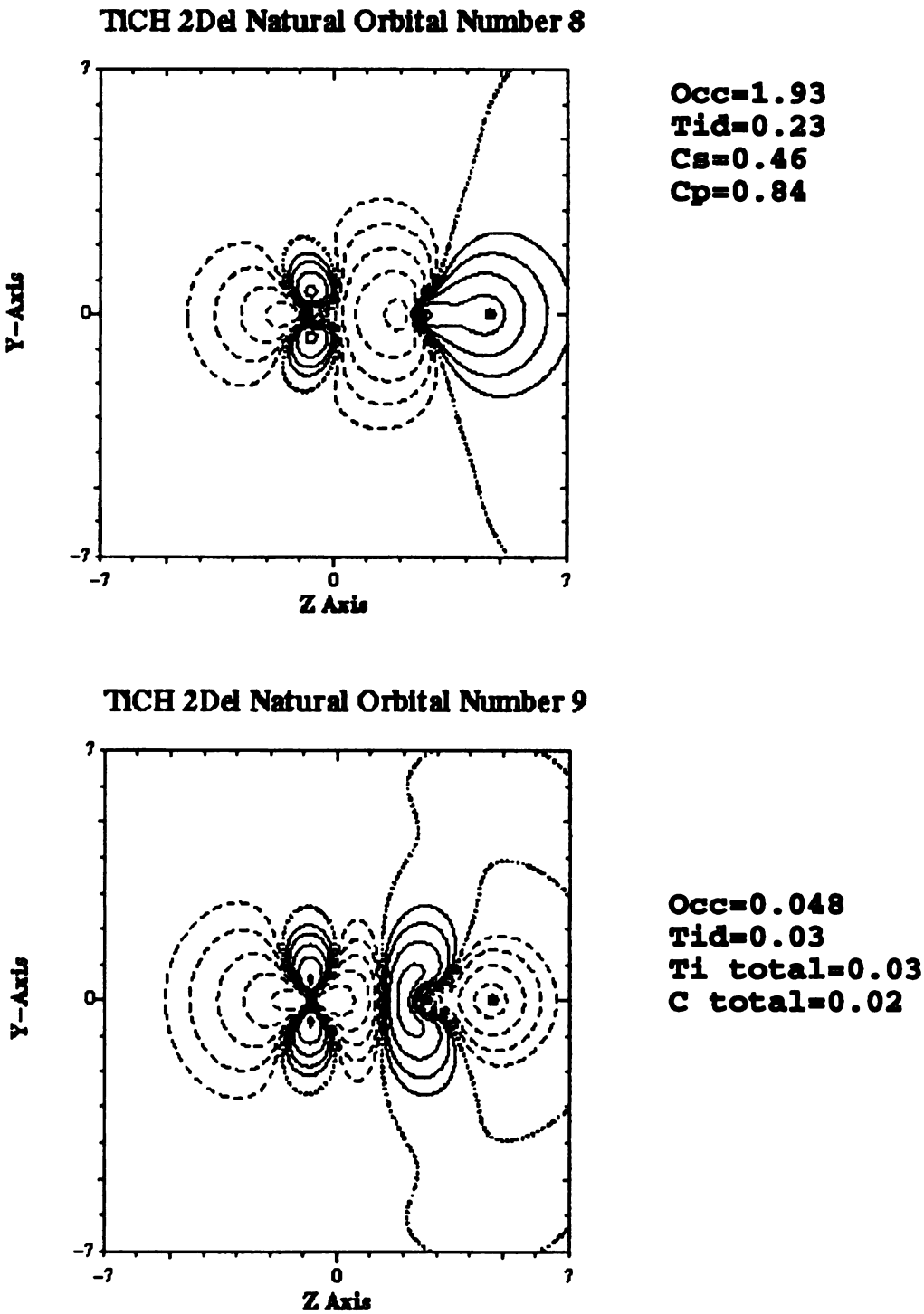

Figures 40 and 41 are the electron density contour plots of natural orbitals 8 and 9 of the TiCH molecule in the $^2\Delta$ state. The occupations and the mulliken population condensed to a basis function type are reported for each orbital.

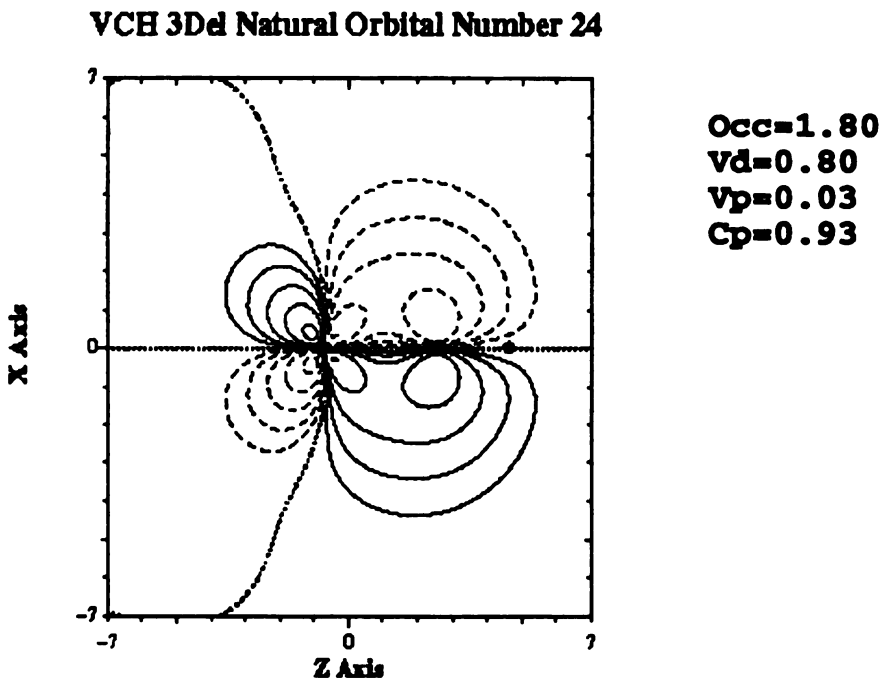

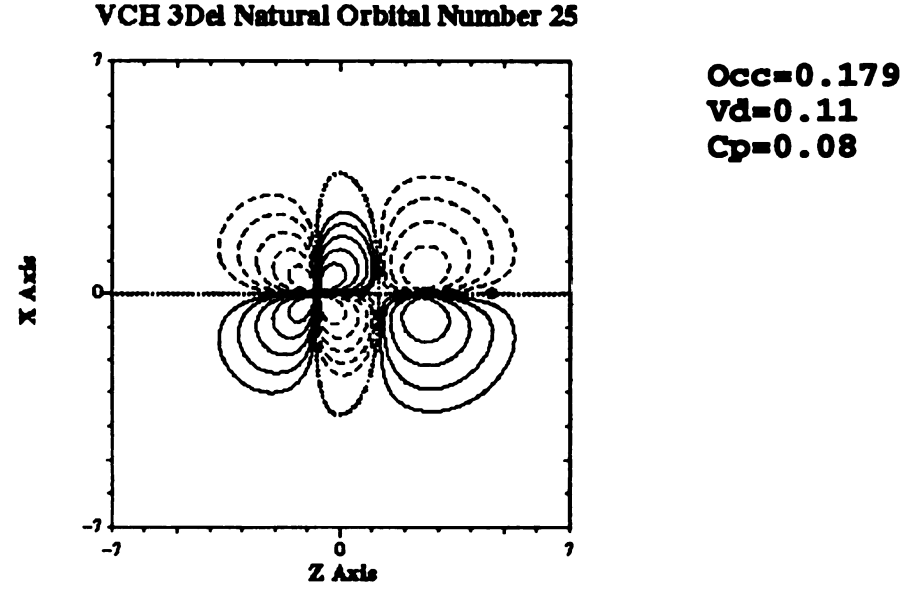

Figures 42 and 43 are the electron density contour plots of natural orbitals 24 and 25 of the VCH molecule in the $^3\Delta$ ground state. The occupations and the mulliken population condensed to a basis function type are reported for each orbital.

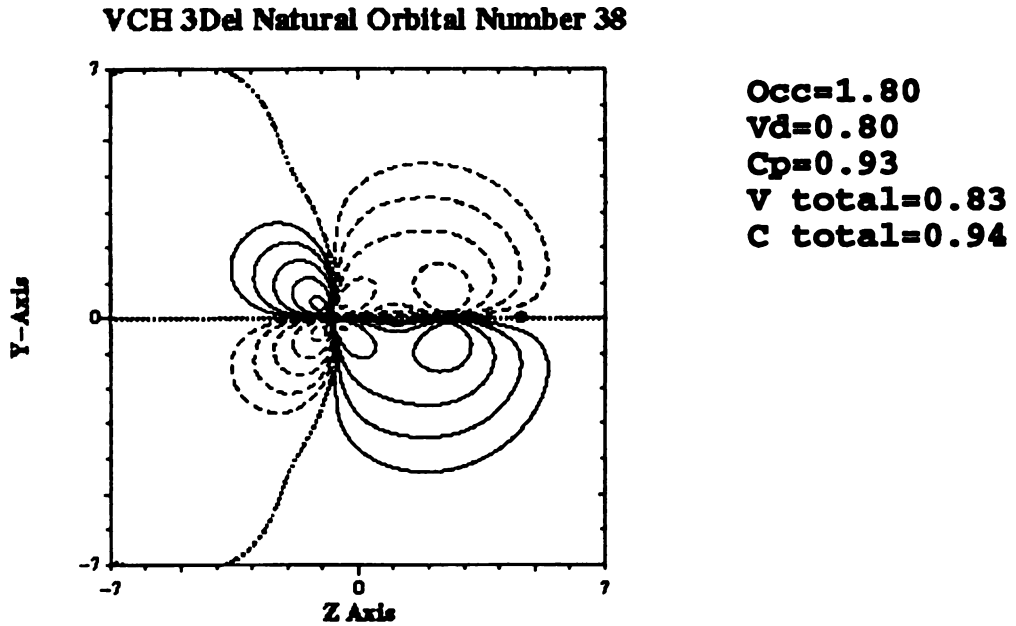

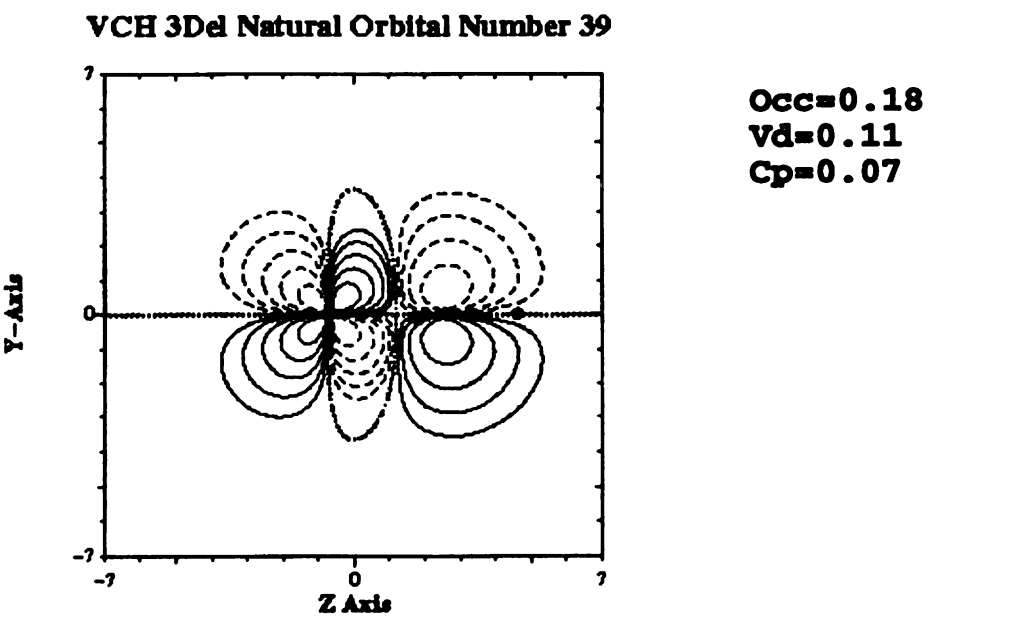

Figures 44 and 45 are the electron density contour plots of natural orbitals 38 and 39 of the VCH molecule in the $^3\Delta$ ground state. The occupations and the mulliken population condensed to a basis function type are reported for each orbital.

symmetric π_x and π_y orbitals between Ti and carbon. The populations are slightly different than those of TiN (0.05 Ti $4p_\pi$, 0.75 Ti $3d_\pi$).[1j]

The contours of the selected natural orbitals of two low-lying excited states of TiCH are shown in Figures 32-41. The contour plot of NO 8, the Ti-C sigma bond in the $^2\Pi$ state, has almost identical occupations and populations to that of the ground state and $^2\Delta$ states NO 8 of the TiCH molecule. The $^2\Pi$ NO 10, anti-bonding C-H sigma bond, is slightly different in structure than that of the NO 10 of the $^2\Sigma^+$ state, However, the bonding and the anti-bonding orbitals are almost identical in the $^2\Pi$ and $^2\Sigma^+$ state(Figures 35, 36, 38, 39 and Figures 20-23), as well as, the $^2\Delta$ state.

Finally, the RHF energies and geometries are found in Table 5a, for the wavefunctions that we were able to construct. The bondlengths are significantly shorter than those of the MCSCF+1+2.

In the case of TiN and TiN+ there is significant charge transfer before reaching the equilibrium geometries; +0.50 and +0.43 au, respectively, on the Ti atom. In TiCH and $TiCH^+$ there is also some charge transfer shown in Tables 9 and 10. The amount of the charge transfer is undoubtedly different due to electronegativity differences.

VCH and VCH+

The bond lengths, energies and dipole moments of VCH and VCH^+ (dipole moment not reported for VCH^+) are also reported. The bond length of V-C in the VCH molecule in the ground state $^3\Delta$ state using the MRCI level of theory is 1.725 Å (Table

11). The corresponding separation using DFT theory is 1.750 Å while the C-H bond length was calculated to be 1.090 Å.

The VCH molecule is constructed analogously to the CrCH molecule absent a lone electron in the $3d_{\delta+}$ orbital on the V atom. The isoelectronic VN has a much shorter triple bond. The experimental results for VCH in the ground $^3\Delta$ state are given in Table 11.[34] Our calculated vibrational frequencies are in good agreement with experiment. The carbon-hydrogen bond length is in relatively good agreement with experiment. The metal-carbon bond length calculated in this work is slightly longer than experiment (1.705 Å) at 1.750 Å (DFT calculation) and 1.725 Å (MRCI) (Shown in Table 11).

Going from VCH to VCH^+, a lone electron in the 4s orbital of vanadium would be removed to leave VCH^+ in the $^2\Delta$ state. The VN^+ state is predicted to have a triple bond between the V and N atoms.[1h] Harrison and Swaisgood[1d] predict a triply bonded VCH^+, $^2\Delta$, ground state like the one reported in this work. Their bond lengths are V-C 1.745 and C-H 1.091 Å while our results predict a V-C separation of 1.599Å at the DFT level and a C-H separation of 1.083Å at the DFT level. Using the more correlated MCSCF wavefunction we calculated a V-C separation of 1.720 Å and a C-H separation of 1.088 Å (Table 12). There is evidence of a significant difference in the sigma system of VCH^+ relative to the other TM-CH^+ molecules. In VCH^+ there is slight (dative) sigma bond between vanadium and carbon. The carbon atom holds almost two electrons in the 2s orbital, Figure 46, while forming a dative pi bond V⇒C in Figure 47. Despite being in effect a double bonded system, our results report a shorter V-C separation than the triply-

bonded V-CH molecule reported by Swaisgood *et. al.*[1d] The isoelectronic VN^+ in the $^2\Delta$ state exists with a much shorter triple bond.[1h]

The occupations shown on the contour plots of the π systems of VCH describe more correlation with the π^* orbitals than the pi systems of TiCH and ScCH. The populations are given in Figures 42-45. The populations of VCH and VCH^+ in the ground state and some excited states are given in Table 13 and 14, respectively.

An excited state of VCH, the $^3\Pi$ state, at the MCSCF level has 70,860 configuration state functions (CSF's). The geometries and energies are given in Table 9. Another excited state, the $^3\Phi_{\pi,\delta+}$ state, is also reported. The $^3\Phi_{\pi,\delta+}$ energies, geometries and frequencies are reported in Tables 11 and 7, respectively.

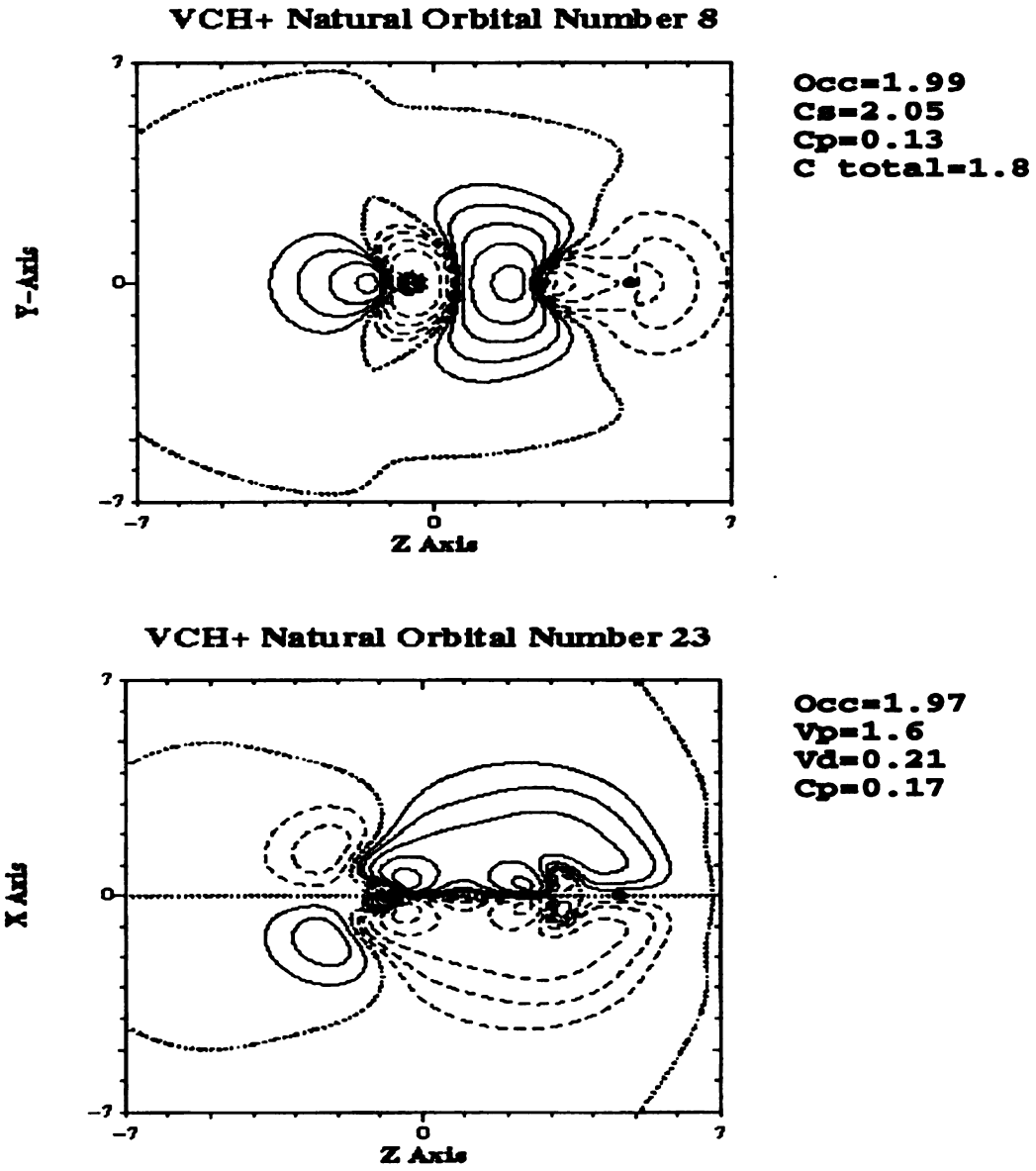

Figure 46 and Figure 47

Figures 46 and 47 are the electron density contour plots of natural orbitals 8 and 23 of the VCH^+ molecule in the $^2\Delta$ ground state. The occupations and the mulliken populationcondensed to a basis function type are reported for each orbital.

CrCH and $CrCH^+$

The CrCH molecule in the $^4\Sigma^-$ ground state is analogous to VCH with another lone electron in the Cr $d_{\delta+}$ orbital. Tables 15 and 7provide the MCSCF, MRCI, and DFT geometries, energies, dipole moments, frequencies and populations for CrCH in the $^4\Sigma^-$ state. The CrCH bond is much longer than the isoelectronic CrN at (1.619Å) at all levels of theory. The dipole moments are quite similar at 2.7 (this work) and 2.0 Debye (CrN).[1j] CrN had a large charge transfer from the Cr to the N atom of +0.5 atomic untis.[1j] In CrCH that charge transfer is half that at +.25 au. (See Table 17) The geometry presented in Table 16 for CrCH $^4\Sigma^-$ using a MCSCF wavefunction included 71,213 CSF.

In $CrCH^+$ an electron is removed from the 4s orbital of Cr in CrCH in the $^4\Sigma^-$ state to leave lone electrons in the $3d_{\delta-}$ and $3d_{\delta+}$ orbitals of Cr. The natural orbitals are shown in Figures 54-57 show the highly correlated pi system of Cr relative to the other TM-CH molecules. The bondlengths, energies, dipole moments, frequencies, and populations for $CrCH^+$ are displayed in Tables 16, 18, and 8.

Conclusions

The results reported for the TMCH were in fair agreement with experiment for VCH and TiCH in terms of geometries at the MRCI level. The density functional theory frequency calculations on the TiCH ground state were in good agreement with experiment. The VCH vibrational frequencies calculated were slightly smaller for the V-C stretch

All of the same ground electronic states for the TMCH and TMN molecules are predicted and follow the same bonding patterns. Comparisons between the metal-nitrides and TM-CH molecules suggest similar structures with much shorter bondlengths and greater charge transfer in the nitrides than in the TM-CH molecules. In fact the character of the bonding in the sigma systems were extremely close. Upon examining the $TM\text{-}CH^+$ molecules, all of the structures again remain similar in structure except for the case of the VCH^+ where our results are in slight disagreement with Swaisgood's previous results.[1g]

Restricted Hartree-Fock calculations are also reported. These results can be found in Tables 5, 6, 12, and 15. These resultant bondlengths are not in agreement with those of the MRCI, and MCSCF results.

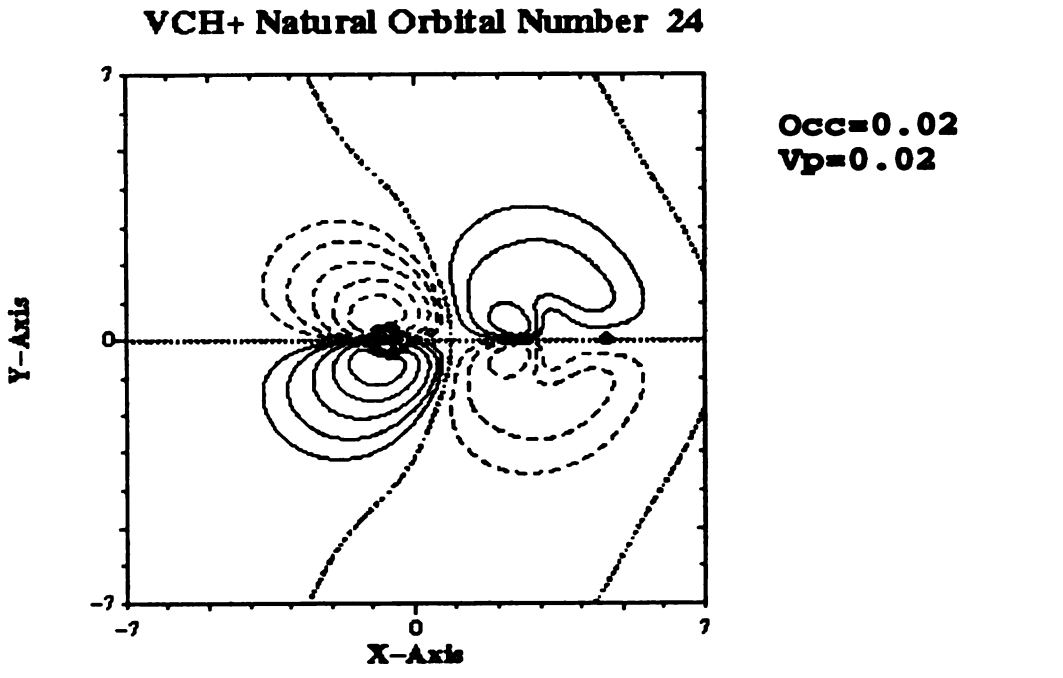

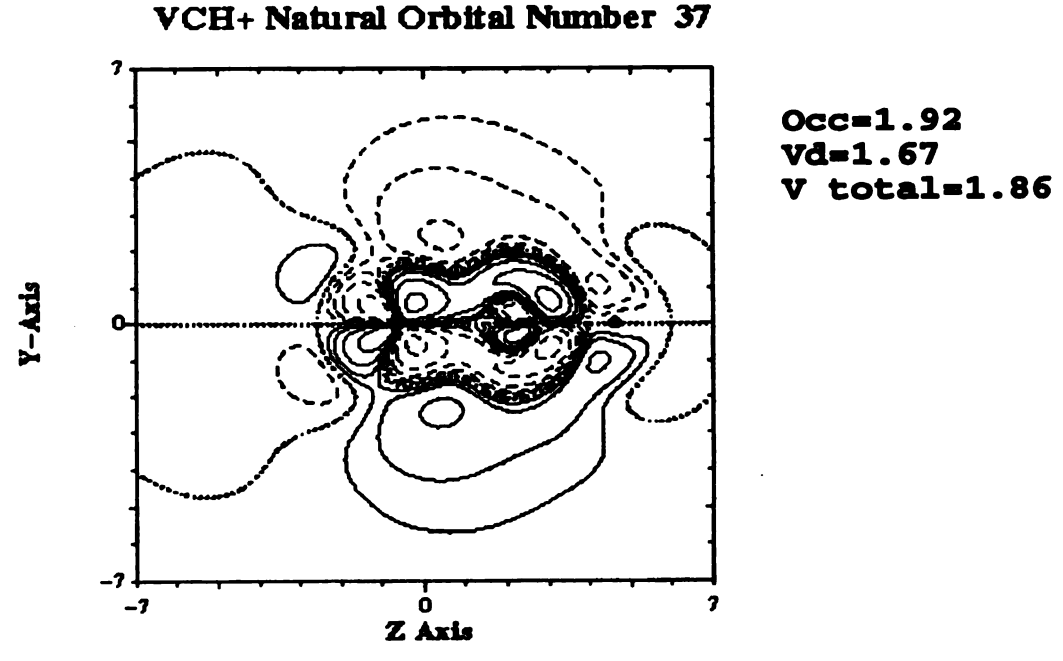

Figure 48 and Figure 49

Figure 48 and 49 are the electron density contour plots of natural orbitals 24and 37 of VCH+ in the 2Δ ground state. The occupation and mulliken population condensed to a basis function type are reported for each orbital

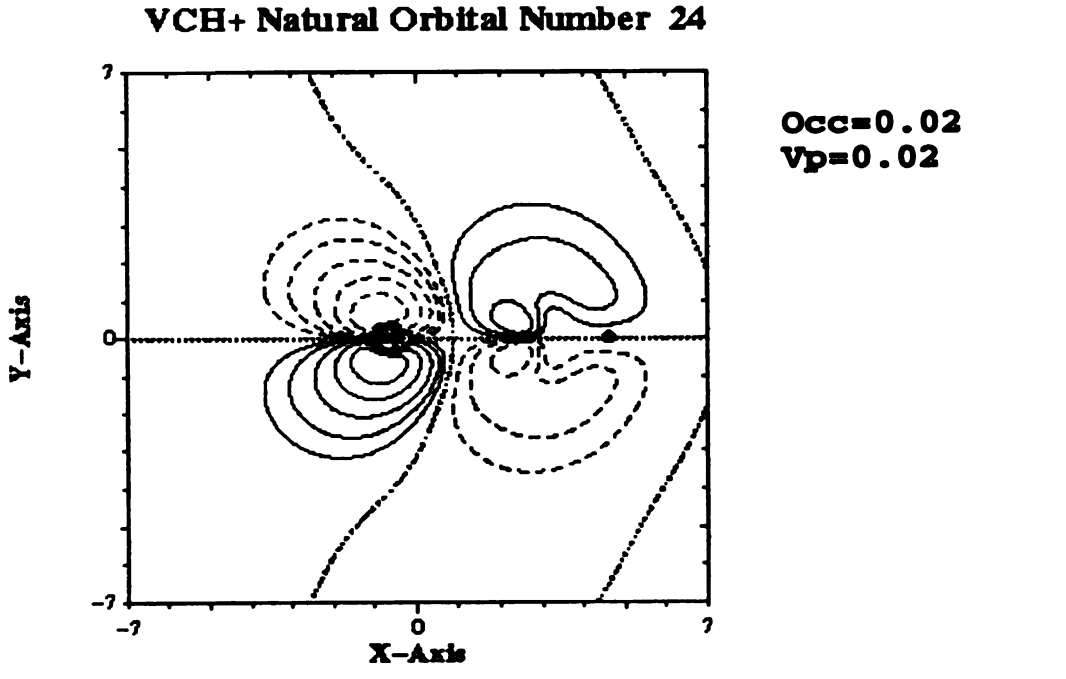

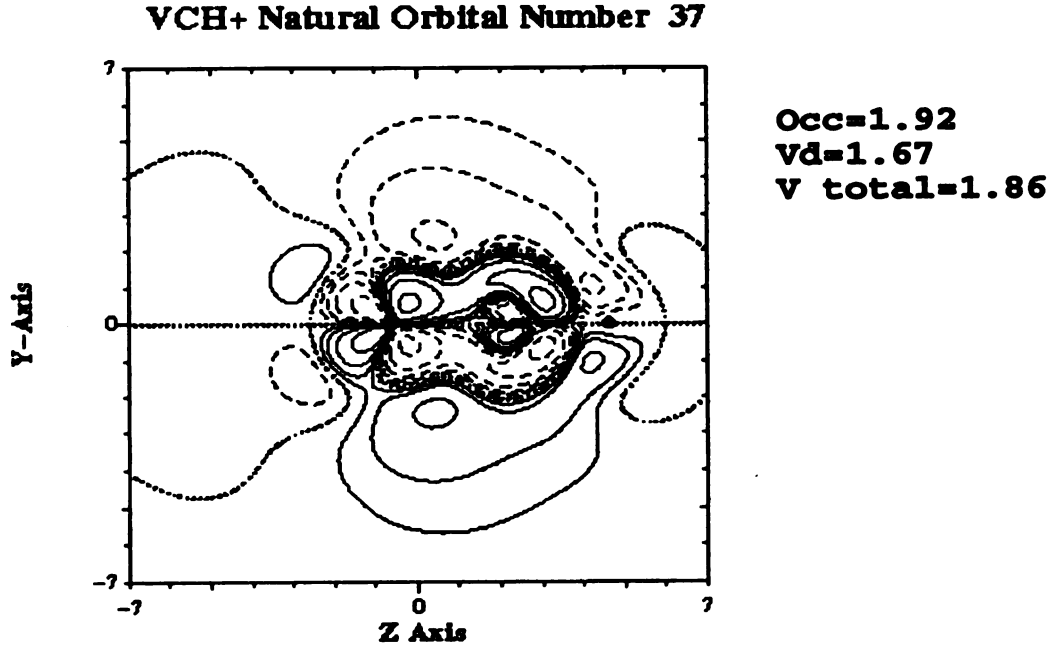

Figure 48 and Figure 49

Figure 48 and 49 are the electron density contour plots of natural orbitals 24and 37 of VCH+ in the 2Δ ground state. The occupation and mulliken population condensed to a basis function type are reported for each orbital

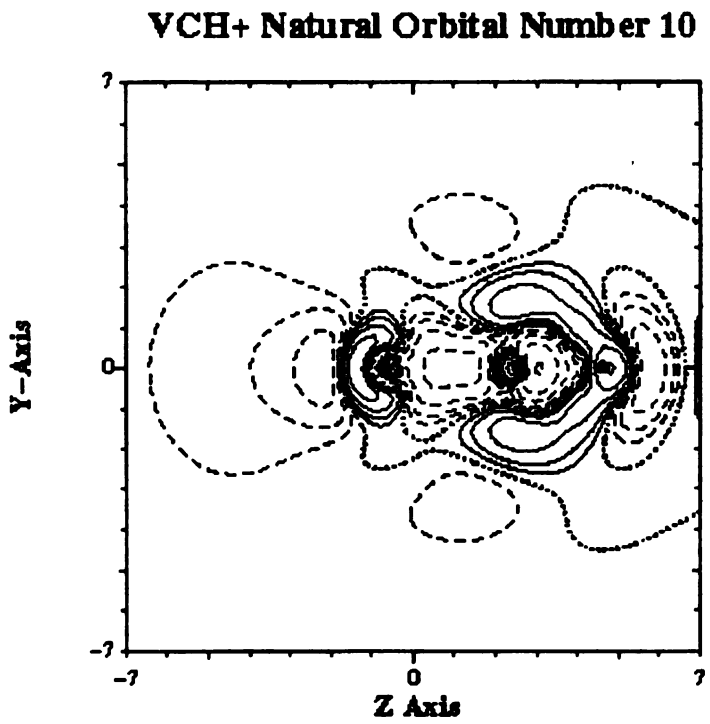

Figure 50

Figure 50 is the electron density contour plot of natural orbital 10 of VCH^+ in the $^2\Delta$ ground state. The occupation and mulliken poupulatin condensed to a basis function is also reported.

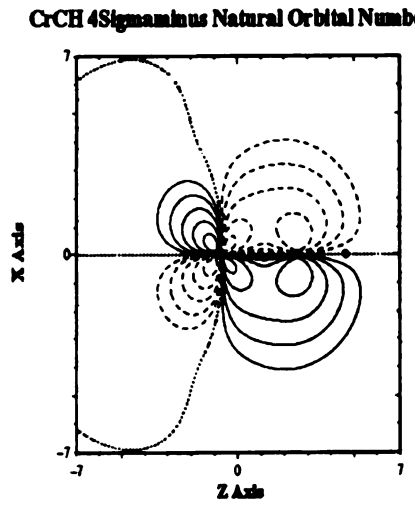

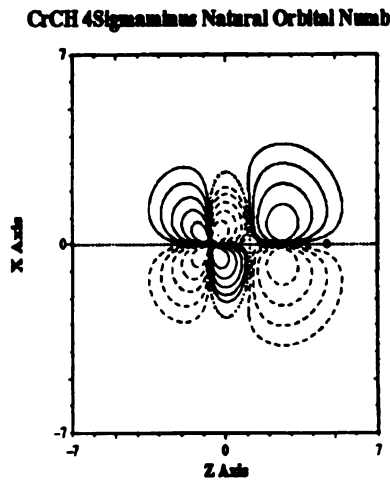

Occ=1.68 Crd=0.84 Cp=0.80
Cr total=0.87 C total=0.81

Occ=0.300 Crd=0.16
Cr total=0.16 C total=0.14

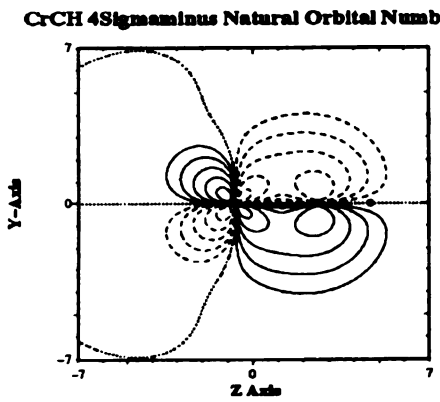

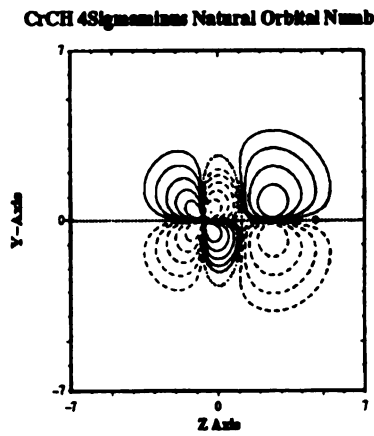

Occ=1.68 Crd=0.84 Cp=0.80
Cr total=0.87 C total=0.81

Occ=0.300 Crd=0.16
Cp=0.14 C total=0.14
Cr total=0.16

Figure 51, 52, 53, 54 (Clockwise)

Figures 51 through 54 are the electron density contour plots of natural orbitals 25, 26, 40, and 39 of the CrCH molecule in the $^4\Sigma^-$ ground state. The occupations and the mulliken population condensed to a basis function type are reported for each orbital.

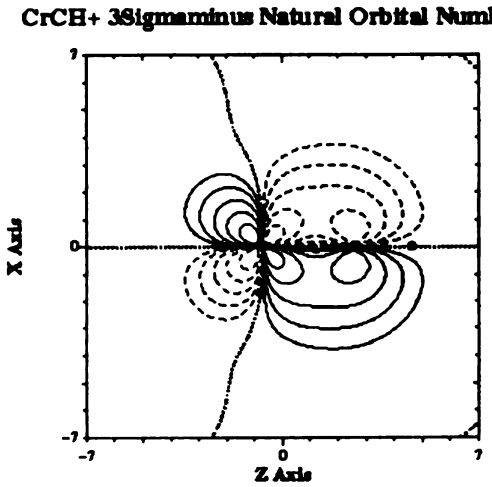

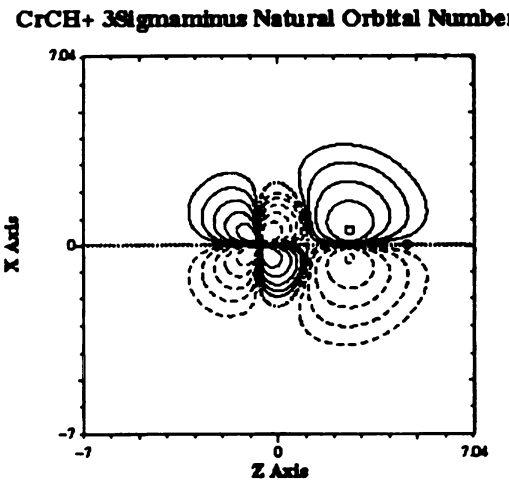

Figure 55 and Figure 56

Figure 55 through 56 are the electron density contour plots of natural orbitals 24 and 25 of the $CrCH^+$ molecule in the $^3\Sigma^-$ ground state. The occupations and the mulliken populations condensed to a basis function type are reported for each orbital.

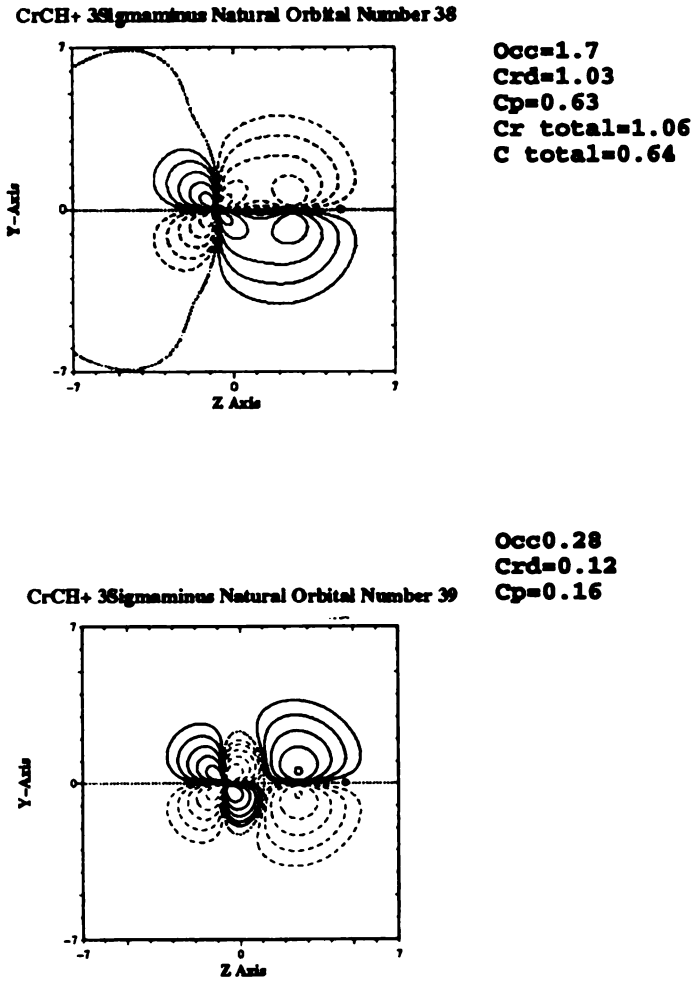

Figure 57 and Figure 58

Figure 57 and 58 are the electron density contour plots of natural orbitals 38 and 39 of the $CrCH^+$ molecule in the $^3\Sigma^-$ ground state. The occupations and the mulliken population condensed to a basis function type are reported for each orbital.

Tabulated Results

Table 1. The equilibrium metal-carbon, ReqScC(Å), and carbon hydrogen, ReqCH(Å), bond lengths, energy, and dipole moment of ScCH in the ground $^3\Pi$ state using the AWACH basis at the MRCI, MCSCF, DFT, and RHF levels (MRCI[a] corresponds to a MRCI wavefunction with an extra orbital of a_1 symmetry in correlation of the MCSCF[a] reference).

State	Level	Basis	ReqScC(Å)	RopCH(Å)	Energy(Hartrees)	Dipole(Debye)
$^3\Pi$	MRCI[a]	AWACH	1.95411	1.09288	-798.27363	-2.1857
$^3\Pi$	MRCI	AWACH	1.95570	1.09252	-798.27204	-2.1767
$^3\Pi$	MCSCF	AWACH	1.99972	1.10322	-798.14097	-1.8010
$^3\Pi$	MCSCF[a]	AWACH	1.99569	1.10430	-798.14912	-1.8314
$^3\Pi$	DFT	AWACH	1.89238	1.09588	-799.24958	-2.7912

Table 2. The equilibrium metal-carbon, ReqScC(Å), and carbon hydrogen, ReqCH(Å), bond lengths, and energy of $ScCH^+$ in the ground $^2\Pi$ state using the AWACH basis at the MRCI, MCSCF, DFT, and RHF levels (MRCI[a] corresponds to a MRCI wavefunction with an extra orbital of a_1 symmetry in correlation of the MCSCF[a] reference).

State	Level	Basis	ReqScC(Å)	ReqCH(Å)	Energy(Hartrees)
$^2\Pi$	MRCI	AWACH	1.92960	1.08886	-798.05745
$^2\Pi$	MCSCF	AWACH	2.09038	1.08108	-797.85422
$^2\Pi$	MRCI[a]	AWACH	1.92813	1.08913	-798.05887
$^2\Pi$	MCSCF[a]	AWACH	1.96458	1.09889	-797.94483
$^2\Pi$	DFT	AWACH	1.86108	1.09419	-799.02300

Table 3. The mulliken population analysis of ScCH in the ground $^3\Pi$ state using the AWACH basis at the MRCI and MCSCF level (MRCI[a] corresponds to a MRCI wavefunction with an extra orbital of a_1 symmetry in correlation of the MCSCF[a] reference).

MRCI[a]		Analysis by Basis Function Type				
State	Atom	s	p	d	Total	Charge
$^3\Pi$						
	Sc	7.03910	12.24748	1.24790	20.56429	+0.43571
	C	3.66683	2.83314	0.02900	6.52897	-0.52897
	H	0.85269	0.05405	0.0000	0.90674	+0.09326
MRCI						
$^3\Pi$						
	Sc	7.04266	12.26294	1.24566	20.57782	+0.42218
	C	3.68906	2.83702	-0.00968	6.51639	-0.51639
	H	0.87517	0.03062	0.00000	0.90578	+0.09422
MCSCF[a]						
$^3\Pi$						
	Sc	7.02360	12.26939	1.23059	20.54779	-0.45221
	C	3.71419	2.83522	-0.00109	6.54832	-0.54832
	H	0.87620	0.02679	0.00000	0.90389	+0.09611
MCSCF						
$^3\Pi$						
	Sc	7.02659	12.27048	1.23397	20.55485	+0.44515
	C	3.71926	2.83325	-0.00604	6.54647	-0.54647
	H	0.87093	0.02775	0.00000	0.89868	+0.10132

Table 4. The mulliken population analysis of $ScCH^+$ in the ground $^2\Pi$ state using the AWACH basis at the MRCI (MRCI[a] extra orbital of a_1 symmetry in correlation of the MCSCF[a] reference).

MRCI Level			Analysis by Basis Function Type				
State $^2\Pi$	Level MRCI	Atom	s	p	d	Total	Charge
		Sc	6.07716	12.00787	1.43886	19.5469	+1.45315
		C	3.76075	2.80089	0.01642	6.57806	-0.57806
		H	0.82843	0.004665	0.00000	0.87508	+0.12492
$^2\Pi$	MRCI[a]						
		Sc	6.06521	12.01081	1.44511	19.54704	+1.45296
		C	3.75060	2.78928	0.04670	6.58657	-0.58657
		H	0.80360	0.06279	0.00000	0.86639	+0.13361

Table 5. The equilibrium metal-carbon, ReqTiC(Å), and carbon hydrogen, ReqCH(Å), bond lengths, energies, and dipole moments of the ground state, $^2\Sigma^+$, and three excited states of TiCH using the AMES, and AWACH basis at the MRCI, and MCSCFlevel (extra orbital of a_1 symmetry in correlation of the MCSCF reference), DFT, and experimental geometry (ground state) and experimental separation between the ground state and $^2\Pi$ state.

State	Level	Basis	ReqTiC(Å)	ReqCH(Å)	Energy(Hartrees)	Dipole(Debye)
$^2\Sigma^+$	MRCI	AMES	1.75024	1.08921	-887.01450	-1.4490
$^2\Delta$	MRCI	AMES	1.79931	1.09566	-886.98351	-7.3121
$^2\Pi_{linear}$	MRCI	AMES	1.72217	1.09202	-886.94941	-3.6733
$^2\Pi_{bent170^0}$	MRCI	AMES	1.72217	1.09202[a]	-886.94725	-3.7013[b]
$^2\Sigma^+$	MRCI	AWACH	1.75123	1.08865	-886.97672	-1.8860
$^2\Delta$	MRCI	AWACH	1.80085	1.09503	-886.94619	-7.3964
$^2\Pi_{linear}$	MRCI	AWACH	1.77341	1.09130	-886.91247	-3.8275
$^2\Sigma^+$	MCSCF	AMES	----------	----------	----------	----------
$^2\Delta$	MCSCF	AMES	1.81461	1.10775	-886.82464	-7.3361
$^2\Pi_{linear}$	MCSCF	AMES	1.72770	1.08500	-886.81038	-2.9747
$^2\Pi_{bent170^0}$	MCSCF	AMES	1.72217[a]	1.09202[a]	-886.81104	-3.6346[c]
$^2\Sigma^+$	MCSCF	AWACH	1.75479	1.10500	-886.84447	-1.4142
$^2\Delta$	MCSCF	AWACH	1.81982	1.08427	-886.81271	-7.3674
$^2\Pi_{linear}$	MCSCF	AWACH	1.77240	1.07884	-886.78921	-3.1484
$^2\Sigma^+$	DFT	AWACH	1.69140	1.09490	-888.00013	-2.6910
$^2\Delta$	DFT	AWACH	1.74240	1.09570	-887.97967	-6.1826
$^2\Pi_{linear}$	DFT	AWACH	1.72300	1.09310	-887.94060	--------
$^2\Sigma^+$	Experiment		1.7277	1.085	$X^2\Sigma^+-^2\Pi$ ~62.8mH	-------
	Our DFT Results				$X^2\Sigma^+-^2\Pi$ 59.5mH	

Table 5a. The equilibrium metal-carbon, ReqTiC(Å), and carbon hydrogen, ReqCH(Å), bond lengths, energies, and dipole moments of the ground state, $^2\Sigma^+$, and three excited states of TiCH using the AWACH basis at the RHF level.

State	Level [a]	Basis	ReqTiC(Å)	ReqCH(Å)	Energy(Hartrees)	Dipole(Debye)
$^2\Sigma^+$	RHF	AWACH	----------	----------	----------	----------
$^2\Delta$	RHF	AWACH	1.73569	1.08239	-886.66760	-3.4093
$^2\Pi_{linear}$	RHF	AWACH	1.76599	1.08152	-886.63119	-2.4709
$^2\Pi_{bent170}{}^0$	RHF	AWACH	1.77217	1.09202	-886.63025	-2.5001

(Applies to Table 5 and 5a.)

a. The $^2\Pi_{bent170}{}^0$ state bondlengths were not optimized. The bondlengths used were those of the optimized $^2\Pi_{linear}$ state.

b. The dipole moment reported corresponded to the z-component of the dipole moment. The y-component calculated was -0.07227 debye. The TiCH molecule was constructed with the C-H bond bent in the yz plane while the TiC bond was along the z-axis.

c. The dipole moment reported corresponded to the z-component of the dipole moment. The y-component calculated was -0.009446 debye. The TiCH molecule was constructed with the C-H bond bent in the yz plane while the TiC bond was along the z-axis.

Table 6. The equilibrium metal-carbon, ReqTiC(Å), and carbon hydrogen, ReqCH(Å), bond lengths, and energy of $TiCH^+$ in the ground $^1\Sigma^+$ state using the AWACH basis at the MRCI, MCSCF, DFT, and RHF levels.

State	Level	Basis	ReqTiC(Å)	ReqCH(Å)	Energy(Hartrees)
$^1\Sigma^+$	MRCI	AWACH	1.73983	1.08999	-886.75643
$^1\Sigma^+$	MCSCF	AWACH	1.73844	1.10157	-886.63855
$^1\Sigma^+$	DFT	AWACH	1.66905	1.09440	-887.74598
$^1\Sigma^+$	RHF	AWACH	1.67270	1.08051	-886.43718

Table 7. The vibrational frequencienes, ω_e, of several states of ScCH, TiCH, VCH and CrCH using DFT, the AWACH basis on metal and 6-31G** basis on C and H.

Molecule	State	ω_e (cm-1)			
ScCH	$^3\Pi$	487.2	513.5	802.1	3114.7
TiCH	$^2\Sigma^+$	600.30	600.30	953.14	3119.2
Experiment	$^2\Sigma^+$	578	578	855	~3000
	$^2\Delta$	496.74	496.74	860.66	3098.7
	$^2\Pi_{linear}$	-804.27	651.54	908.55	3139.0
	$^2\Pi_{bent17^0_0}$	-	-	-	-
VCH	$^3\Delta$	577.28	577.28	693.95	3148.2
Experiment	$^3\Delta$	564	564	838	~3000
	$^3\Phi_{\pi,\delta^+}$ [a]	------	631.95	776.79	3174.4
CrCH	$^4\Sigma^-$	545.74	545.74	640.39	3155.2

$^2\Sigma^+$ TiCH Experiment	TiCH Our DFT Results
$X^2\Sigma^+-^2\Pi$ ~62.8mH	$X^2\Sigma^+-^2\Pi$ 59.5mH

a. $^3\Phi_{\pi,\delta^+}$ frequencies calculated using MCSCF equilibrium geometry

Table 8. The charge distribution and vibrational frequencienes, ω_e, of $ScCH^+$, $TiCH^+$, VCH^+, and $CrCH^+$ in their ground states using DFT, the AWACH basis on metal and 6-31G** basis on C and H.

Molecule	State	ω_e (cm-1)			
$ScCH^+$	$^2\Pi$	552.84	605.21	815.09	3154.5
$TiCH^+$	$^1\Sigma^+$	677.61	677.61	994.28	3156.3
VCH^+	$^2\Delta$	847.91	848.22	1064.1	3229.8
$CrCH^+$	$^3\Sigma^-$	589.95	589.95	692.46	3179.0

Table 9. The mulliken population analysis of TiCH in the ground $^2\Sigma^+$ state and three excited states using the AMES and AWACH basis sets at the MRCI level (MRCI[a] extra orbital of a_1 symmetry in correlation of the MCSCF[a] reference).

MRCI[a] AMES basis	Analysis by Basis Function Type					
State	Atom	s	p	d	Total	Charge
$^2\Sigma^+$						
	Ti	7.19463	12.39523	2.53457	22.16185	-0.16185
	C	3.30996	2.71314	0.05006	6.07316	-0.07316
	H	0.74872	0.01628	0.0000	0.7650	+0.2350
$^2\Delta$						
	Ti	6.40492	12.2005	3.14550	21.77167	+0.22833
	C	3.38170	2.94461	0.06773	6.39405	-0.39405
	H	0.79626	0.03802	0.00000	0.83428	+0.16572
$^2\Pi_{linear}$						
	Ti	6.41862	12.71552	2.68921	21.85400	+0.14600
	C	3.37103	2.90426	0.08161	6.35689	-0.35689
	H	0.76191	0.02719	0.00000	0.78910	+0.21090
$^2\Pi_{bent170^0}$						
	Ti	6.93920	12.28476	2.67499	21.92097	+0.07903
	C	3.35917	2.88907	0.03675	6.28499	-0.28499
	H	0.76475	0.02929	0.00000	0.79404	+0.20596
MRCI[a] AWACH basis						
State						
$^2\Sigma^+$						
	Ti	7.16397	12.12480	2.44044	21.75934	+0.24066
	C	3.57442	2.75750	0.02458	6.35650	-0.35650
	H	0.85221	0.03195	0.00000	0.88416	+0.11584
$^2\Delta$						
	Ti	6.14121	12.09255	3.10044	21.35628	0.64372
	C	3.67550	2.94460	0.05251	6.67261	-0.67261
	H	0.89372	0.07739	0.00000	0.97111	+0.02889
$^2\Pi_{linear}$						
	Ti	6.07742	12.67113	2.57873	21.35389	+0.64611
	C	3.75619	2.98626	0.02418	6.76663	-0.76663
	H	0.86770	0.01178	0.00000	0.87948	+0.12052
MRCI AWACH basis Analysis by Basis Function Type						
State	Atom	s	p	d	Total	Charge
$^2\Sigma^+$						
	Ti	6.94413	12.197613	2.69711	21.859557	+0.140444
	C	3.45601	2.74343	0.01524	6.259891	-0.214687
	H	0.91186	0.01390	0.00000	0.925757	+0.074243
$^2\Delta$						
	Ti	6.28269	12.20102	3.27497	21.771917	+0.228082
	C	3.44709	2.81591	0.01256	6.27554	-0.275540
	H	0.93837	0.01418	0.00000	0.952541	+0.047458
$^2\Pi_{linear}$						
	Ti	6.22478	12.77718	3.76464	21.829147	+0.170853
	C	3.45446	2.78006	0.01382	6.248332	-0.248332
	H	0.90843	0.01129	0.00000	0.922521	+0.077479

Table 10. The mulliken population analysis condensed to basis function type of $TiCH^+$ in the ground $^1\Sigma^+$ state using the AWACH basis at the MRCI (MRCI[a] extra orbital of a_1 symmetry in correlation of the MCSCF[a] reference).

MRCI[a] Level		Analysis by Basis Function Type				
State $^1\Sigma^+$	Atom	s	p	d	Total	Charge
	Ti	6.00942	11.97325	2.59793	22.60728	+1.39272
	C	3.77514	2.73443	0.04343	6.55300	-0.55300
	H	0.79754	0.04218	0.00000	0.83972	+0.16028
MRCI Level $^1\Sigma^+$						
	Ti	6.00893	11.96726	2.62095	20.61658	+1.38342
	C	3.77242	2.72439	0.01836	6.51517	-0.51517
	H	0.83568	0.03257	0.00000	0.86825	+0.13175

Table 11. The equilibrium metal-carbon, ReqVC(Å), and carbon hydrogen, ReqCH(Å), bond lengths, energy, and dipole moment of the ground state, $^3\Delta$, and an excited state (DFT level) of VCH using the AWACH basis at the MRCI and DFT level. The experimental bond length for the ground state is also reported.

State	Level	Basis	ReqVC(Å)	ReqCH(Å)	Energy(Hartrees)	Dipole(Debye)
$^3\Delta$	MRCI	AWACH	1.72539	1.08954	-981.46786	-1.75693
$^3\Delta$	MCSCF	AWACH	1.74828	1.10044	-981.31299	-1.3349
$^3\Delta$	DFT	AWACH	1.69704	1.09301	-982.54778	-1.0039[a]
$^3\Phi_{\pi,\delta+}$	DFT	AWACH	1.71391	1.08991	-982.36029	-1.3852[a]
$^3\Delta$	**Experiment**		1.702	1.080	----------	
$^3\Pi$	MCSCF	AWACH	1.76573	1.09988	-981.25522	-1.6782

a. Dipole moment in atomic units

Table 12. The equilibrium metal-carbon, ReqVC(Å), and carbon hydrogen, ReqCH(Å), bond lengths, and energy of VCH^+ in the ground $^2\Delta$ state using the AWACH basis at the MRCI, MCSCF, DFT, and RHF levels.

State	Level	Basis	ReqVC(Å)	ReqCH(Å)	Energy(Hartrees)
$^2\Delta$	MRCI	AWACH	1.72000	1.08852	-981.23573
$^2\Delta$	MCSCF	AWACH	1.73289	1.09849	-981.09832
$^2\Delta$	DFT	AWACH	1.59877	1.08329	-982.02962
$^2\Delta$	RHF	AWACH	1.64713	1.08003	-980.86841

Table 13. The mulliken population analysis of VCH in the ground $^3\Delta$ state using the AWACH basis at the MRCI level.

		Analysis by Basis Function Type				
State $^3\Delta$	Atom	s	p	d	Total	Charge
	V	7.17346	12.12899	3.53824	22.85340	+0.14660
	C	3.55884	2.73373	0.00149	6.29108	-0.29108
	H	0.86257	0.00705	0.00000	0.85553	+0.14448

Table 14. The mulliken population analysis condensed to basis function type of VCH^+ in the ground $^2\Delta$ state using the AWACH basis at the MRCI and MCSCF level.

MRCI Level		Analysis by Basis Function Type				
State $^2\Delta$	Atom	s	p	d	Total	Charge
	V	4.99914	12.04193	3.70996	20.75104	+2.24896
	C	5.58519	1.79378	-0.23210	8.14687	-1.14687
	H	0.43145	-0.32935	0.00000	0.10210	+0.29059
MCSCF Level						
$^2\Delta$						
	V	6.00942	12.00620	3.70600	21.73610	+1.26390
	C	3.70986	2.69805	0.02298	6.43089	-0.43089
	H	0.81742	0.01559	0.00000	0.83301	+0.16699

Table 15. The equilibrium metal-carbon, ReqCrC(Å), and carbon hydrogen, ReqCH(Å), bond lengths, and energy of the ground state, $^4\Sigma^-$, of CrCH using the AWACH basis at the MRCI, MCSCF, DFT and RHF levels.

State	Level	Basis	ReqCrC(Å)	ReqCH(Å)	Energy(Hartrees)	Dipole(Debye)
$^4\Sigma^-$	MRCI	AWACH	1.74257	1.08754	-1081.91311	-2.3398
$^4\Sigma^-$	MCSCF	AWACH	1.77857	1.09811	-1081.71636	-2.0085
$^4\Sigma^-$	DFT	AWACH	1.74670	1.09127	-1083.03970	-2.7418
$^4\Sigma^-$	RHF	AWACH	1.91023	1.07540	-1081.42992	--------

Table 16. The equilibrium metal-carbon, ReqCrC(Å), and carbon hydrogen, ReqCH(Å), bond lengths, and energy of $CrCH^+$ in the ground $^3\Sigma^-$ state using the AWACH basis at the MRCI, MCSCF, DFT, and RHF level.

State	Level	Basis	ReqCrC (Å)	ReqCH (Å)	Energy(Hartrees)
$^3\Sigma^-$	MRCI	AWACH	1.72025	1.08642	-1081.66315
$^3\Sigma^-$	MCSCF	AWACH	1.74314	1.08442	-1081.51000
$^3\Sigma^-$	DFT	AWACH	1.71720	1.09189	-1082.76612
$^3\Sigma^-$	RHF	AWACH	1.74314	1.07660	-1081.44267

Table 17. The mulliken population analysis condensed to basis function type of $CrCH^+$ in the ground $^3\Sigma^-$ state using the AWACH basis at the MRCI level (extra orbital of a_1 symmetry in correlation of MCSCF).

		Analysis by Basis Function Type				
State $^3\Sigma^-$	Atom	s	p	d	Total	Charge
	Cr	6.33761	12.02527	4.34514	22.71373	+1.28627
	C	3.91776	2.61937	0.03973	6.57686	-0.57686
	H	0.72393	-0.01452	0.00000	0.70941	+0.29059

Table 18. The mulliken population analysis condensed to basis function type of CrCH and $CrCH^+$ in their ground states using the AWACH basis at the MCSCF level (extra orbital of a_1 symmetry in correlation).

		Analysis by Basis Function Type				
State $^4\Sigma^-$	Atom	s	p	d	Total	Charge
	Cr	6.93200	12.15021	4.65970	23.74754	+0.25246
	C	3.63180	2.78929	0.02117	6.44225	-0.44225
	H	0.83284	-0.02263	0.00000	0.81021	+0.18979
$^3\Sigma^-$						
	Cr	6.33761	12.02527	4.34514	22.71373	+1.28627
	C	3.91776	2.61937	0.03973	6.57686	-0.57686
	H	0.72393	-0.01452	0.00000	0.70941	+0.29059

BIBLIOGRAPHY

BIBLIOGRAPHY

1. Publications in this series include: (a) Alvarado-Swaisgood, A. E.; Allison, J.; Harrison, J. F. J. Phys. Chem. 1985, 89, 2517. (b) Alvarado-Swaisgood, A. E.; Harrison, J. F. J. Phys. Chem. 1985, 89, 5198. (c) Harrison, J. F. J. Phys. chem. 1986, 90, 3313. (d) Mavridis, A.; Alvarado-Swaisgood, A. E.; Harrison, J. F. J. Phys. Chem. 1986, 90, 2548. (e) Alvarado-Swaisgood, A. E.; Harrison, J. F. J. Phys. Chem. 1988, 92, 2757. (f) Alvarado-Swaisgood, A. E.; Harrison, J. F. J. Phys. Chem. 1988, 92, 5896. (g) Alvarado-Swaisgood, A. E.; Harrison, J. F. 1988, 46, 155. (h) Harrison, J. F.; Kunze, K. L. Journal of Physical Chemistry 1989, 93, 2983.(I) Tientega, F.; Harrison, J. F. Chem. Phys. Letters, 1994, 223, 202. (j) Harrison, J. F.; Kunze, K. L.. "Gas Phase Organomettaliic Chemistry", Freiser, B; Ed.; Kluwer Academic Publishers: Netherlands, 1995, Chapt. 2, 89-121.

2. Publications of the theoretical groups: (a) Schilling, J. B.; Beauchamp, J. L.; Goddard, W. A., III; J. Am. Chem. Soc. 1987, 109, 4470. (b) Schilling, J. B.; Goddard, W. A., III; Beauchamp, J. L. J. Am. Chem. Soc. 1987, 109, 5573. (c) Schilling, J. B.; Beauchamp, J. L.; Goddard, W. A., III J. Am. Chem. Soc. 1987, 109, 5565. (d) Carter, E. A.; Goddard, W. A., III J. Am. Chem. Soc. 9186, 108, 2180, 4746. (e) Pettersson, L. G. M. ; Bauschlicher, Jr., C. W.; Langhoff, S. R.; Partridge, H. J. Chem. Phys. 1987, 87, 481. (f) Blomberg, M. R. A.; Siegbahn, P. E. M.; Backvall, J. E. J. Am. Chem. Soc. 1987, 109, 4450. (g) Siegbahn, P. E.; Blomberg, M. R. Chem. Phys. 1984, 87, 189. (h) Bauschlicher, C. W. Chem. Phys. Letters, 1983, 100, 515. (I) Allison, J. N.; Goddard, W. A. , III Chem. Phys. 1983, 81, 263. (j) Shim, I.; Gingerich, K. A. Int. J. Quant. Chem., 1993, 46, 145. (k) Gingerich, K. A. J. Chem. Phys. 1968, 49, 19. (l) Musaev, d. G.; Koga, N. ; Morokuma, K. J. Phys. Chem. 1993, 97, 4064. (m) Blomberg, R. A.; Siegbahn, P. E. M.; Svensson, Matts, Inorg. chem. 1993, 32, 4218. (n) Elkhattabi, S.; Daoudi, A.; Berthier, G.; Flament, J. P. 1997 to be published.

3. Publications of experimental groups: (a) Elkind, J. L.; Armentrout, P. B. J. Chem. Phys. 1987, 86, 1868. (b) Sunderlin, L. ; Aristov, N.; Armentrout, P. B. J. Chem. Phys. 1987, 109, 78. (c) Aristov, N.; Armentrout,P. B. J. Phys. Chem. 1987, 91, 6178. (d) Reents, W. D.; Strobel, F.; Freas, R. B.; Wronka, J.; Ridge, D. P. J. Phys. Chem. 1985, 89, 5666. (e) Hettich, R. L.; Freiser, B. S. J. Am. Chem. Soc, 1987, 109, 3543. (f) Radecki, B. D.; Allison, J. Organometallics 1986, 5, 411. (g) McElvany, S. W.; Allison, J. Organometallics 1986, 5, 1219. (h) Hanratty, M. A.; Beauchamp, J. L.; Illies, A. J.; van Koppen, P.; Bowers, M. T. J. Am. Chem. Soc. 1988, 110, 1. (I) Schilling, J. L.; Beauchamp, J. L. J. Am. Chem. Soc. 1988, 110, 15. (j) Schilling, J. L.; Beauchamp, J. L. Organometallics 1988, 7, 194. (k) Tolbert, M. A.; Mandich, M. L.; Halle, L. F.; Beauchamp, J. L. J. Am. Chem. Soc. 1986, 108, 5675. (l) Kang, H.; Beauchamp, J. L. J. Am. Chem. Soc. 1986, 108, 5663. (m) Kang, H.; Beauchamp, J.

L. J. Am. Chem. Soc. 1986, 108, 7502. (n) Lebrilla, C. B.; Schulze, C.; Schwarz, H. J. Am. Chem. Soc. 1987, 109, 98. (0) Lebrilla, C. B.; Drewello, T.; Schwarz, H. Int. J. Mass Spectrum. Ion Proc. 1987, 79, 287. (p) Schulze, C.; Schwarz, H. J. Am. Chem. Soc. 1988, 110, 67. (q) Stepnowski, R.; Allison, J. Organometallics, in press. (r) Bernath, P. F.; Ram, R. S. J. Mol. Spect. 1994, 165, 97.

4. Bernath, P. F.; Ram, R. S. J. Chem. Phys. 1992, 96, 6344.

5. Dunn, T. M.; Hanson, L. K.; Rubinson, K. A. Can. J. Phys. 1970, 48, 1657.

6. Peter, S. L.; Dunn, T. M. J. Chem. Phys. 1989, 90, 5333.

7. Howard, J. C.; Conway, J. G. J. Chem. Phys. 1965, 43, 3055.

8. Dunn, T. M.; Roa, K. M. Nature 1969, 222, 266.

8a. B.H Botch, T.H. Dunning, Jr., and J.F. Harrison, J. Chem. Phys., 75, 3466 (1981)

9. Bates, J. K.; Dunn, T. M. Can. J. Phys. 1976, 54, 1216.

9a. E. A. Carter and W. A. Goddard III, J. Phys. Chem., 88, 1485 (1984).

10. Bates, J. K.; Gruen, D. M. J. Chem. Phys. 1979, 70, 4428.

11. Knight, L. B., Jr.: Steadman, J. J. Chem. Phys. 1982, 76, 3378.

12. Balasubramanian, K.; Das, K. K. J. Chem. Phys. 1990, 93, 6671.

13. Simard, B.; Balfour, J.; Vasseur, M.; Hackett, P. A. J. Chem. Phys. 1990, 93, 4481.

14. Wachters, A. J. H. J. Chem. Phys. 1970, 52, 1033.

15. S.P. Walch and C. W. Bauschlicher, Jr., J. Chem. Phys., 78, 4597 (1983).

16. Hay, P. J.; Wadt, W. R. J. Chem. Phys. 1986, 82, 5606.

17. Dunning, T. H. J. Chem. Phys. 1971, 55, 3958.

18. Harrison, J.F.; Edwards, J.; NOBCChE '96. 23rd Annual National Conference: Proceedings of the National Organization for the Professional Development of Black Chemist and Chemical Engineers, 1996.

19. Martin, R. L.; and Hay, P. J. J. Chem. Phys. 1981, 75, 4539.

19a. Stewart, R.F.; J. Chem. Phys. 52, 1, 431-438, (1970).

20. MOLPRO is a package of ab-initio programs written by H.J. Werner and P.J. Knowles, with contributions from J. Almof, R.D. Amos, M.J.O. Deegan, S.T. Elbert, C. Hampel, W. Meyer, K. Peterson, R. Pitzer, A. J. Stone, P.R. Taylor, R. Lindh, M.E. Mura, and T. Thorsteinsson.

21. Moore, C. E. Atomic Energy Levels; National Standard Reference Data Series; National Bureau of Standards: Washington DC, 1971; Vol. I and II, Circular 35.

22. Mulliken, R. S. J. Chem. Phys. 1955, 23, 1833.

23. Peterson, G. A. , and Al-Laham, M. A.. J. Chem. Phys. 94, 608 (1991).

24. Muller, J.; Angew, Chemie, 11, 653 (1972).

25. MSUPlot Program, J. F. Harrison, Michigan State University, Chemistry Department, E. Lansing, MI 48824.

26. MSUProp Program, J. F. Harrison, Michigan State University, Chemistry Department, E. Lansing, MI 48824.

27. Plotmtv is a plotting program for the visualization of scientific data. It was developed under the Computational Science Education Project by the U.S. Department of Energy. Copyright © 1991-95.

28. Bauschlicher, C.W.; Ricca, A.; Chemical Physics Letters 245 (1995) 150-157.

29. *Gaussian 94*, Revision A. 1, M. J. Frisch, G. W. Trucks, H. B. Schlegel, P. M. W. Gill, B. G. Johnson, M. A. Robb, J. R. Cheeseman, T. A. Keith, G. A. Petersson, J. A. Montgomery, K. Raghavachari, M. A. Al-Laham, V. G. Zakrzewski, J. V. Ortiz, J. B. Foresman, J. Cioslowski, B. B. Stefanov, A. Nanayakkara, M. Challacombe, C. Y. Peng, P. Y. Ayala, W. Chen, M. W. Wong, J. L. Andres, E. S. Replogle, R. Gompets, R. L. Martin, D. J. Fox, J. S. Binkley, D. J. Defrees, J. Baker, J. P. Stewart, M. Head-Gordon, C. Gonzalez, and J. A. Pople, Gaussian, Inc., Pittsburgh PA, 1995.

30. A. Daoudi, and S. ElkHattabi Laboratoire de Chimie Theorique, Faculte des Sciences Dhar Mehraz, BP.; G. Berthier, Laboratoire de Radioastronomie Millimetrique, Ecole Normale Superieure, France; J. P. Flament, Lavoratoire de Dynamique Moleculaire et Photonique, Universite USTL de Lille, France; *On the Electronic Structure and Spectroscopy of the ScN Molecule*, submitted for publication.

31. Patridge and Bauschlicher, private communication.

32. M. Barnes, A.J. Merer, and G. F. Metha, Journal of Molecular Spectroscopy 181, 168-179 (1997).

33. Basis set was obtainedfrom the Extensible Computational Chemistry Environment Basis Set Datatabase, Version 1.0, as developed and distributed by the Molecular Science Computing Facility, Environmental and Molecular Sciences Laboratory, which is part of the Pacific Northwest Laboratory, P.O. Box 999, Richland, Washington 99352, USA, and funded by the U.S. Department of Energy. The Pacific Northwest Laboratory is a multi-program laboratory operated by Battelle Memorial Institute for the U. S. Department of Energy under contract DE-AC06-76RLO 1830. Contact David Feller, Karen Schuchardt, or Don Jones for further information.

34. M. Barnes, A.J. Merer, and G. F. Metha, J. American Chemical Society, 177, No. 7, 2096-2097 (1995).

35. See Chapter 1 and references therein.

APPENDIX

APPENDIX

LISTING OF PUBLICATIONS

1. **"Ab-Initio Studies of the Scandium Nitride Dimer" J. Edwards and J. F. Harrison, Proceedings NOBCChE 95, 1995, 22, 122.**

2. **"Ab-Initio Studies of Several Low-Lying States of YN" J. Edwards and J. F. Harrison, Proceedings NOBCChE 96, 1996.**

3. **"Electronic Structure of Early Transition Metal Carbynes" J. Edwards and J. F. Harrison, to be submitted to Journal of Molecular Spectroscopy.**